

POST-CAPTURE SYNTHESIS OF IMAGES USING MANIPULABLE
INTEGRATION FUNCTIONS

THESIS

A thesis submitted in partial
fulfillment of the requirements for
the degree of Doctor of Philosophy
in Computer Science in the Stanley
and Karen Pigman College of
Engineering at the University of
Kentucky

By
Paul Selegue Eberhart
Lexington, Kentucky

Director: Dr. Henry G. Dietz, Professor of Computer Science
Lexington, Kentucky 2024

Copyright© Paul Selegue Eberhart 2024

ABSTRACT OF THESIS

POST-CAPTURE SYNTHESIS OF IMAGES USING MANIPULABLE INTEGRATION FUNCTIONS

Traditional photographic practice, as dictated by the properties of photochemical emulsion film, mechanical apparatus, and human operators, largely treats the sensitivity (gain) and integration interval as coarsely parameterized constants for the entire scene, set no later than the time of exposure. This frame-at-a-time capture and processing model permeates digital cameras and computer image processing.

Emerging imaging technologies, such as time domain continuous imaging (TDCI), quanta image sensors (QIS), event cameras, and conventional sensors augmented with computational processing and control, provide opportunities to break out of the frame-oriented paradigm and capture a stream of data describing changes to scene appearance over the capture interval with high temporal precision. Captured scene data can then be computationally post-processed to render images with user control over the time interval being sampled and the gain of integration, not just for each image rendered but for every site in each rendered image, allowing the user to ideally expose each portion of the scene. For example, in a scene that contains a mixture of moving elements some of which are more brightly lit, it becomes possible to render dark and light portions with different gains and potentially overlapping intervals, such that both have good contrast, neither one suffers motion blur, and little to no artifacting occurs at the interfaces.

This thesis represents a preliminary exploration of the properties, application, and tooling required to capture TDCI streams and render images from them in a paradigm that supports functional post-capture manipulation of time and gain.

KEYWORDS: Computational photography, Exposure, Image capture, Postprocessing, Video Processing

Author's signature: Paul Selegue Eberhart

Date: July 9, 2024

POST-CAPTURE SYNTHESIS OF IMAGES USING MANIPULABLE
INTEGRATION FUNCTIONS

By
Paul Selegue Eberhart

Director of Thesis: Henry G. Dietz

Director of Graduate Studies: Simone Silvestri

Date: July 9, 2024

ACKNOWLEDGMENTS

I would like to acknowledge the many friends, family, and colleges who have been patient about the large chunks of time, energy, and attention I devoted to the work that lead to this thesis, and also about the large chunks of time devoted to other priorities during the interim.

I would specifically like to acknowledge two former committee members, Dr. Raphael Finkel and Dr. Nathan Jacobs, who left the University of Kentucky before I finished but gave me a great deal of excellent advice during their involvement.

TABLE OF CONTENTS

Acknowledgments	iii
Table of Contents	iv
List of Figures	vi
List of Tables	viii
Chapter 1 Introduction	1
1.1 TDCI	2
1.2 New Work	2
Chapter 2 Background	3
2.1 TDCI	3
2.2 The Camera	5
2.3 Camera Pipeline	22
2.4 Scene Model	25
2.5 Image Processing and Compression	27
Chapter 3 Experiments	31
3.1 ISOLess	31
3.2 Temporal Super-Resolution	34
3.3 Shutter Artifacts	34
3.4 Camera Motion	36
3.5 Non-Uniform	39
3.6 Exposure Interval	39
3.7 Film Speed	40
3.8 Precedent for Non-Uniform Exposure	42
3.9 Non-Uniform Over Time	44
3.10 Non-Uniform Over Space	46
3.11 The Octave Prototype	49
3.12 Findings from the Octave Prototype	51
3.13 Camera Hackin'	52
3.14 NUTIK	65
Chapter 4 Discussion	75
4.1 A Better Way To Use a Digital Camera	75
4.2 Capture, Then Integrate	76
4.3 Violating Assumptions Makes Everything Harder	77
4.4 Changes in Cameras	78

Chapter 5 Conclusion	84
Appendix A Non-Uniform Proof Of Concept: Matlab Prototype	85
Appendix B NUTIK parts	88
Bibliography	122
Vita	129

LIST OF FIGURES

2.1	Common Sensor Sizes	12
2.2	Shutter angle and exposure time	14
2.3	A typical sensor stack	15
2.4	Bayer-type CFA	16
2.5	Adelson Checkerboard Illusion	27
2.6	LED Light Waveform	29
3.1	ISOLess Test Camera Spread	32
3.2	A4000 Exposure Comparison	33
3.3	Shutter Mode Artifacts	35
3.4	Electronic First Curtain Artifacts	35
3.5	Measurement Orientations for ShAKY attached to a Canon 5DIV	37
3.6	A completed ShAKY device, showing the internal electronics	38
3.7	Typical ShAKY data for a Sony A6500 (IBIS and EFC disabled) camera still on a tabletop (left) vs. hand-held (right)	38
3.8	Example Integration Function from Octave prototype	44
3.9	Capture of riding mower integrated with the function shown in Fig. 3.8	45
3.10	Two integration functions	48
3.11	Mask specifying two areas of the scene to integrate with different functions.	49
3.12	Capture of a single pendulum carrying a foam penguin and rock, exposed with the mask and functions from fig. 3.10 and 3.11	50
3.13	Binwalk results for the liro.ko module on an a6000	54
3.14	Process table of Canon native processes	57
3.15	Rough layout of DIGIC 5 SoC	57
3.16	The packed layout of Canon 14-bit RAW encoding	58
3.17	First screen of EDMAC live monitoring	58
3.18	EDMAC DMA Transfer Behavior	59
3.19	EDMAC Memory Layout, with Offsets	59
3.20	The LAFODIS160 polar slow-scan camera	64
3.21	An in-progress full-coverage scan for LAFODIS160	64
3.22	EBNF grammar of the internally developed language for specifying exposure functions	66
3.23	HalfSharpFn2.fn	69
3.24	Visualization of HalfSharpFn2.fn	70
3.25	Half Mask	70
3.26	Rendered Frame	70
3.27	FeatureExtraction.fn	71
3.28	Visualization of FeatureExtraction.fn	71
3.29	Rendered Frame showing exaggerated differences	72
3.30	RampFn2.fn	72
3.31	Visualization of RampFn2.fn	72

3.32	Vertical Half Mask	73
3.33	Rendered Frame showing the effect of ramp functions	73
4.1	A mockup of a limited UI for re-timing a frame from a scene model . . .	83

LIST OF TABLES

2.1	NetPBM Magic Numbers	4
3.1	Selected properties of cameras used in the ISO-invariance experiments. .	32

Chapter 1 Introduction

This work is, fundamentally, an exploration into a simple question: "What if we stop treating digital cameras like film cameras?"

This idea began as an intrusive thought while working on experiments supporting other imaging research projects, extended into a rather broad and surprisingly abstract inquiry, and has homed in on a series of desirable properties achievable in a digital camera system which are obscured or obstructed by assumptions carried over from film cameras and affordances for feeble computers in the early years of digital imaging. Such a situation is not surprising; permanent photographic processes emerged from several sources in the 1830s, and the first primitive digital image sensors only appear in 1969 [1]. This hundred and forty year interim provided ample time and market penetration for techniques, terminology, and practices to develop and refine into a powerful cultural inertia.

Fundamentally, a digital camera consists of a number photosensitive sensels, an interface for reading out those sensels, and an attached computer system to control the readout and to process and store the resulting data. These sensels and read-out mechanisms may be constructed in a wide variety of ways, but the vast majority of them share a number of properties, and many of those properties are distinct from the behavior of photo-chemical film. First, sensels are relatively independent. While many cameras share one analog-to-digital converter across a section of sensels, digital cameras are not bound by the restriction that the sampling of the entire frame must be simultaneous, as film cameras are. In fact, excluding a small but growing number of global shutter cameras, the majority of cameras do not have precisely correlated global readout. Furthermore, digital cameras do not require that the readout of the sensels be *correlated*; different sections of the sensor/scene may be sampled not only at different times, but with different parameters to suit the brightness, motion, or other scene properties.

The control mechanism also distinguishes modern cameras from their photo-electro-mechanical predecessors. A basic film camera fundamentally has three relatively coarse controls; the sensitivity (film speed) of the installed film, selected from a set of manufacturer options and set long before the time of capture, the shutter speed, and the aperture of the lens. While film cameras picked up various sorts of automation, like several varieties of automatic exposure control, over the decades, the presumption is that those parameters are controlled by a human operator to produce approximately the desired image "through the lens," or automation designed to mimic what a human operator would have done.

Finally, digital cameras do not require that the measurement of incident light and the generation of an image from that sampled data be coupled. In a film camera, those processes are very closely coupled; the photochemical processes in the emulsion at the time of exposure closely bound the resulting image. Some after-the-fact control is possible by manipulating the development process, but the resulting image is largely restricted to relatively small changes effected by relatively blunt instruments like

dodging and burning with hand-cut masks.

1.1 TDCI

Much of this work follows from an earlier, related body of work around the concept of **Time Domain Continuous Imaging** (TDCI). Though a significant body of prior work exists on the TDCI concept, there are a few additions and alterations to the terminology around it I have developed in the current work.

Since the first publications on TDCI [2] in 2014, as in many discussions of camera systems, the process of converting incident light into an image has been referred to as “integration.” This terminology is pleasing for a number of ways; it suggests the mathematical term integration - as in area under a curve - which roughly describes the way in which gathered incident light over a period of time (as determined by the shutter) is converted into an image, modulated by a gain function (colloquially, film speed).

Similarly, much of the current work has taken the approach of viewing TDCI as a variation on a derivative sensing system; that is, a sensor system that records the derivative of the phenomena being sampled rather than directly capturing the values.

Specifically, the TDCI sensors which have been proposed or simulated approximately record the *second* derivative of the incident light - each record is an update to the rate of change of the incident light at a particular sensel. This choice of terminology is substantially less common, but is extremely useful in thinking about the action of various camera-system components.

1.2 New Work

Much of the precursor work for this thesis, and even a significant amount of the work covered here, was in service of developing systems based on “Time Domain Continuous Imaging” (TDCI). Originally, the intention of this thesis was, in essence, to develop a more sophisticated TDCI system, which would use “prosumer” grade cameras for capture, and allow for non-uniform integration of the captured data. As the work has progressed, the ideas have grown rather independent of the TDCI implementation, and the focus has shifted to exploring the capabilities of systems with decoupled sampling and integration, especially focusing on non-uniform integration. There is also a significant amount of content devoted to investigating how and why assumptions held across the vast majority of imaging systems came into being, and have impeded moves toward more flexible timing and exposure models that the rise of digital photography could have enabled. Many of the experiments were conceived with the intention of supporting the development of a TDCI based system, so this work still employs TDCI tooling to construct prototypes, and explores a variety of issues in modifying existing camera systems to support decoupled image synthesis. The focus is firmly on the implementation requirements and possibilities presented by decoupled, non-uniform image synthesis.

Chapter 2 Background

2.1 TDCI

Work on TDCI technology has proceeded for a period of years prior to the initiation of this thesis. The publication record begins in 2014 with “Frameless, Time Domain Continuous Image Capture” at that year’s IS&T/SPIE Electronic Imaging conference [2], which lays down the fundamental approach, and has continued with the development and publication of a series of testbeds, refinements, techniques, and applications.

Much of this work has centered on developing a family of TIK (**T**emporal **I**mage **K**ontainer) file formats, and the software tools to manipulate and convert them.

TIK

TIK is, slightly unfortunately, a dual-use acronym, referring to both the **T**emporal **I**mage from **K**entucky tools, and the **T**emporal **I**mage **K**ontainer format they operate on. This TIK project [3] has been at the center of existing TDCI work. The TIK software and formats create a testbed for performing time domain continuous imaging using conventional still images and/or video captures. The existing TIK tools consist of a set of open-source programs and specifications that allow the generation of noise models, rendering of TDCI streams from series of frames, and the rendering of virtual exposures from existing TDCI streams.

These three functions are performed offline, using recorded images and taking nontrivial time and computational resources to perform the renderings.

TIK file Formats

The TIK formats extend the NetPBM [4] family of image formats. The NetPBM format suite was developed in the mid 1980s by Jef Poskanzer. NetPBM formats include **P**ortable [**B**it — **G**rey — **P**ix] **M**aps, as well as several less-common extensions, such as the PAM (**P**ortable **A**rbitray **M**ap) format, which allows for arbitrary pixel encodings. Each standard NetPBM format type can be encoded in two modes, ASCII, which initially served as a way to safely transmit image data through plaintext-only channels such as email, and now provides a convenient representation for direct manipulation by a human or primitive text-oriented tools, and Binary, which is more compact, and also very convenient to directly manipulate when memory-mapped. The NetPBM formats all begin with an ASCII magic number, the meanings of which are described in 2.1, and support *comments* in the form of lines beginning with #.

The TDCI extensions exploit the comment mechanism in the NetPBM format to generate files which appear as valid NetPBM images to tools expecting them, but contain extra data and metadata for TDCI applications. This enables image

Type	Magic Number		Extension	Colors
	ASCII	Binary		
Portable BitMap	P1	P4	.pbm	0/1 (White/Black)
Portable GrayMap	P2	P5	.pgm	0-255 (Grays)
Portable PixMap	P3	P6	.ppm	0-255 (RGB)

Table 2.1: NetPBM Magic Numbers

previews, appropriate MIME behavior, and other user-friendly features with no additional development effort. Some common tools, such as `ffmpeg` or ImageMagick’s `display` support concatenate NetPBM files, which can be used for automatic support of uncompressed TDCI data. This header format is so flexible that it can be used to prepend appropriate metadata to formats ingested by the TIK tools which are not able to carry their own, such as folders of frames or conventional video files, by including a `.tik` containing only metadata.

The TDCI extensions to NetPBM start with a TDCI version header, which must be the first comment in the NetPBM, of the form:

```
# TIK V version format [parameters]
```

where *version* is an eight-digit ISO-style date representing the date on which the TIK tool, and *format* is which kind of encoding is used in this file, as well as any parameters to that format. Fields are delimited by one or more whitespace (space or tab) characters. For example, a file beginning

```
# TIK V 20160712 RGB
```

would signal a file compliant with the 20160712 version of the TIK specification, containing a normal P6 PPM file, a 0 byte, and a stream of RGB-encoded pixel updates. The 20160812 TIK standard has been published as a part of *TIK: a time domain continuous imaging testbed using conventional still images and video* [3].

In-Camera TDCI

Over the summer of 2016, Katie Long, an undergraduate working with the KAOS research group, developed a first *in camera* implementation of TDCI capture [5]. Her implementation builds on CHDK (the **C**annon **H**ack **D**evelopment **K**it) to encode a TIK stream directly in a consumer digital camera.

This CHDK TIK implementation is necessarily extremely minimal and limited, as the target cameras for this method are, unfortunately, not particularly well suited for TDCI capture, lacking any sort of low-level sensor addressing, nor computationally powerful enough to cover for their deficiencies. The ELPH115 and 160 cameras used for the initial implementation possess only a pair of ARMv5TE processors at about 83 MIPS, and 36MB of RAM, which supports a memory bandwidth of roughly 59Mb/s for writes and 21Mb/s for reads.

These restrictions limit the TIK captures performed with this technique to the live view resolution of the host camera, 720x240 in the case of the original targets. Operating on the live view stream presents a number of difficulties and advantages. As a substantial benefit, it frees up the RAW buffer; the section of main memory used to store full-resolution, full-depth sensor data before it is converted to JPEG and/or written out. The raw buffer is the bulk of main memory in the camera; in the case of the ELPH160, the 20MP sensor at 12bpp consumes roughly 30MB of main memory, leaving only roughly 3MB for user code if it is in use. In terms of disadvantages, other than the obvious extremely restricted resolution, the live view data is delivered at an inconsistent framerate, and the data is delivered in a peculiar packed YUV format which requires decoding, and only provides one U and V value for each group of 4 pixels.

The CHDK TIK capture mechanism is built on top of the motion detect hooks in CHDK, exploiting the similarities between TDCI and various established motion-extraction techniques discussed further in 2.5. The latest 20161130UYVYYY implementation even offers the ability to render frames from specified intervals, albeit in an extremely awkward and limited way, producing images encoded in a format the camera itself is unable to display.

2.2 The Camera

Because much of this work is focused on new modes of operation enabled by digital cameras, and the persistent assumptions that impede their use, it is important to ground the behavior and terminology around camera systems. A camera is comprised of a photosensitive element to record incident light, an optical lens to form an image on the photosensitive element, and a shuttering mechanism to control the exposure of the photosensitive element to the image projected by the lens. Particular cameras can vary widely in how these elements are constructed, and which and how parameters of the system can be manipulated by the end user. Relevant details of the construction of these elements are discussed in this section.

Optics of Lenses

While optical lenses themselves are an area of considerable study, for the purposes of imaging work, a small subset of optics is useful in imaging applications, and specifically toward the proposed work. This focuses on the bulk characterization of optical assemblies - primarily the sort sold as photographic lenses, which are somewhat confoundingly also referred to simply as lenses.

Lenses can be characterized in a variety of ways, most straightforwardly by focal length: the distance between the point of convergence and the sensor plane, measured in millimeters. Longer focal lengths result in a more “zoomed in” image for the same other parameters.

Another basic lens property is “lens speed”; the ratio of the system’s focal length to the diameter of the entrance pupil - essentially, the amount of light admitted by the

lens. Faster lenses represent a relatively larger entrance pupil, and hence admit more light. Lens speed is generally expressed as “ f /numbers” or “ f -stops”, the reciprocal of the relative aperture. This encodes the amount of light admitted into a geometric series of powers of the square root of two.

More formally, optical systems can be characterized by a set of mathematical functions. The image of a point-source passed through an optical system forms the PSF (**P**oint **S**pread **F**unction), essentially the impulse response of the lens. The PSF for a system, or at least a good approximation thereof, is easily obtained by simply imaging an approximate point source with the system in question. Mechanically, an image is the sum of all non-occluded portions of the point spread function, for all points of light in the scene. More easily applicable to imaging is the OTF (**O**ptical **T**ransfer **F**unction), which represents the response of the optical system to sine-wave input; formally, this is the Fourier Transform of the PSF. The OTF is a complex-valued function, but for imaging applications the more convenient real-valued MTF (**M**odulation **T**ransfer **F**unction), formally the absolute value of the OTF, is used, justified by an assumption of (approximate) radial symmetry.

Legacy of Film

Many photographic conventions were set in the pre-digital era, and have been carried into the digital age. Most of these carryover assumptions are reasonable and contribute to the ergonomics of camera use, but many others impede or mislead productive use of modern digital-sensor based cameras. Even years after the transition to more flexible digital sensors, cameras are still designed and operated under assumptions adopted during the film era.

In a film camera, the image is captured by a timed exposure of a surface doped with photosensitive chemicals. The details of the various chemistries used for this purpose are dramatically out-of-scope for this work, a number of the behaviors of this medium, and the parameters used to characterize it, have survived into the digital age. More details of the relevant parameters are detailed below in the discussion of the APEX system.

A number of systems existed for describing the sensitivity of photocemical emulsion film - early systems tended to be specific to a vendor, but eventually standards such as the ASA scale (formally ASA Z38.2.1, later refined into ASA PH2.5 and ANSI PH2.21 for color film) and eventually the ISO 5800 (for color negative film) and related ISO6 and ISO2240 for black-and-white and color negative film respectively. The concept of “film speed” or “ISO” in a digital context is a convenient abstraction for gain, but is chiefly an analogy - a somewhat stretched analogy the rather complicated mathematical details of which are established by ISO 12232 [6] - to allow techniques developed for film exposure to apply to digital cameras.

Another assumption from the pre-computer era which continues to hold sway over camera design is the idea that images, as captured, should be suitable for human consumption. In digital imaging systems, this is often not the case; the consumer of the images is likely to be a computer, which may be programmed to extract specific

information from the image, rather than a human who attempting to interpret the capture. Even if the image is ultimately intended for a human viewer, a large degree of computational post-processing is *mandatory* to convert the digitized, color-mosaic image data into an image a human can view, and the collection of parameters and defects which can readily be manipulated in this rendering process are different and much broader than what could be readily manipulated in a chemical exposure process. This leads to unfortunate choices in optical systems; for example, when designing a system intended to capture text for character recognition, designers may choose a well-corrected lens which makes compromises in terms of sharpness in order to produce a more-pleasing image, while the OCR system would be better served by extremely sharp images with situationally harmless but visually displeasing color fringing.

Without this presumption, it starts to become possible to build different kinds of camera, which are better suited for capturing information about a scene, rather than pleasing images. Pleasing images can then be synthesized after the fact to create the desired image or images, with the ability to manipulate exposure parameters in ways that are traditionally set at time of exposure, or not manipulable at all. Sensors could be placed behind lenses designed to perform specific functions (computations) rather than capturing a perceptual model of the scene. For example, a lens could be designed to project regions of a scene down to a small number of points aligned with the sensels of a very low-resolution sensor. Each sensel can then be read out for changes, resulting in segmented motion detection in the scene without any computational image processing, or even, strictly speaking, imaging.

The most pernicious of these assumptions is that a capture must be a single, uniform integration of the received light across the whole sensor area during a uniform interval. None of the above is true of digital sensors; it is possible and often desirable to expose different sections of a sensor for different intervals, compose an image from multiple samples, integrate after the fact, integrate over different intervals for different parts of the frame, or even weight integration with one or more functions in time over the scene. Occasionally, these assumptions are conditionally violated; HDR (**H**igh **D**ynamic **R**ange) images often use different integration intervals for different parts of the scene, though typically this is performed by taking a sequence of images with different exposure settings and selectively composing them after the fact, rather than by controlling or sampling the sensor in a non-uniform way.

Photographers will sometimes also deviate from simple single-exposure captures of relatively-static images for artistic and/or documentary purposes. Multiple-exposure images were used in early scientific chronophotography to capture motion in a single scene, such as a series of overlaid exposures capturing intervals of an animal's gait. In modern times, a similar effect is sometimes created by after-the-fact layered multiplication of several separate exposures rather than by repeatedly exposing the same photosensitive surface, such that the image remains normally exposed, but changed portions of the image are overlaid, creating a time-lapse effect, and/or allowing the same subject to appear multiple times in the same image. The other common use of multiple-exposure images is for artistic effect; multiple exposures can create translucent portions of images, mask of portions of one exposure by saturating them with another, or other more complicated composition performed by controlling the scenes

and photographic parameters at the time of exposure. Typically, these long or multiple exposure images imposed on a single photosensitive surface are not fully separable after the fact like a series of independently exposed frames or TDCI capture would be, as information is lost by saturation or occlusion.

APEX

The APEX system (**A**dditive system of **P**hotographic **EX**posure), designed in 1960 for use with monochrome film and encoded in ASA PH2.5-1960 [7] is still, with minor modifications, the dominant method for discussing exposure parameters. The APEX system is based on the equation

$$\frac{A^2}{T} = \frac{BS_x}{K}$$

where

- A is the f-number, the reciprocal of the relative aperture.
- T is the exposure time, the 'shutter speed', in seconds.
- B is the average scene luminance, the 'brightness', in foot-lamberts.
- S_x is the photographic sensitivity of the medium, the 'film speed', in the ISO system.
- K is the light-meter calibration constant, in cd/m^2

The full equation is rather complicated for manual field use, both due to arithmetic intensity and behavior which will provide several equivalent sets of parameters any of which may or may not be achievable with any particular camera system. Because of this impractical complexity, some set of simplifications are typically applied in practical applications. One option is to use a mechanical or electronic calculator capable of producing suitable settings with some parameters fixed, as with a particular lens or film speed.

To simplify the arithmetic and range of choices, it is common to collapse the various parameters into a single *exposure value* (E_v) equivalent to the \log_2 of either side of the equation,

$$E_v = \log_2 \frac{A^2}{T} = \log_2 \frac{BS_x}{K}$$

Another simplification, known as the "additive" or "logarithmic" system not only takes the \log_2 of either side, but separates the fractions such that the whole calculation can be performed with addition:

$$E_v = A_v + T_v = B_v + S_v$$

where

- E_v is the exposure value, as above.

- A_v is the aperture value; $A_v = \log_2(A^2)$
- T_v is the time value; $T_v = \log_2(\frac{1}{T})$
- B_v is the speed (or sensitivity) value; $A_v = \log_2(NS_x)$
- S_v is the brightness (or luminance) value; $B_v = \log_2(\frac{B}{NK})$
 - N is a constant which converts between ASA arithmetic film speed (S_x) and speed value (S_v), $2^{-7/4}$ (approximately 0.30)
 - K is the reflected-light meter calibration constant

Photographic systems with computer control, especially digital cameras, the computation is often further simplified into the APEX96 system, which multiplies standard APEX values by 96 to allow exposure calculations to be easily and accurately performed using only integer math.

The Exif [8] system which is used to include metadata in image files uses the APEX values to encode exposure parameters, albeit with occasional marketing-related inaccuracies in certain values, or strange selections of the K and N constants by some versions of the standard and/or manufacturers.

Sensors

Modern cameras almost exclusively capture with analog sensors whose values are digitized. These sensors are comprised of an array of photosensitive cells (sensels) which convert incoming photons into electrical charge, and ADCs (Analog to Digital Converters) which convert the charges imparted to the sensels into digital values. These basic parts are typically accompanied by a variety of filters and other support elements, forming a sensor stack.

On the sensor, each sensel accumulates charge from photon interactions, which ideally accurately samples a scene. A number of effects can interfere with sampling accuracy, particularly in extreme lighting conditions. If the number of photons striking a sensel is extremely high, a sensel may saturate, reaching the maximum amount of charge it can store, thus clipping signal, or even leak charge into adjacent sensels [9]. If the number of photons striking a sensel is extremely low, the sampling can be overwhelmed with noise from the sensor, such as inaccuracies in the charge handling or ADC, or simply *photon shot noise*, the natural statistical variation in emission rate. The existence of photon shot noise requires that many photons be captured to accurately sample the scene, as the variation may otherwise distort the signal.

There are two major ways in which sensors are constructed; CCD (**C**harge **C**oupled **D**evelopers) sensors, and CMOS (**C**omplimentary **M**etal **O**xide **S**emi **C**onductor) devices. CMOS sensors are often referred to as “active pixel” sensors by contrast to CCD’s “passive pixel” mechanisms, though it is possible to build passive-pixel sensors consisting of only a photodiode and selection logic from CMOS technology.

The basic action of a CCD was designed at Bell Labs in the late 1960s, initially for use as a digital memory device [10], but by 1970 had been adapted for imaging applications there, primarily by the work of Michael Francis Tompsett [11].

A CCD sensor is comprised of one or more rows of PN junctions; silicon structures of p or p++ doped silicon, covered by thin layer of n-doped silicon, separated into individual regions. Each of these regions is exposed to light, and acts as a capacitor or charge-well, converting arriving photons into charge via the photoelectric effect. Between each pair of wells sits an electrode contact, separated from the doped layers by an insulating layer of SiO_2 . In order to read the charges collected in each well, the electrodes can be energized in sequence, creating potential wells into which electrons from the un-energized neighboring region will flow, in effect allowing the sensor to be used as an analog shift register. The output of the shift register can then be sampled by a relatively large and sophisticated readout mechanism, in digital sensors this will be an ADC (Analog to Digital Converter) possibly in combination with an amplifier.

Many commercial CCDs use a more sophisticated architectures in order to better suit imaging applications. Some CCD sensors are designed with one set of exposed PN junctions to accumulate charge, and a second set of junctions blocked from receiving light, into which the entire set of sampled charges can be shifted in a single operation. These may be constructed in several ways, such as with a contiguous sensing area and storage area of equal size, or with alternating rows of imaging and storage elements. This latter interline approach allows for faster readouts with fewer transfers but reduces the fill factor to around 50%, making such sensors prone to spatial artifacts or requiring the introduction of microlenses and/or an anti-aliasing filter to redirect the light striking the surface uniformly into the sensitive regions.

CCDs with separate sensing and storage elements offer an advantage in that they can be used without a mechanical shutter, and potentially at very high framerate; the sensor is grounded out, setting the sensor to the dark state, then the exposed junctions are allowed to accumulate charge for an interval. The control electrodes can then be energized to simultaneously shift the entire set of captured charges into the covered row, ending integration.

CCDs have a number of interesting design properties. CCDs are well-suited to ultra high sensitivity applications, as they possess an inherently high quantum efficiency, and the sensels can further be readily modified with features like photo-multipliers in front of the sensing wells, or electron multipliers (essentially avalanche diodes) in the readout path, allowing the reading of charges as small as a single photon. However, CCDs are susceptible ‘spillover’ effects such as blooming or smearing; if some charge wells become saturated, the electrons will shift into neighboring wells, contaminating the sample. Blooming occurs when the charge escapes to neighboring cells in a direction-independent way, while smearing occurs when the excess charge escapes down the lower-resistance shift path, creating bright line artifacts. The act of introducing the control charges heats the sensor, increasing dark current and hence noise. Thus, CCDs must either be operated with a duty-cycle that allows for cooling intervals, or, for greater complexity and expense but improved performance, be actively cooled.

In contrast to the charge wells employed in CCD sensors, each sensel of an active-pixel CMOS sensor is comprised of a photodiode and some number of control transistors to perform functions such as resetting the charge across the junction, and dumping the charge onto a readout bus. To use the photodiode as a sensor, it is first reverse biased to a known potential using a reset transistor, then exposed. Photons striking the photodiode during exposure will *reduce* the charge on the junction, which can then be sampled to read the amount of light at that location.

Many CMOS sensors are more sophisticated, with the addition of specialized structures such as a pinned photodiode which provides separate sensing and readout junctions, with the charge moved between them via a bias applied by an additional transfer transistor. In addition to providing better isolation, pinned photodiode sensors also have improved noise properties because of their correlated double sampling; readings are taken as the *difference* between the freshly-reset readout diode, and the charge on the readout diode after transferring the sense diode's charge onto it, giving a continuously self-referenced calibration. A common way of classifying CMOS sensors is by the number of transistors per sensel; 3T, 4T and 5T sensors are common, with increasing sophistication, usually leading to a lower fill-factor but better noise properties.

There are two partially-independent size factors in sensors; the overall dimension of the entire light-sensitive area, and the area of each sensel in the area. A small sensor with large sensels will necessarily offer low resolution, but otherwise the two factors are relatively independent, and induce different effects on the properties of the captured image.

Larger sensors are obviously physically larger, but also require larger optics to project an image which covers the sensor.

Sensor size is often measured in terms of “crop factor” relative to a “Full Frame” 35mm light-sensitive area of 36mm x 24mm. This convention allows for easier comparison of photographic properties; the effective behavior of a full frame lens attached to a crop sensor body will be multiplied by the crop factor. For example, the common APS-C sensor size of 25.1mm x 16.7mm is said to have a 1.5x crop factor, meaning a 100mm focal length lens for a 35mm camera were attached to a APS-C body, the lens would behave like a $100mm/1.5 = 66.67mm$ lens with the same aperture size. Many cameras and lens systems are marked in 35mm equivalent fields of view (pre-multiplied by the crop factor) rather than actual parameters, which can lead to in comparisons.

Larger sensors will, given the same optics and other parameters, offer a shallower depth of field. This shallower depth of field may be desirable, as in portraits or other tasks with sharply delineated foreground and background, or undesirable, as when capturing landscapes or for gathering the maximum amount of information about the scene.

The measure of resolution itself is more complicated than it first seems. Resolution is, in essence, a measure of the amount of detail in an image. However, resolution can be measured along a number of dimensions (pixel resolution, spatial resolution, tem-

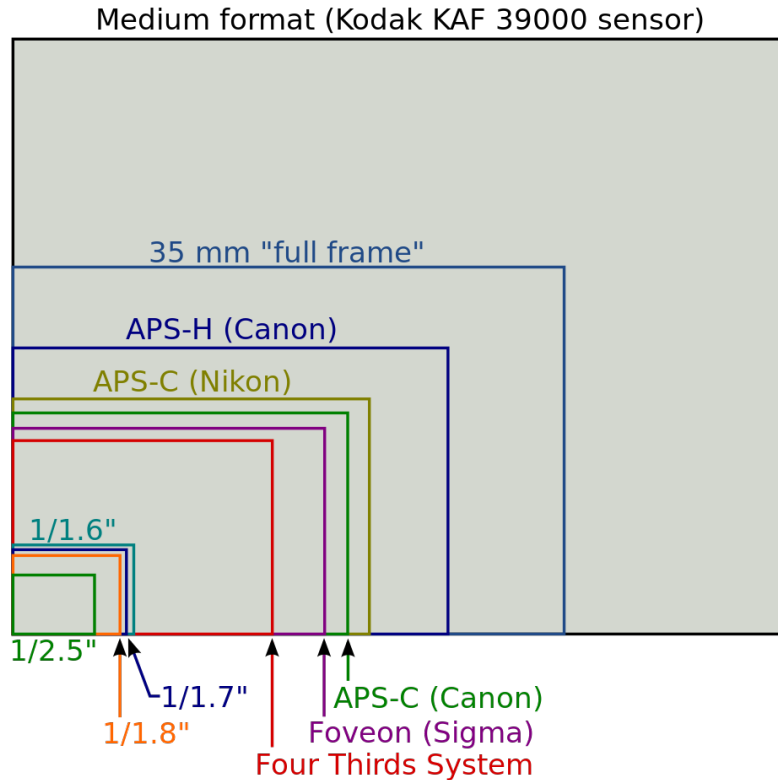


Figure 2.1: Common Sensor Sizes ©Moxfyre/Wikimedia Commons/CC-BY-SA-3.0

poral resolution, spectral resolution, etc.), and the methods for measuring resolutions along those various axes may produce wildly different results.

The most obvious measure of resolution for digital imaging systems is pixel resolution; the total number of individually distinguishable light-sensitive dots on a sensor, usually expressed as “pixels.” Pixel resolutions are typically expressed either in resolution along the X and Y axis (eg. 640x480, 1920x1080), which also encodes information about aspect-ratio, or simply in terms of the total count, usually expressed as megapixels (MP). While manufacturers often market a camera based on the number of megapixels of the sensor, this metric is easily manipulated, ignores optical effects, and generally does not provide a faithful representation of the qualities of the image produced.

Some of the sensitive area of most sensors is not used for image capture; some pixels around the edge are typically kept dark to provide a black reference, some pixels may be excluded from the processed image due to transformations to correct for lens distortion, and some fraction of pixels will typically be “dead” and not contribute to the gathered data. Furthermore, the stack of filter elements between the lens and sensels (discussed below) will cause some pixels to be ganged together, as with anti-aliasing filters that spread a point of light out across several pixels, or in a

color imaging application, the color filters themselves which isolate subsets of pixels to specific narrow frequency bands (colors). In video applications, pixel resolution can be misleading because it is possible not all pixels will be updated in each interval. For example, some encoding schemes *interlace*, updating alternating rows of the image on alternating frames. Pixel resolution can also be deceiving because it is possible to arbitrarily scale digital images with a variety of scaling algorithms which do not add any additional information about the scene (and may create artifacts), but do increase the apparent pixel resolution.

A different method for measuring spatial resolution uses properties of the captured images rather than a characterization of the capture device. For this measure, one determines the smallest features which can be distinguished in a controlled image. The most typical of these measures is line pairs per millimeter (lp/mm); a measure of how many alternating black and white lines can be distinguished at the sensor/film plane. Lp/mm is a very suitable measure for characterizing lenses in isolation, as the test can be performed by simply arranging sample cards with different-density lines and observing the projected image. Unfortunately, lp/mm becomes somewhat ambiguous when used to characterize whole imaging systems, especially digital systems, as the size of the reproduced image will likely be altered from the (possibly unknown) size of the photosensitive element during development in film systems, and will always be altered and resized during reproduction by the display device in the case of digital imaging, making the concept of “per unit length” suspect. Measures of lp/mm in digital systems is further complicated by processing steps in the digital imaging pipeline, which may artificially sharpen or soften the image, experience aliasing at certain spatial frequencies, or otherwise throw the measure. For digital imaging systems, a measure of pixels per inch (ppi) is perhaps the most faithful representation of the informational density of an image. The ppi measure is, in essence, the number of *independent* pixel values per unit length. ppi thus encodes the limiting factor on the spatial resolution across the optical elements, sampling device, and processing pipeline.

Other measures of resolution work along other dimensions. Temporal resolution measures the precision of image measurement with respect to time, corresponding roughly with sample rate in other sensing applications. The most common measure of temporal resolution for video capture is Frames per Second (FPS), roughly the number of full-scene updates per second. FPS does not always accurately represent the temporal resolution with which particular details in a scene can be determined. For example, just as for spatial resolution above, some video encodings may not update the whole frame simultaneously. Temporal resolution is also confounded by exposure times. In the common case for a single capture device, frame rate and exposure time are interrelated - the maximum exposure time is the reciprocal of the frame rate, and exposure times shorter than that imply periods in which no information is collected. This relation is described as *shutter angle*. A shutter angle of 360° says that the shutter is open for the entire inter-frame interval, while a 180° shutter angle has the shutter open only for the first half of each interval. Setting shutter angle

appropriately is a matter of both the imaging devices' sensitivity to light, and the desired effect. An illustration of shutter angle is shown in 2.2.

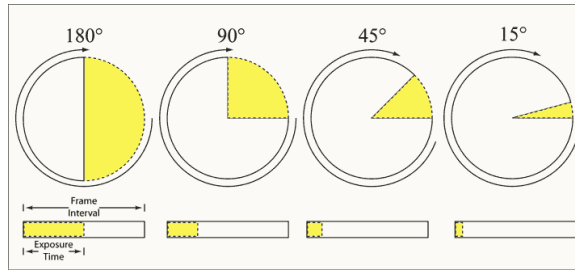


Figure 2.2: The relationship between shutter angle and exposure time. ©Plowboy/lifestyle/Wikimedia Commons/CC-BY-3.0

Some higher-temporal-frequency features may be extracted with lower reliability by analyzing features within a single exposure, most directly through techniques like measuring the spatial dimensions of a motion-blur and dividing by the exposure time. Also like spatial resolution, temporal re-sampling is possible, and unless special efforts are made, can result not only in no additional information, but distracting artifacts. TDCI complicates this measure as the temporal resolution of a TDCI Stream is likely (and preferred) to be non-uniform across the frame, thus defeating many of the uniformity-assuming techniques, and necessitating statistical and/or temporally-integrated measures, which will complicate direct comparisons.

The Sensor Stack

Typical imaging sensors are not just the exposed array of sensels, rather, a collection of protective layers, filters, and optical elements are superimposed on the sensor, forming a *sensor stack*. This stack converts the array of photon detectors into an imaging device, and the design decisions in the construction of the sensor stack substantially affect the properties of the data captured by the sensor. Common sensor stack elements in addition to the sensor itself include a protective layer, various blocking filters, a color filter array, a microlens array, and an antialiasing filter. The specific function of these elements are described in detail in figure 2.3.

The front-most element of most sensor stacks is simply a layer of “clear” glass which acts to protect the other elements of the stack from physical damage. This layer is typically 1-4mm in thickness [12] for commercial cameras.

Another critical layer in the sensor stack are band-pass filters which block or attenuate certain frequency bands of light from reaching the sensels. Infrared blocking filters are included in most visible-light cameras to compensate for the natural sensitivity peak of the Silicon they are constructed from in the near infrared (around 750nm) [13] band. This biases the sensor toward human visible portions of the spectrum, which is desirable in sensors capturing image for human viewing. Sensors in

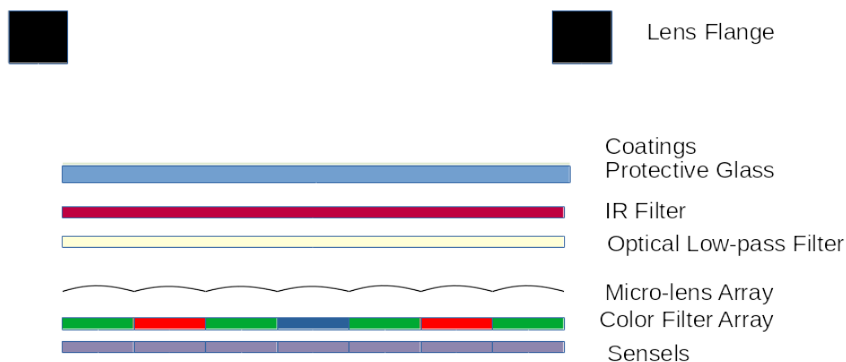


Figure 2.3: A typical sensor stack

applications other than capturing scenes such that the images match human perception, such as astrophotography, low-light imaging (“nightvision”), or in use in FTIR (**F**rustrated **T**otal **I**nternal **R**election) touch surfaces often omit this filter, as the infrared sensitivity is desirable in these applications. Other bands may be excluded according to application, either in the sensor stack or, more often, using removable elements mounted to the lens assembly. For example, UV blocking filters may be added when photographing in bright sunlight to lessen the appearance of fringing due to Ultraviolet light refracting spatially away from the well-corrected visible bands. Clever applications of a variety of band-pass filters in conjunction with image processing techniques are important to Multispectral Imaging.

For color imaging, a color filter array is superimposed over the sensor to allow for separation of color data, and hence capture of color images. Each individual sensel in conventional sensors is only a photon collector; it cannot distinguish colors without external filtering. In most camera sensors, a *Bayer filter* [14, p. 3.2.2] is superimposed over the sensor, consisting of alternating stripes of green/red and green/blue alternating color filters. This pattern is chosen largely on human physiology grounds; human eyes are most sensitive to green light, peaking somewhere around 550nm [15], so favoring green in the color filter array maximizes the capture of detail. A typical bayer pattern is shown in 2.4. Other patterns may be chosen to optimize particular spectral properties; some cameras use various RGBW arrangements in which a standard bayer pattern has some unfiltered sensels interspersed to increase the total amount of light admitted and hence improve overall sensitivity. Similarly, some sensors have been designed with CYYM or CYGM filter arrays filtering for secondary colors in order to, again, increase the total admitted light. Other cameras may have additional filter channels to alter the In many applications, the green channel of a Bayer-filtered sensor is an adequately close approximation of the luminance to be used directly as an approximation. Several well-known image processing tools weight Red 0.3, Green 0.59, and Blue 0.11 by default when performing conversion to grayscale. [16]

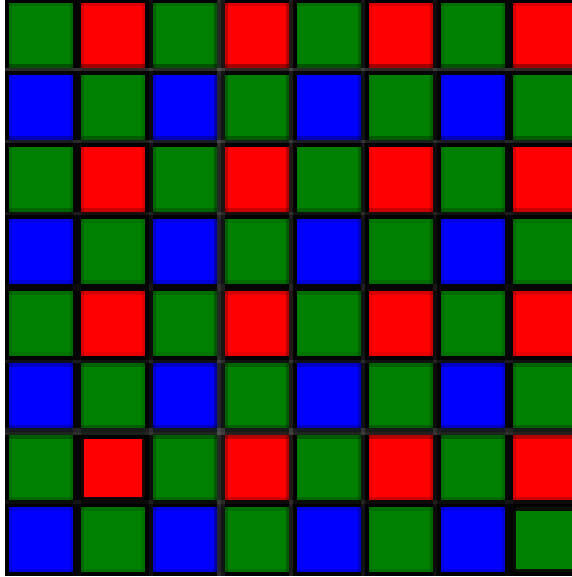


Figure 2.4: Bayer-type CFA pattern

Various *demosaicing* techniques are used to convert the interlaced color information into a full-color image. These techniques will necessarily cause some aliasing, blurring, or other delocalization of color data and/or a dramatic reduction in image resolution. An example extremely simple demosaicing algorithm would simply assign the value from the nearest neighbor sampling a particular channel to that channel in each pixel, which is straightforward to implement but tends to “smear” colors, particularly where there are sharp gradients between regions. Another simple example method would generate single colored pixel from each 2x2 block of sensels, deriving the red channel from the red-filtered sensel, the blue from the blue-filtered sensel, and the green from the two green-filtered sensels. This method is also conceptually straightforward, but rarely used because it cuts the image resolution by a factor of four, and is still prone to color corruption. In most applications, more sophisticated demosaicing algorithms are applied, with a minimum ante of bilinear interpolation, and a tendency toward more scene-aware techniques using pixel correlation or grouping to minimize color smearing.

Demosaicing is known to be a dual-problem with *super-resolution* [17], a term covering any technique that improves the effective resolution of an already-captured image via postprocessing. Early promising experiments for temporal super-resolution [18] with TDCI streams are likely to also yield effective temporal demosaicing techniques.

Most image sensors include an antialiasing filter somewhere in the filter stack. This filter, which is sometimes described as an optical low-pass filter, acts to spread each point of light out over a region of the sensor, allowing for more accurate sampling. The primary need for an antialiasing filter in a camera sensor stack is to prevent moiré patterns; high-frequency repeating patterns in a scene beating with the placement and spacing of sensels in the sensor layer. This spread also helps to compensate for

the fill factor of the sensor in another way; by spreading each point of light, features go undetected by “slipping into” the non-photosensitive regions of the sensor. There is a significant tradeoff in the degree of the antialiasing filter; a too-aggressive AA filter will limit the spatial resolution, visibly blurring the captured image, while a too weak AA filter will still allow certain scene content to produce aliasing artifacts. An ideal antialiasing filter will eliminate all spatial frequencies above the Nyquist frequency of the imaging system, while faithfully passing all below-Nyquist features. Antialiasing filters are typically implemented with several layers of birefringent material [19] inserted into the sensor stack. Birefringent materials have a refractive index which is dependent on the direction and polarization of light, splitting the beam into two spatially separated components. Careful selection and arrangement of several birefringent layers produces a filter which splits an incident beam into a desired number of components; typically four to cover a cell of a color filter array; and whose dispersion distance matches the Nyquist frequency of the underlying sensor. In most practical sensors, the antialiasing filter is implemented in several layers of Quartz or Lithium Niobate [19].

The depth of the optical path in the sensor stack creates a variety of surprising artifacts. These artifacts may compromise image quality in a variety of ways. The physical thickness of the sensor stack begins to have effects even before the light reaches the device. In an increasingly common case, cameras employing an electronic first curtain shutter suffer from gradients in the exposure, as the electronic first curtain is in the film plane, and thus not subject to angular selectivity, while the mechanical second curtain is in front of the film plane, by at least the thickness of the sensor stack and a safety margin, and thus selectively admits off-angle rays. This (and several related) phenomena were documented in a paper I co-authored [20].

Deeper in the sensor stack, in order to compensate for the fill-factor of the sensor and the depth of features above and through the light-sensitive area, the microlens array will attempt to focus light into light-sensitive areas, but irregularities and light leaks in system, as well as intentional cross-contamination from the antialiasing filter, creates contamination and dependency between neighboring sensels. These artifacts may bypass the color filter array, if present, further complicating the contamination. Even lower in the stack, physical structures in the manufacturing of sensels may interfere with neighbors; for example, the partially occluded sensels used for phase-detect auto-focus [21] in many sensors have a metal layer on top of the sensitive area to accomplish the occlusion. In addition to receiving less light than regular sensels, requiring the data from these cells be processed differently or discarded and interpolated over, this metal layer can shade or reflect additional light into neighboring sensels, creating line artifacts.

ADCs

Once incident light has been converted to an electrical charge, those charges must be read out as quantized values. This conversion is done in one or more **Analog to Digital Converters**. Typically, the ADC component in a imaging sensor will include some amplification or other preprocessing, but these can safely be regarded as part of

the conversion process. There are a number of design decisions around the ADCs in a sensor, setting aside implementation details of the ADC itself, which is out-of-scope for this work but well covered elsewhere [22].

Different sensor designs will include different numbers of ADCs; some sensors, especially CCD sensors, may use a single ADC, shifting rows of (analog) charges ‘down’ sensel rows, then ‘across’ a readout row to a single converter. This method is relatively slow, and the extended analog path can introduce noise from the charge transfers, but the use of the same ADC device for each conversion avoids artifacts due to differences between the ADCs, or calibration and post-processing steps to normalize them.

Others sensor designs, typically CMOS sensors, are read out with an ADC per-row or per-column. This configuration allows for much faster readouts, as the conversion process is parallelized, at the cost of considerably more ADC hardware, and a slight loss of consistency as different ADCs may exhibit minor performance variations.

Typical sensors are not designed with per-sensel ADCs, as a matter of cost and complexity, though some of the exotic and/or specialized sensor technologies discussed below may approximate independent per-sensel sampling. For example, designed-for-TDCI sensor would not employ any conventional ADCs, but would detect charge threshold crossings at each individual sensel.

There is another design compromise that arises a consequence of the row or column-oriented readout in the vast majority of sensors, between *rolling* or *global* shutters.

In global shutter mode, the entire frame is read out before any sensels are exposed or allowed to begin integrating. In rolling shutter mode, rows/columns that have already been read out are exposed while the readout process continues, such that each sensel is exposed for the same amount of time, but the exposure intervals are staggered across the frame. Rolling shutter allows for higher frame-rates, and a slight reduction in noise due to analog effects on captured charges at rest, but at the cost of potential distortion. The most severe (and intuitive) of these distortions is that fast moving objects may “smear” in an image captured with a rolling shutter, such that objects moving along the axis of readout will appear elongated or compressed as consecutive intervals sample the object in different positions. Many cameras can be operated in either mode to suit situational needs, or in combination with an external mechanical shutter as in “electronic first curtain”.

A final variation in sensor ADC design that bears mention is that sensors may be constructed with the ADC(s) in the same chip and manufacturing process, or with a separately-constructed ADC, coupled to the sensor at the die or package level. Advantages of on-chip ADC designs include better noise properties, as the length and number of junctions in the analog transmission path increases noise, and a potential cost decrease at volume, as it lowers the numbers of components. Advantages of

off-chip ADC designs include being able to use tailored fabrication processes for each component, and a potential cost savings because it allows the use of commodity ADC components.

Other Sensor Technologies

Quanta image sensor

A competing design for next-generation image sensors provides interesting contrast to the design decisions in TDCI. Eric Fossum’s QIS (**Q**uanta **I**mage **S**ensor) design [23] operates on a basis of photon counting; each QIS sensel (termed “jot” in their writings) is a detector for a single photon over an interval. Each jot in a QIS sensor array is sampled on the order of 1000fps, and provides a single bit of output at each sample, 1 for a photon interaction, or 0 for none, which are then collated into a bit field, representing a frame. A series of bit fields are collected into a three dimensional bit field in (x,y,t) , x and y being the spatial grid of the sensor layout, and t being the time series of samples. Images are synthesized post-capture by sampling into the data, in a process not entirely dissimilar to TDCI. QIS sampling is envisioned as combining along all three axes; pixels are synthesized by combining an (x,y) region of jots summed over an interval. The dimensions of the region and interval can be controlled dynamically, giving desirable options for compression and extended dynamic range which are impractical with conventional sensors, advantages which are shared with TDCI-based imaging.

QIS jots must be much smaller *and more closely spaced* than the diffraction limit of the optical system in front of the sensor, which poses challenges in both fabrication technology and energy density for practical sensors, as compact energy efficient single photon detectors are not yet practically realizable.

QIS differs from TDCI in several key ways. Most importantly, QIS is still frame-based - each QIS sample is an (approximately) simultaneous sample across the whole surface of the sensor while TDCI imaging operates on a series of waveforms updated only when the rate of change for a particular sensel changes. A QIS sensor must, therefore, be able to sustain the data rate of updating the entire sensor capture at the sampling rate. This produces an obvious saturation risk; if the (probable) arrival and detection rate of photons is high relative to the sampling rate, the sensor will saturate, capturing no meaningful scene information.

QIS is also based in a different set of assumptions - where TDCI is based on the premise that image data is a model of a consistent physical scene, sampled by observing light reflected or emitted from it, QIS imaging assumes the arriving light *is* the model of interest.

Combining the two ideas above from a different perspective, TDCI is based on photon arrival *rate*, while QIS is (at least in principle) in photon arrival *count*. To

give an (intentionally oversimplified) example, if a sensel is struck by a single photon between $t = 0$ and $t = 1$, no photons between $t = 1$ and $t = 2$, and two photons between $t = 2$ and $t = 3$, an arrival-rate sensor will regard the value during the interval from $t = 1$ to $t = 2$ as $2/3$. In a count-oriented sensor, the illumination of the point in question during interval $t = 2$ will be considered 0, giving no information about the scene.

Photocell arrays

A possible implementation of a sensor suitable for TDCI, which is sadly outside the scope of the current work, could be constructed from an array of easily fabricated photocells or photo-diodes, with each diode paired with a small computational element. These computing elements could be extremely simple, essentially only needing a few hundreds of transistors per sensel, as proposed in work on Nanocontrollers in the early 2000s [24].

Event Cameras

Event cameras are another recent sensing technology which bears significant similarity to TDCI designs. Like TDCI, event cameras are based on recording only a stream of records for changes in the scene. Unlike TDCI, event cameras' change records are typically only a time, location, and polarity, while TDCI records additionally include a new value - including an initial baseline sample. This lack of a magnitude update (or recorded absolute magnitude) in the update record has several consequences.

First and most problematic is that means an event camera will produce *no* information about static parts of the scene, so no amount of processing will be able to fill in scene features that do not move during the sampling interval without additional out-of-band sensors. Some experimental event cameras have contained a second set of sensels, a second sensor, dual-mode sensels, or other out-of-band system to establish ground truth [25], but this will typically result in problems in the optical path, such as a low fill-factor because the sensels are larger or interspersed, or a complicated optically-degrading beam splitting solution to create two images. More problematically, correlating and integrating the event stream and frame-based capture data is computationally difficult, and, based on recent surveys [25] not even fully solved in general.

Secondly, polarity-only change records (rather obviously) restrict the information in an event; all an update can tell is that that site has changed by more than a threshold.

The particular thresholding configuration may use a fixed threshold level for the sensor, a configurable (by user dictate or feedback) level for the whole sensor, some manner of automatic feedback in individual sensels, or some combination thereof.

Finally, in a problem shared with TDCI systems, event cameras may suffer from saturation. If a large number of changes happen at the same time, event data will be offset or lost as the amount of data being read exceeds the throughput at which records can be stored. This situation would typically be caused by some sort of

correlated change in the scene, trivial examples including things like camera motion or sudden lighting changes. This risk of saturation due to correlated events can be mitigated with techniques such as flicker filters (to eliminate predictable, periodic lighting changes, such as power-line-frequency sinusoids), or more sophisticated scene modelling to describe changes correlated due to camera motion or similar systematic behavior in a higher-level representation.

Philosophically, TDCI and event cameras are rather different approaches - TDCI is largely inspired by designing to suit the readily realizable apparatus of cameras and computers, while event cameras are Neuromorphic in inspiration, and tilt their designs toward similarity to biological vision. This does, interestingly, mean that some research directions explored for event cameras and regarded as “less favorable” for neuromorphic work provide interesting information for TDCI work, like some event cameras designed to provide PPM or PWM magnitude representations in [26].

The current primary player in event cameras is inivAktion AG, formed by researchers at ETH Zurich and the University of Zurich who piloted many of the technologies. InivAktion’s DVS (“Dynamic Vision Sensor”) products represent the commercial state of the art for event camera systems, and provide a good baseline for comparison. In particular, their state-of-the-art commercial product, the DAVIS346 produces a 346x260 grayscale event record, saturates at approximately 12M events per second, and costs 6600CHF (approx \$6687 US at time of writing).

Light Field Cameras

Another family of cameras which allow for a significant degree of manipulation of photographic parameters after the fact are light field (or plenoptic) cameras [27]. Unlike conventional cameras, light field cameras attempt to measure not just the magnitude (intensity) and perhaps wavelength (color) of recorded incident light, but a vector quantity also encoding the direction of the incident light. This is desirable because it allows for the depth of scene features to be reconstructed after the fact either to generate 3D images, or to allow optical or computational adjustment of the focus and depth of focus within a range determined by the optical system in conventional images rendered from the recording.

Broadly, Light Field photography is accomplished by imposing a 2D array of micro-lenses somewhere in the optical stack of a camera - typically between the main lens and photosensitive element - to project an array of micro-images. The “Integral photography” name derives from the fact that that conventional images are rendered from the gathered light field by summing - in modern systems computationally, though early experiments used lens arrays to do so optically - the contribution from the same relative position in the set of micro-images to render a final image.

There are significant disadvantages to light field cameras - the largest being that the resolution of output images is roughly - and with differences between implementations - bounded by the number of micro-lenses in the capture device. There is also a substantial computational requirement to render output images, a user interface problem in designing tools by which an operator can set the range of focus, and the final focus and depth of field of the output image. Also like the work proposed in

this thesis, this is a set of problems which is considerably outside conventional image processing software tools and conventional photographic practices and intuition, which creates a substantial barrier to entry for making a consumer-facing device.

Light field imaging has considerable historical pedigree, going as far back as 1908 when the concept was proposed by Gabriel Lippmann - best known for his work on color photography based on interference which earned him the the 1908 Nobel Prize in Physics - under the name “Integral photography” in the same year. Lippmann’s proposal predated the technology to fabricate micro lens arrays (also sometimes termed “lenticular screens”) for several decades, though early implementations began to appear by the 1920s. Once the technology to mechanically construct large, extremely well matched, and very precisely offset lens arrays to render images from the gathered light field is available, it is possible to impose a matching set of lens arrays in a camera and on a print to produce novelty lenticular prints which appear 3D as the viewer’s perspective through the lens array shifts. Later, digital cameras and computer technology allowed the rendering process to be computational rather than optical. Critically, in 1992, Adelson and Wang described a mechanically and computationally tractable design for a light field camera from which depth information can be automatically derived by computationally analyzing the correspondence between the micro images[28]. Reversing the depth estimation process - that is altering the stride by which an output image is summed from the micro images - allows for the focus and depth of field of the output to be altered after exposure, in much the same way the work in this thesis proposes to do for time and gain.

The most visible modern commercial implementation of light-field imaging technology was from Lytro, a company founded in 2006 by Yi-Ren Ng to commercialize light-field camera work from his PhD work at Stanford [29]. Lytro operated until 2018, and produced two models of consumer light field camera **illum** as well as the software to manipulate their captures during that time. A decade and \$140 Million of investor money later [30], Lytro produced the Illum, a \$1,500 one-trick-pony tech demo where both the device and rendering software were brittle, buggy, and slow, and the target audience of trained photographers who might buy such a device were frustrated by the required changes in practice for composition and processing and underwhelmed by the quality of the resulting images **illum**. Of note, such a large fraction of the Lytro staff were hired by Google when the company shut down that there were (later proven false) rumors of an acquisition [30] - likely but not verifiably to work on the computational artificial depth of field features that appeared in Android camera software around the same time. A few scientific imaging companies, most prominently Raytrix GmbH [31], have been offering plenoptic cameras and proprietary software for rendering images and 3D reconstructions from their streams for a more limited, less photographically inclined audience before and after Lytro’s brief presence on the market.

2.3 Camera Pipeline

A typical digital camera contains a small computer, which controls the user interface, camera functions and parameters, storage management, and basic image processing.

This computer will govern both photographic tasks, such as auto-focus, mechanical stabilization, and metering; and digital transformations, such as demosaicing, encoding into output formats, and potentially more sophisticated transformations including correction for dead pixels, black levels, or even lens distortion. In-body correction for lens artifacts is most common in fixed-lens cameras, but may also be performed by interchangeable lens cameras using data stored in a ROM in the lens. The integration of these controls into a single device also enables a variety of higher-level features, such as automatically focusing on detected faces, automatically shooting suitably-bracketed bursts to process into HDR images, and a wide variety of other convinces.

This computer is likely a System-on-chip design, integrating a processor, dedicated image-processing hardware, and I/O controllers for storage and user interface hardware. In the modern era the host processor is typically one or more licensed ARM processor cores. Many camera vendors have long-term ASIC families for these on-board computers, such as Canon’s DIGIC, Sony’s BIONZ, or Nikon’s EXPEED lines. Most vendors also have long-running operating system families shared along their camera line; Canon ran a system built on top of VxWorks until around 2007, and subsequently switched to an in-house operating system known as DRYOS [32], while Sony runs a Linux-based stack [33].

RAW Image capture

Many cameras have an option to capture sensor data with a minimum of processing. This is a typical feature in “professional” cameras, and is often easily added to other models via software hacks [32]. Primarily, RAW capture avoids the lossy compression methods, such as JPEG (described elsewhere), which will remove some information from the capture, and may cause artifacts. Secondly, raw captures will lack many of the processing steps normally performed in-body; typically, the image will still have the color filter array pattern un-interpolated giving a “mosaiced” view, contain regions of the sensor not typically included in output images such as unlit black-reference areas, and lack any automated lens or sensor correction, etc. Skipping the automatic execution of these steps in the camera body allows the photographer, or a later editor, to manually control the details of the process, apply more computationally-intensive methods, or extract information which might be lost during conventional processing.

A major issue with RAW capture is that RAW formats are not well standardized; because there is very little processing, most cameras have unique or near-unique output, and require a suitable RAW conversion tool to access the generated files. Many commercial image-manipulation tools have support for a wide but not exhaustive selection of camera RAW formats, and Dave Coffins `dcraw` [34] utility aims to offer an open-source decoder for a nearly exhaustive selection of cameras.

There are also semi-RAW formats, such as Adobe’s DNG (**D**igital **N**egative) format, an open lossless container format which bundles a set of metadata for interpreting the data, based on the TIFF image format, which is itself a specialization of the EXIF metadata standard [8], and under consideration for ISO standardization.

Few cameras directly export DNG files, though many vendor-specific RAW formats are also based on TIFF.

Compression

Most digital cameras default output format is, in contrast to the RAW image data described above, a compressed, post-processed, image provided with metadata in a standardized format. The vast majority of cameras use the JPEG lossy compression method, and subsequently export images in exif format [8], giving an interchange format which bundles the compressed image data with metadata. JPEG compression is based on a number of human-perception optimizations, whose broad strokes are interesting as examples, but whose exact algorithmic details, choice of constants and methods in the color mapping step, basis functions, etc. are specified by a number of mutually-incompatible standards, and not particularly relevant to the project at hand.

JPEG compression is performed in a YCbCr color space, which represents colors as luminance (Y) and Cb and Cr color components, which are the blue and red differences from the luma. This expression is useful for compression as it easily allows the prioritization of luminance (discarding of color) data, more or less corresponding to human perceptual sensitivity. JPEG compression also splits each resulting data component into 8x8 blocks, which are converted into a frequency-domain representation via a discrete cosine transform, which essentially transforms the block into a linear combination of 64 basis functions. This representation can then be quantized, by dividing each coefficient by a constant (typically a different constant for each component) then rounded, which, since we are operating in the frequency domain, essentially removes the high-frequency components to which humans are least sensitive. This quantization step is the only one which is necessarily lossy, though in practice several of the other steps are likely to lose information due to limitations of the implementation of the arithmetic. The resulting simplified coefficients are then (losslessly) entropy encoded, typically via a mixture of run-length and Huffman encoding.

In addition to the desirable effect of providing an interchange format, and compression typically in the vicinity of 10-20:1, a number of undesirable things happen as a result of JPEG compression. Since the compression is based largely on the elimination of high-frequency data and color information, these are the places where JPEG compression will be most visible. In particular, JPEG-compressed images are prone to artifacts around high-contrast edges due to the approximation of intensity transitions via combinations of smooth functions, an introduced "blocky" appearance in smoothly-shaded areas of the image where adjacent 8x8 blocks' processing produce different results, and a general loss of detailed color information. Because there are a number of different standards and implementations for JPEG compression and file encoding, there are also a variety of opportunities for errors to be introduced during

decoding via improper choice of methods or constants.

2.4 Scene Model

Image capture techniques can be split along a number of conceptual axes. One fundamental distinction among imaging techniques is separated by whether the objective of imaging is conceptualized as recording photons or or creating a scene model.

In a photon-recording model, the objective is to faithfully record the light arriving at the sensor during an interval. This view is appealing in several ways; it is analogous to film, conceptually simple, and requires minimal computational resources. It also has several serious problems, the most fundamental of which have to do with the properties of light itself. The particle nature of light causes photon shot noise (Also sometimes called “photon noise” or “Poisson noise”); a statistical uncertainty [35].

Photon shot noise is worthy of more detailed explanation, as it is Central to the justification for non-photon-recording sensing; the number of photons N measured by a sensel over time t sampling a scene illuminated such that λt is the expected incident photon count is given by the discrete probability distribution

$$Pr(N = k) = \frac{e^{-\lambda t} (\lambda t)^k}{k!}$$

, a standard Poisson distribution. Being a standard Poisson distribution, its variance is equal to its expected value, $E[N] = var[N] = \lambda t$; or more usefully, shot noise (the standard deviation of the signal) grows with the square root of the sampled signal.

Another weakness of photon-recording is that of lighting/color corruption. The lighting in the scene may interfere with the sampling of the scene. Low or narrow-band lighting in particular can easily cause incorrect representation . In the simplest example, a surface which primarily reflects red light, such as a brick, in as scene lit entirely with blue light will most likely appear black in a conventional image, as none of the available light will be reflected from the surface to the sensor. A human observer is likely to recognize the brick remains red, particularly if the scene lighting is varying, due to their expectation of scene and color constancy. The issue of the relationship between color and light discussed further elsewhere in this document, in subsection 2.4.

In contrast, if the objective of image capture is conceived as capturing an accurate model of the scene, a different set of design choices are selected. In the scene-modeling view, arriving photons are viewed as unreliable, stochastic samples of scene properties. Successive samples are used to refine a model of the scene; an area with very few incident photons can be sampled over several intervals to obtain data that trends over the noise level. An area which is saturated during one interval still has information in the scene model from previous samples. TDCI falls firmly into the ‘scene model’

family.

A different framing which turns out to result in nearly the same division is whether the sensor is interpreted as measuring photonic arrival *rate* or photonic arrival *count*. This is an important but somewhat subtle point about quantizing photonic arrival energy at sensels. Traditionally, the charges stored in the sensels are interpreted as photon arrival *counts*; the charge accumulated in a sensel during the sampling interval is directly interpreted as the desired output. This provides a film-analog behavior. In digital sensors, it is also possible to interpret photonic arrival in terms of photonic arrival *rates*; the charge accumulated in a sensel for any given interval informs not only the instantaneous value of that sensel, but also the rate-of-change of that value. This rate-based view requires that multiple samples be considered, and leads to other consideration of multiple samples; averages over many samples can be used to derive information in areas where the instantaneous arrival rates are below the noise level. These multi-sample considerations encode an assumption of scene consistency, and lead to essentially the same behaviors as the scene modelling approach above.

Lighting Model and Scene Appearance

The notion of colors as specific frequencies/wavelengths of light does not correspond precisely to human vision. A human viewers' perception of colors is surprisingly subjective, owing to both the physical mechanism by which human eyes sense light, and . Human eyes contain a number of light sensitive cone cells, in three varieties whose sensitivities have respective center frequencies of approximately 420 ("blue"), 530 ("green"), and 560 ("red")nm wavelength [15]. The output signals from these cone cells are then differentiated by opponent process cells, which also come in three varieties; luminance opponent cells, which are stimulated by all three cone cell outputs, C_g opponent cells, which are stimulated by red and blue cone responses and inhibited by green cone responses, giving red-green discrimination, and C_b opponent cells, which are stimulated by red and green cone responses, and inhibited by blue cone responses, giving blue-yellow discrimination.

This subjectivity carries useful advantages and disadvantages, mostly based on the concept of *color constancy*; a viewer's ability to recognize an object maintains its color despite changes in lighting which can alter the wavelength or quantity of reflected light. One such consequence is Metamerism; colors which can be situationally perceived as the same, despite containing dissimilar spectral power distributions. Metamerism is critical to color reproduction; for any given stimulus, a perceptually identical color can be generated by mixing different intensities of three RGB primary-colored light sources, allowing for compact sampling, representation, and reproduction of a large gamut with a simple three-color representation.

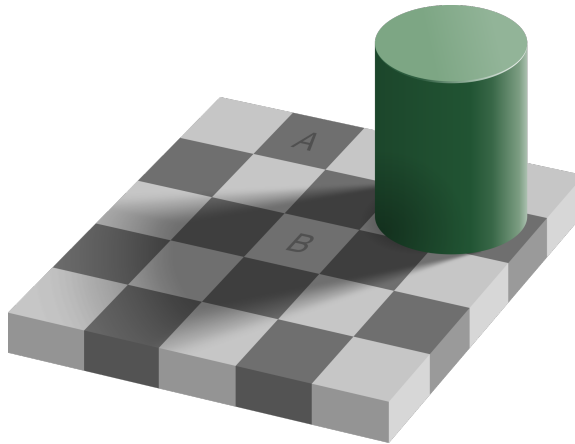


Figure 2.5: Adelson Checkerboard Illusion: Square A is exactly the same shade of grey as square B. ©Pbroks13 /Wikimedia Commons/CC-BY-4.0

2.5 Image Processing and Compression

TDCI technology shares a variety of assumptions and techniques with existing image and video processing techniques. This section discusses a number of adjacent technologies, and their relationship with the concepts and methods of the TDCI approach. Many of these technologies' commonalities are based in their shared notions of scene consistency.

Motion Segmentation

In many computer imaging techniques rely on motion segmentation - the interpretation of sequential scene data into features and trajectories. Motion segmentation is used both for image processing - extracting scene data from images - and video compression - eliminating duplicate information from series of images. The typical form of motion segmentation is *rigid* motion segmentation, the decomposition of a scene into a set of regions or features, and the trajectories of their motion.

Rigid motion segmentation can be implemented in a wide variety of methods, from simple differencing of sequential frames, through statistical classification techniques, wavelet-based methods which distinguish features by scale and frequency, layering techniques, and a variety of other mathematical models. Optical flow, detailed below to provide specific examples, can be used as a form of rigid motion segmentation, typically one which is primarily concerned with the motion extraction function.

Optical Flow

Optical Flow [36] is the study of the apparent motion of objects in a scene, caused by the relative motion of the observer and scene. Optical flow is rooted in psychological, now more trendily referred to as neuromorphic, models to describe motion-sensitive

vision in animals by James J. Gibson in the 1940s [37]. After the advent of computer imaging, the optical flow view has become important in its own right, as it allows computers to make inferences about captured image data in ways that are consistent with the physical scene and/or a human observer of the data.

Like the TDCI model, the optical-flow view is deeply rooted in an assumption of scene consistency, and the idea that the sensor is forming a scene model rather than directly capturing reality. For optical flow to be sensible, much less useful, scenes must be comprised of consistent elements, which can be recognized, moving slowly enough that their motion from frame to frame can be computed.

Optical flow can be computed with a large and growing variety of techniques, descending from a wide variety of fundamental approaches including scene differencing, structure matching and tracking, energy or phase models [36]. Many of these techniques extremely well-established, and have been mainstay image processing primitives for decades.

Optical flow is closely related to motion estimation and video compression. In vision-like applications, computing scene and/or camera motion is often the desired data, and other sensing is largely irrelevant. In video compression, optical flow processing is valuable for allowing storage to be traded for computation; it is much smaller to represent a series of frames as a combination of scene elements, some moving along mathematically encoded paths, rather than a series of separately encoded images. These two uses, though rooted in the same mathematical techniques, differ in one crucial aspect; in compression applications it does not matter whether the camera or objects in the scene are moving, while in vision applications distinguishing the two is both desirable and, unfortunately, typically unknowable.

Some sensors are designed specifically for optical flow imaging. By far the most prolific example of such a device is the sensor used in typical optical computer mice. These mouse sensors are extremely low resolution, low depth, but extremely fast downward-facing cameras, coupled with stark controlled lighting, to enable a simple optical flow computation to generate a series of Cartesian offsets, replacing the continuous rotary encoders found in mechanical mice.

TDCI encoding may enable new, convenient optical flow computation techniques owing to the inherent encoding of per pixel time-difference data. Unfortunately the TIK image format family currently in use does not localize this data in ways that obviously lend themselves to inexpensive optical flow calculations.

Another consistency assumption made in many imaging and sensing applications is that the scene brightness will remain more or less constant for periods much longer than the sampling period. The rise of pulse-width modulation (PWM) controlled LED lighting causes a minor problem for systems that depend on this assumption of brightness consistency, including TDCI. Many modern LED-based lighting systems are controlled by PWM(**P**ulse **W**idth **M**odulation), which produces light-dark cy-

cles at frequencies in the 100-1000Hz range, or with waveforms which are not simple sinusoids or even square waves. As an example, a waveform obtained from a green LED used as a sensor by connecting it across the inputs of a suitably biased Microchip MCP6002 Operational Amplifier, read out with the integrated Oscilloscope of a Digilent Electronics Explorer is shown in figure 2.6, illustrating the waveform of a TaoTronics TT-DL27 LED desk lamp with controllable brightness and color temperature set to an “intermediate” brightness.

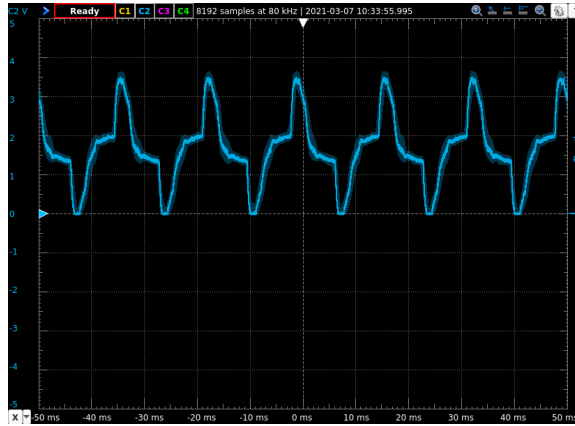


Figure 2.6: Waveform captured from an LED desk-lamp set to less than full brightness. The frequency is around 60Hz, but the shape is decidedly not sinusoidal.

Fortunately, these flickers are imperceptible to humans due to persistence of vision, appearing as the average value of the lighting, so capturing this flickering is not generally desirable in imaging systems. Unfortunately, whether or not they are a feature of interest, large instantaneous scene lighting changes which, unless expressly detected and discarded, can beat with the sampling frequency and/or dramatically explode the size and frequency of scene-change records in imaging systems. Just as many modern video cameras have flicker elimination settings (sometimes auto-ranging, sometimes specific “50Hz” and “60Hz” settings) for eliminating power-line frequency flicker in various regions as exhibited by florescent lighting, a robust capture system system that samples continuously rather than in a frame-oriented manner will require at least some degree of compensation for these phenomena. The most likely candidate is building a model of the lighting so the data rate does not balloon because the periodic change is accounted for in the encoding. With multiple sources operating at potentially a range of frequencies and waveforms, that may be considerably computationally expensive. A series of brief experiments connecting LEDs with different peak sensitivities to a MCP-6002 Operational Amplifier to observe the waveform of the incident light produced by various common light sources were undertaken, but didn’t reveal any patterns worthy of detailed discussion.

It would also be desirable that a capture device be able to model camera movement relative to the scene, maintaining the scene model as constant and compensating for the camera motion. Embedding a motion sensor - as is already commonly done many cameras for for orientation detection, for stabilization, etc. - allows a certain

amount of automation. Existing optical flow techniques also provide potential options for detecting and compensating for camera motion, but they may or may not be tractable for real-time, in-camera capture, as in-camera compute resources are frequently limited.

Poisson Image Editing

One of the underpinning assumptions that makes TDCI practical is the notion of scene constancy. Scene constancy is the notion that the space- and time- rates of change in a scene will be slow relative to the timescale and field of view of the image capture. This constancy is already exploited in a number of widely-used techniques. Elsewhere in this document I have discussed the utility of this tendency for video compression, it is also useful for seamless editing. Poisson image editing [38] is a well-established family of image processing techniques which operate based on similar assertions of scene constancy. Poisson editing is somewhat mathematically absurd but readily intuitively motivate-able. Essentially, this process is to guarantee slow, human-imperceptible gradients in intensity [39] on the edges of features, while setting the interior of a region to a specific desired appearance. In the originator’s own words, this is accomplished with “Poisson partial differential equation with Dirichlet boundary conditions which specifies the Laplacian of an unknown function over the domain of interest, along with the unknown function values over the boundary of the domain.” Fortunately, when discretized (which is the only relevant case) this process reduces to a reasonably manageable quadratic optimization problem.

Chapter 3 Experiments

A number of experiments have been undertaken aiming to explore ways in which modern digital cameras diverge from the abstractions and assumptions under which they are typically operated, and about ways in which those properties can be leveraged to enhance their capabilities. Many of these experiments were published as papers, but collectively they suggest a possibility of re-conceptualizing the use of digital cameras in a way that would allow users to better leverage the properties of the cameras. In particular, changes to the software stack and user interface should allow users to manipulate parameters traditionally considered set at the time the picture is taken post-capture, repeatedly, and with finer granularity than traditional photographic technique.

3.1 ISOLess

One of the motivations for this work, and the TDCI effort in general, is the observation that many digital cameras appear to be “ISO-Less” (or, more formally, “ISO Invariant”) - that is the user-set “film speed” or ISO setting on the camera is partly or entirely implemented as digital gain in the processing pipeline, rather than a change to the gain of the sensor itself. Much of the information about ISO-invariance, especially prior to 2015 when the experiment discussed in this section was performed - came from hobbyist and enthusiast quarters, which tends to be regarded as unreliable in academic circles. This is despite the fact that information from stable pseudonyms on the internet is generally highly reliable, and who has spent a significant amount of time interacting with academic output is acutely aware that results published in academic venues should be considered inflated and untrustworthy until independently verified, as authors respond to the many incentives to hype questionable output. So, the experiment which began my involvement in serious imaging research was working on devising and conducting a series of experiments to determine the degree of ISO-Less behavior in a range of consumer digital cameras.

In this series of experiments, 19 different cameras capable of RAW capture released by Canon, Fuji, and Sony between 2000 and 2014 were tested to determine how ISO-invariant their capture behavior actually is. The spread of cameras tested is described in table 3.1 and pictured in 3.1. These cameras represent quite a wide spectrum; 11 are CCD based while 8 use CMOS sensors. They operate on RAW formats from 10-14BPP, with minimum claimed ISOs from 50-100 and maximums from 400-25600. Their processing pipelines come from different generations and different vendors.

To create an even fairer test, in a subset of cameras where it is reasonably straightforward to do so, images were exposed, digitally boosted, and processed by the same in-camera pipeline as the native-ISO exposures. In the CHDK-enabled Canons, the lua scripting interfaces in [32] expose the controls for the image processing pipeline. These facilities include functions to load a RAW into the in-camera JPEG engine



Figure 3.1: The spread of cameras used in ISO Invariance Experiments

Camera	Model	Year	Prog	Sensor MP	Min ISO	Max ISO	BPP
Canon G1	2000		CCD	3	50	400	10
Sony F828	2004		CCD	8	64	800	14
Canon A620	2005	CHDK	CCD	7	50	400	10
Canon A640	2006	CHDK	CCD	10	80	800	10
Sony A100	2006		CCD	10	100	1600	12
Canon A590	2008	CHDK	CCD	8	80	1600	10
Canon SD770	2008	CHDK	CCD	10	80	1600	12
Sony A350	2008		CCD	14	100	3200	12
Canon A480	2009	CHDK	CCD	10	80	1600	12
Sony SLT-A55	2010		CMOS	16	100	12800	12
Sony NEX-5	2010		CMOS	14	200	12800	12
Fuji X10	2011		CMOS	12	100	3200	12
Sony NEX-7	2011		CMOS	24	100	16000	12
Canon A4000	2012	CHDK	CCD	16	100	1600	12
Canon EOS-M	2012	ML	CMOS	18	100	12800	14
Canon ELPH115	2013	CHDK	CCD	16	100	1600	12
Canon N	2013	CHDK	CMOS	12	80	6400	12
Sony A7	2013		CMOS	24	50	25600	14
Sony A7 II	2014		CMOS	24	50	25600	14

Table 3.1: Selected properties of cameras used in the ISO-invariance experiments.

with control of the parameters, and a facility for adding or averaging RAW frames, which are all that is required for the experiment. To generate the test sets, exposures were taken at the base ISO, multiplied by successive addition, eg. $i=i+i$; $i=i+i$; $i=i+i$; $i=i+i$; to digitally boost by a factor of 16, then run through the in-camera JPEG encoding pipeline with the parameters set as though it was set to ISO1600. A series of crops from an exposure processed in this manner are shown in figure 3.2.

The left-most image is from a native, suitably-exposed ISO1600 exposure, the middle frame is from an exposure shot with all other settings held constant but the gain reduced to ISO100 then the RAW frame multiplied by 16 and rendered through the camera's JPEG engine, and the third crop is the second with a simple de-noise filter applied. The most interesting observation is that the boosted ISO100 image appears to preserve more detail than the native ISO1600 image, but with considerably more noise. If a simple denoise filter is applied, as in the third sample, most of the additional detail is preserved while the majority of noise is eliminated, leaving a image that is not only equivalent to but by most measures superior to the native ISO1600 exposure.



Figure 3.2: JPEG Crops from Canon A4000 at ISO 1600, 16x ISO 100, and 16x ISO 100 Filtered

In a digital sensor, the Sv term in the APEX formula should really be split; $Sv = Sv_{analog} + Sv_{digital}$, where Sv_{analog} is a coarse control set at time of exposure by altering the analog gain of the sensels and/or ADC used for readout, and $Sv_{digital}$ is a fine control applied computationally during processing. Traditional exposure and integration are commingled, but to reiterate the point, in a TDCI-type system, they are separated, and the integration step is manipulable in post-processing.

Conceptually, this work exposes that the ISO film-speed analogy is a crutch for simplifying the computations required to generate a good exposure into something a human operator can do on-the-fly, and in particular was designed around traditional sensitized-emulsion with a fixed sensitivity. The typical formula used to determine exposure from ISO film APEX system, described in section 2.2, or one of its integer-math-friendly variants. APEX is an effective way to generate desired exposure for a particular level of incident light, but is effectively a point computation; in scenes with significant dynamic range, exposing according to APEX requires that the user select the light level at a particular point in the scene or average of an area for correct exposure, and tolerate poor exposure elsewhere - or cover it up later with stitching or manipulation in post-processing.

Some cameras do have controls exposed to manipulate Sv_{analog} at a spatial granularity smaller than the whole sensor at least to a limited degree. In particular, many Canon DSLR models operate on a line-oriented readout, and hackers have determined

that the register controlling the analog gain can be altered between line readouts - as in [40] - sacrificing vertical resolution for extended dynamic range. The fact that this method for HDR imaging is effective further demonstrates that the frame-at-a-time APEX style exposure computation inherited from film does not make effective use of digital image sensors.

Contemplating the implications to exposure practices of this work is the genesis for many of the ideas explored in this thesis.

3.2 Temporal Super-Resolution

By way of brief description, *super resolution* is resolving details smaller than the basic sampling of a system would allow. Typically, super resolution is applied spatially; using techniques on one or more images to distinguish features below the resolution of the sensel size, of the sensor or diffraction limit of the lens, of the noise-floor for the sensor, or other limits of the device used for each capture. A number of well-known techniques have been established going back at least a decade for spatial super-resolution using multiple frames, generally relying on feature alignment and (weighted) averaging and/or confidence modeling, as in [17] and [41]. Temporal super resolution is somewhat less common, and refers to resolving *time* in units smaller than the interval in a capture; typically meaning changes faster than the frame-rate of a video sequence.

Most techniques for temporal super resolution in a typical frame-oriented video system encode a number of assumptions; that the pixel values in each frame are correct, and that most changes in frame content are the result of changes in the scene rather than in the lighting or capture system (“scene constancy”, once again).

In 2019 I was a co-author on a side project investigating the potential for TDCI methods to allow for Temporal Super-Resolution. This culminated in a paper entitled “Temporal super-resolution for time domain continuous imaging” [42] presented at Electronic Imaging in 2019. My involvement in this paper was relatively minor, but a few of the lessons from the work turn out to be important to the focus of this thesis, so it bears discussion.

The methods proposed in this paper operate on a TDCI stream, which already attempts to model an approximation to a continuous waveform of incident light. This slightly changes the problem from the frame-oriented case, but is still fundamentally an exercise in applying knowledge of the capture system and recognition of likely scene properties to model the likely behavior of the incident light. The relevant properties of the capture device include timing artifacts from the shuttering mechanism which generally skew the exact interval over which parts of the frame are captured in a predictable way, a further exploration of which is discussed in the next section.

3.3 Shutter Artifacts

A small related project culminating in a poster at EI2019 explored a number of shuttering artifacts. This paper studied the artifacts created by different kinds of

shutters: vignetting from traditional mechanical shutters not being precisely in-plane and having transit times, and non-global electronic shutters' various sorts of temporal and spatial de-synchronization. Some material from this work is integrated into this document in the front matter in subsection 2.2, the full paper is in [20].



Figure 3.3: A picture of a spinning fan captured by a Sony A7RII under different shuttering modes. Insets show the banding pattern induced by the non-DC lighting interacting with the electronic shutter.

This work was largely ancillary to the TDCI work, but is relevant in that it was making a close study of the timing behavior of widely-used shuttering mechanisms, an understanding of which is required to properly integrate sensor data into an accurate representation of the scene. It also serves as a further justification for TDCI-style decoupling of capture and integration; constructing a model of the incident light at each point from the available data allows many of these artifacts to be computationally avoided - or conversely, to be synthesized to create the appearance of specific historical capture devices.

A specific set of phenomena investigated in this work is illustrated in figure 3.3, showing a 1/8000s exposure from a Sony A7RII pointed at a rotating fan blade, showing both the dislocation of the moving parts of the scene (the distorted fan blades in the third image), and, magnified in the inset, the banding pattern created by the beating of the frequency of the AC light source in the scene and the line-by-line clearing and reading.



Figure 3.4: An image from a Sony A7RII illustrating the effects of the different shutter regimes.

Another less well-known phenomena explored in this work is the artifacts produced by operating cameras in electronic first curtain mode. In this mode, the initial zeroing of the sensor is not accomplished by a mechanical shutter, but by electronically dumping charge from the sensels. The sensor is then allowed to gather light for

the selected interval, and the process is stopped by a mechanical focal-plane shutter, and the result read out. As shown in figure 3.4, the mechanical focal plane shutter creates shading, as it is not exactly in the image plane (allowing off angle light to encroach), not capable of instantaneous acceleration, and its travel is not correlated with the initial clearing.

Furthermore, this work shows that camera users are already interacting with spatially or temporally non-uniform exposures (discussed in a later section). In fact, it exposes several kinds of currently-tolerated non-uniformity: the incident light that creates a rolling shutter effect is obviously not gathered at the same interval for the entire scene, though in an undesirable way not under user control, rather than configured and leveraged to the user’s advantage. These effects are discussed further in the context of desirable non-uniformity.

3.4 Camera Motion

In the introductory discussion about imaging technologies about event cameras, TDCI, and Poisson image editing 2.2, problems due to correlated changes are briefly mentioned. These technologies share a reliance on *scene constancy*: the idea that the contents of the scene are unlikely to change extremely quickly relative to the recording mechanism. For the capture devices, these problems take the form of readout bandwidth saturation due to correlated changes, resulting in lost scene data as the update traffic exceeds the read-out bandwidth. These correlated changes can take several forms, such as sudden changes to scene lighting, or motion of the camera itself. These features also cause problems for conventional frame-oriented capture devices, introducing undesired artifacts like flicker or blur. More sophisticated modeling that incorporates lighting or camera motion can reduce the severity of these problems. As noted in the introductory material, employing some degree of lighting model in the capture device is well established in the form of filtering for line-frequency flicker elimination. More recently, analyzing camera motion in an effort to cancel blur has become common. Many modern digital cameras contain an IMU (Inertial Measurement Unit) tied to a IBIS (In Body Image Stabilization) or OIS (Optical Image Stabilization) mechanism which can move the sensor or lens elements to correct for small amounts of camera motion. The sensors embedded in cameras are not terribly consistent, and the data they generate is not generally stored in a user-accessible way.

Therefore, as a preliminary step to study camera motion, in the summer of 2019 members of the KAOS lab developed a hardware/software system and test protocol to instrument a camera in use, capture detailed motion data synchronized with the exposure along several axes shown in 3.5, and convert the data into forms suitable for study.

This system, with the somewhat tortured name “ShAKY” (SHift Angle Kentucky) includes several hardware and software components. On the hardware side, 3D Printed module which attaches to common cameras via a standard 1/4 – 20 UNC camera mount thread contains an Arduino Pro Micro ATmega32U4 development board, a MPU-9250 9-axis IMU to read motion, and a 3.5mm TRS connector to interface with the flash sync signal of cameras which support it. An Arduino sketch

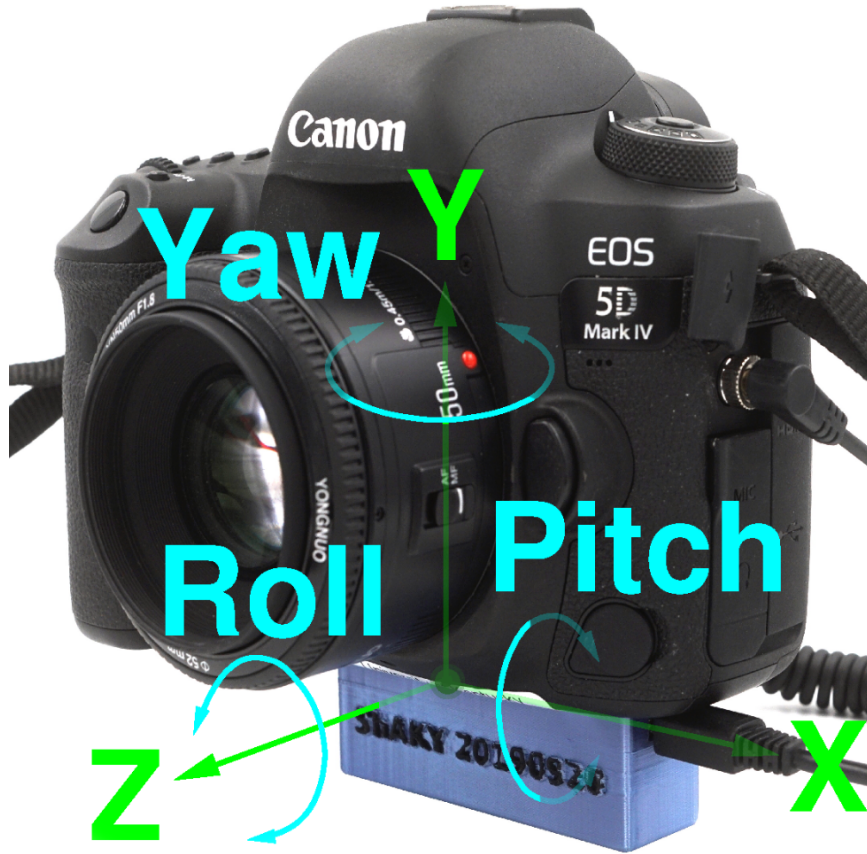


Figure 3.5: Measurement Orientations for ShAKY attached to a Canon 5DIV

flashed to the Pro Micro to calibrate and read out the IMU and monitor for sync signals, both of which are streamed to a host computer via USB. This module is shown in figure 3.6.

On the host computer, a single-file C program `hostshaky.c`, which shells out to GNUPlot [43] for visualization, performs integration, filtering, and analysis of the raw sensor data into motion data. The processing is performed on a host computer to maximize data-rate; the micro-controller in the camera-attached module is programmed to sample and encode sensor readings at the highest rate sustainable for the device and connection to maximize temporal resolution, while the more computationally intensive analysis happens on the much larger resources of a modern PC.

The experimental procedure is then implemented by a web form displayed on a relatively 4k television set, which presents a questionnaire for relevant details about the camera, lens, human subject under test, and experimental conditions, then encodes them into a QR code integrated into a test pattern for the subject to photograph. This photograph of a QR code is thus inherently tagged by the image content with the experimental data, and by the camera-generated EXIF data with finer details of the exposure for later analysis. An example readout is shown in 3.7

Only a small amount of user testing was performed with this device, but the

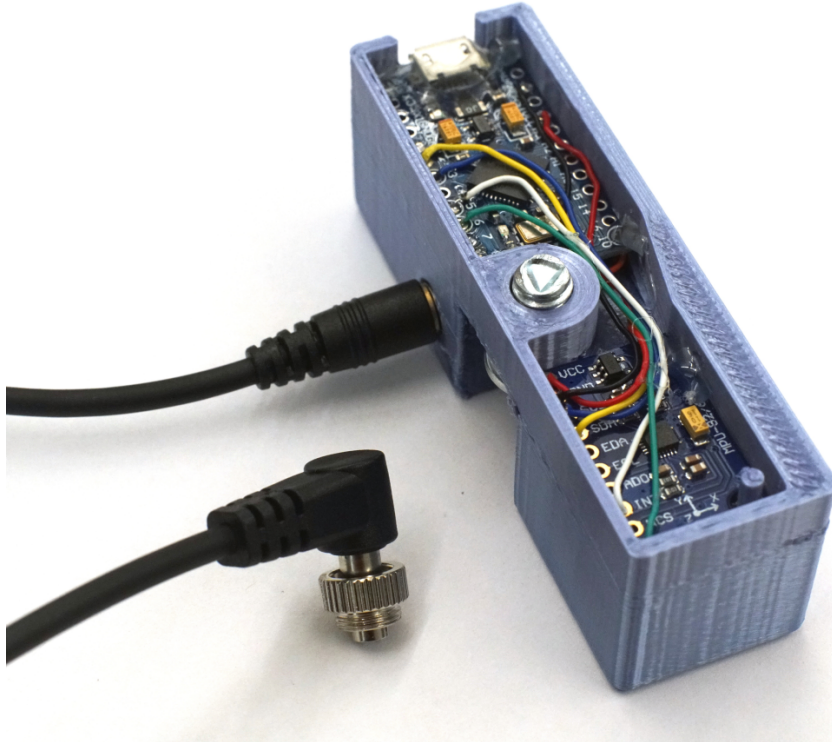


Figure 3.6: A completed ShAKY device, showing the internal electronics

preliminary results do indicate this simple, low-cost, open-source device can provide insights into camera motion. Many of the preliminary findings were not particularly surprising: using a viewfinder (and hence holding the camera closer and making a third point of contact between the operator and camera) roughly halves the amount of measured camera motion. Using electronic first curtain shooting on cameras which support electronic or mechanical shuttering tends to meaningfully reduce shake at the time of exposure.

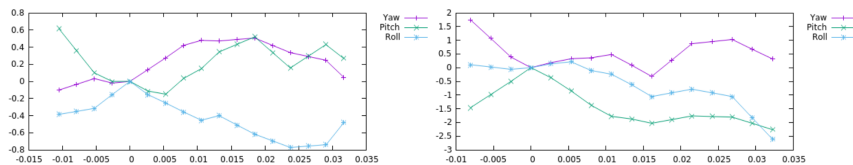


Figure 3.7: Typical ShAKY data for a Sony A6500 (IBIS and EFC disabled) camera still on a tabletop (left) vs. hand-held (right)

Other results were more surprising: individual operators are not particularly consistent, the camera itself produces a substantial amount of the observed motion. A particularly surprising finding is that, relative to a single-handed grip, holding the camera with two hands not only does not result in reduced camera motion, but tends to convert less-photographically-problematic x,y,z motion into more problematic pitch and roll.

This work was published as "Characterization of camera shake" at Electronic Imaging 2020 [44].

3.5 Non-Uniform

A major promise of TDCI-like pipelines which has not been previously explored is the ability to produce exposures which are spatially or temporally non-uniform. To define terms, a spatially non-uniform exposure is one where the exposure parameters for each site in the rendered image is not the same - the gain or time interval from which light is integrated can be varied over the area of the rendered image. A temporally non-uniform exposure is one in which the integrated light is not handled consistently across time. Conventional exposure approximately - excluding previously discussed shutter artifacts - treats exposure as a single interval at a constant gain for the entire frame. Temporally non-uniform exposure consists of integrating incident light from multiple different periods, weighting light from different times in the exposure interval differently, or (overlapping with spatial non-uniformity) building the frame from different intervals.

If, for example, the dynamic range of a scene exceeds the dynamic range of the sensor, a traditional integrate-at-exposure camera cannot generate an image which preserves detail in the entire scene. However, if the integration is performed computationally after the fact, there is no restriction that all spatial segments be integrated with the same function, and suitable parameters can be chosen for sections of the image independently.

3.6 Exposure Interval

In a conventional frame-based camera, the photosensitive element - film or digital sensor - is exposed to light for a fixed interval by the opening and closing of a shutter. In the archetypal camera this is accomplished with the use of a focal-plane shutter; a pair of light blocking curtains which slide over the sensor one after the other, with the intervening time comprising the shutter speed.

With a focal plane shutter, and a relatively long exposure, a first curtain opens, allowing light through the lens to reach the sensor, and some time later the second curtain closes, cutting off the exposure. This scenario provides a very good approximation of the whole sensor being exposed for the same time interval, but that is not always desirable. In scenes with very large variations in brightness, exceeding the dynamic range of the sensor, a uniform exposure time will over or under expose parts of the scene. That is, if the bright areas of a scene are properly exposed to capture a maximum amount of detail, the darker areas may be under-exposed and simply appear dark, losing information in that part of the scene. Conversely, if the darker areas of a scene are properly exposed, the brighter areas may be over-exposed and saturate, losing information about that part of the scene.

For very short exposure intervals, a focal plane shutter allows light to strike the sensor by moving both curtains at the same time, releasing them with an offset less

than their individual travel time, thus traversing a slit between the first and second curtain across the sensor. This scenario is a poorer approximation of the entire sensor being exposed for the same interval - while the amount of time each sensel is exposed for approximately the same amount of time, the area along the leading edge of the frame is exposed at an earlier absolute time than the area at the trailing edge of the frame. This offset can result in smearing or other artifacts, particularly if objects are moving in the scene fast enough to create substantial displacements during the shutter interval. Other shuttering methods, such as iris leaf shutters or various electronic dump-and-readout schemes are also employed and create their own distinct artifacts in the resulting image, several of which are detailed in [20].

Some photographers may alter the exposure interval in intentional ways to create specific desired effects. The best-known of these alterations is to shoot multiple exposures on the same photosensitive frame, effectively compositing the incident light during multiple images into a single photo. These techniques, however, are physically complicated to set up, difficult to predict the results of, and require that the setup be executed perfectly at the time of image capture(s). The difficulty of physically realizing complicated exposures, and simplicity of achieving similar effects by computationally compositing images after the fact mean these effects are already most often accomplished by post-processing.

Non frame-based capture schemes like TDCI allow photographers to avoid these problems with exposure by computationally integrating the incident light over one or more interval(s) to create the final image. This means different portions of the scene are not competing for exposure parameters, as they are being sampled independently. Likewise, even the possibility of shuttering artifacts is eliminated, since if the sensels are continuously independently sampled, there is no correlated scan pattern which could produce artifacts. Most importantly, computational integration separates the processes of sampling the scene and exposing the image, so once sampled, the same interval of incident light can be exposed over and over to produce images, allowing the photographer to tweak the exposure parameters repeatedly, viewing the resulting image and adjusting until the desired effect is achieved.

3.7 Film Speed

In a conventional frame-based camera, the sensitivity to incident light (gain) is set as a whole-frame parameter, referred to as “Film Speed” for historical reasons. In an actual film camera, this gain is set by the photo-chemical sensitivity of the film being used, measured in modern times with the ISO 5800 system. In a digital camera, the gain is determined by the “ISO Setting” in the camera. This setting’s properties are specified by analogy to the behavior of film in the ISO 12232 [6] standard. In either case, this setting is fixed for the entire frame, for the entire interval of exposure. This whole-scene gain setting is often undesirable as it limits the dynamic range which can be represented in a single capture. Much as for the exposure interval, setting the gain to suit one part of a scene will often leave other parts dramatically under- or over- exposed, losing information about those areas as they saturate or fail to fill in details.

When performing integration computationally after the fact, there is no reason the gain must be uniform for the entire scene. In this scenario, a photographer can specify different gains, or gain functions as above, for different portions of the scene such that each portion of the scene is exposed as desired. There is significant precedent for the desirability of such a feature, as a number of “tricks” allow modern digital cameras to evade whole-scene exposure settings, albeit with significant caveats. First, modern digital cameras with computer-controlled optical paths often have built-in support to take rapid bursts of exposures while automatically varying exposure settings. This method is typically referred to as “HDR Bracketing”, as it allows capture of a High Dynamic Range image by “bracketing” - taking exposures with either the aperture or shutter speed varied in steps around an estimated center value. This allows photographers to extend the dynamic range of a processed image by taking the series of frames exposed differently, and ideally correctly for different regions of the scene, and composing them in photo editing software after the fact. This method suffers from several serious limitations. The most obvious limitation is that because the exposures are taken successively, any motion in the scene or camera will cause the successive frames to not line up perfectly, creating artifacts in the composite image. More fundamentally, images generated by HDR bracketing still require that every part of the scene is properly exposed in at least one of the series of frames, requiring the photographer (or camera), to properly estimate the required number and range of exposure settings at the time of capture.

A second extant technique for cheating whole-sensor gain with modern digital cameras is that the sensor ISO setting is often applied, all or in part, as a digital multiplier in the post-processing [45] after the sensor has been read out, rather than by changing the behavior of the sensels. This property is, lately, referred to as “ISO Invariance” or “ISO-Less shooting”. This after-the-fact gain function means information is only gained or lost based on the ISO setting during the image processing pipeline, not during capture. As a result, if images are captured at an ISO invariant camera’s base ISO, all the scene information the sensor is capable of capturing will be captured and retained, albeit typically with less-than-pleasing brightness. The image can then be brightened in post-processing, essentially applying digital gain later when the photographer has the advantages of time, multiple tries, and additional compute power to make superior decisions about the gain factor. The gain can also be spatially non-uniform - selectively brightening or darkening parts of the scene is an extremely common post-processing manipulation. If the camera used was ISO Invariant this practice is effectively equivalent to selectively changing the sensitivity of the capture device. This technique, however, does not extend the range of the captured data beyond what the sensor can represent for a fixed interval, and may actually shrink it if the brightening or darkening range-clips any pixels. Employing this technique also complicates selecting an appropriate shutter speed, since the captured image will be intentionally under-exposed at the time of capture.

By leveraging TDCI encoding, similar effects can be produced while avoiding many of the disadvantages of the methods that rely on traditional photographic modes. Some methods for using TDCI processing to generate images with larger dynamic range and fewer artifacts were previously explored in [46], but the techniques in that

work retained the practice of using a single uniform sensitivity and exposure time. Specifically, if the incident light is recorded as a waveform and sampled after the fact, all of the differently-integrated regions can be integrated with time centered at the same instant, avoiding the issue of artifacts due to changes in the scene between sequentially-shot bracketed exposures. Even better, recording the incident light variation rather than a series of exposed images removes the requirement that the parameters for each of the constituent exposures be pre-selected. Since there are no pre-determined exposures under this scheme, there is no danger of clipping regions of the scene due to lack of data or saturation. This allows the selection of the parameters with which regions of the scene are exposed to be done after the fact, as many times as is necessary, until precisely the desired exposure parameters for each part of the scene are found.

3.8 Precedent for Non-Uniform Exposure

There is precedent for the concept of generating variously non-uniform exposures, but existing techniques for generating non-uniformity photochemical or digital photography come with significant limitations which should be improved upon by the techniques proposed in this work.

Many of the closest precursors to arbitrary non-uniformity are darkroom techniques. Dodging and Burning [47], the practice of adding or removing light during the print making process allow a degree of spatial control over effective exposure. Dodging is the process of selectively shielding the print paper from light passing through the film, by physically interposing shaped opaque masks between the film and print over the areas to be affected when it is exposed on an enlarger, casting shadows which effectively lighten the affected region. Burning, conversely, is the practice of selectively allowing additional light to fall on specific regions of the paper to create a darker area, typically by imposing an opaque mask with holes cut in the desired areas part way through the print exposure interval, cutting off the rest of the frame.

Typically, these effects are achieved by manually cutting a mask of the desired shape and size in a piece of opaque non-reflective material- such as dark colored card stock- then hand-holding it in the optical path of the enlarger with wire or line. The support structure can be hidden by keeping it in constant motion, and the edges of the affected area can be modulated by modifying (perhaps over time) the distance between the mask and paper - a mask very close to the paper produces sharp edges, and they edges become larger and more diffuse as it is drawn further away. Adams also suggests techniques like dripping developer solution at different concentration or temperature to effect local changes.

All these techniques are manual, labor intensive, bound to specific photochemical processes, and restricted to locally altering the interpretation the light gathered during the exposure rather than actually altering the interval or gain of that light. Analogous digital practices - selecting areas of an image for selective lightening, darkening, or dynamic range manipulation - are certainly less laborious but only slightly more flexible. The analogy of masks to guide exposure has been extremely valuable in the development of the techniques presented in this work.

Other extant methods of generating non-uniform exposures with existing technologies are based on multiple exposures. These techniques are quite wide ranging; the multiple exposures can be performed on a single piece of film or sensor readout at the time of capture by repeatedly opening and closing the shutter, or by after-the-fact compositing of several single exposures during the development process. In a controlled environment, similar effects can also be accomplished by modulating the light on the scene rather than the shuttering mechanism, as in stroboscopic photography when the shutter is opened for a relatively long interval, and a flash is fired for multiple controlled shorter intervals.

The content and parameters of the separate composited images can vary widely. For artistic purposes, the multiple exposures may be related only by the intent of the photographer. For more consistent compositions of multiple exposures, a common practice “stacking” in combination with “bracketing”: taking a series of exposures with different parameters with the possibility of combining the desired features of several to achieve effects not possible through the lens. Exposure can be manipulated by stepping the shutter speed, aperture, or (in a digital camera) sensitivity across a range, then regions of the frames exposed as desired in the constituent frames can be combined. Compositions of multiple differently exposed frames can produce a dynamic range larger than is achievable directly with the same equipment.

In digital camera systems the technique can again be extended in various ways; as digital cameras are not bound by the static sensitivity of a roll of film or the parameter modification speed of a human operator. As a simple example, when bracketing, the onboard computer can vary parameters between successive frames almost as fast as the limit of the desired shutter time. Another even broader example is that where optical techniques are restricted to additive composition of multiple exposures digital setups may use other compositing schemes, such as blending or subtraction. Digital techniques for compositing multiple exposures also afford more flexibly an easily mask out which parts of the final image come from which exposure, including employing various sorts of automation to make the decision without a human operator. Some digital cameras, or cameras integrated into computerized devices even allow some of these techniques to be automatically executed in-body; features with names like “Auto HDR” or the automatic focus stacking features advertised by Olympus [48].

However, the extended digital features do not remove the restriction that the intervals represented by the time individual exposures cannot be overlapping, creating issues for composition, such as discontinuities in the case of moving scene elements. It also does not allow wide after-the-fact adjustment of individual exposures; for example, if a portion of a scene is dramatically over- or under- exposed for every frame of a bracketed sequence, nothing can be done after the fact to recover information about that part of the scene.

Focus bracketing and stacking bears mention as it continues the analogy of this work to plenoptic cameras’s ability to adjust focus post capture; while focus stacking allows a series of frames which were correctly focused, and the focus correctly spaced, at the time of capture to generate extended depth of field, a plenoptic camera can generate extended depth-of-field without relying on a set of step-wise components which were focused correctly at exposure time.

Many of the tools developed in the current work are inspired through a lens of enabling more general, more flexible, and more powerful versions of these existing techniques.

3.9 Non-Uniform Over Time

When performing integration of incident light computationally after capture, there is no restriction that the virtually admitted light must be uniformly “exposed” over a single interval as with a physical shutter. Integration gain functions can be specified which simulate mechanically implausible shutter behaviors with only a small amount of extra difficulty. For example, the gain function can have multiple distinct peaks, producing an effect analogous to multiple exposures. Even less physically realizable, the gain function can slope, vaguely physically analogous to imposing a time-varying neutral density filter over the lens, or (somewhat less precisely, as slope variations will not affect depth of field) iris-ing the aperture during the exposure. It is, of course, entirely possible integrate with gain functions that could not be practically realized by a mechanical means, though the more radical the exposure function, the less unprecedented the effects will be.

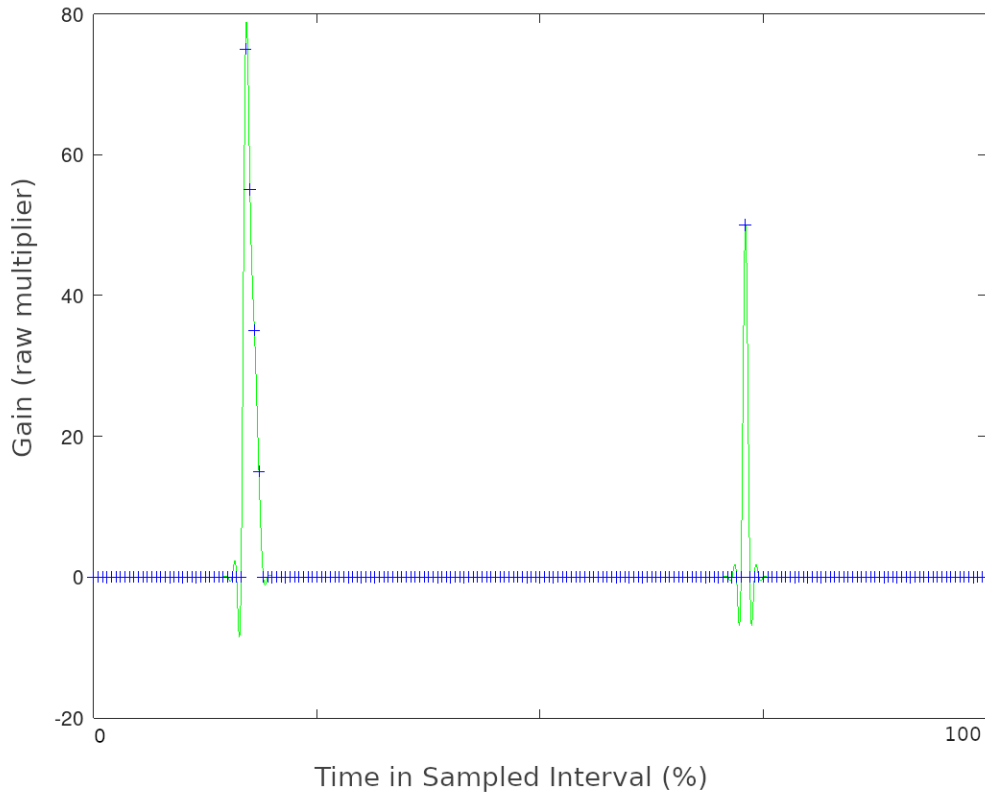


Figure 3.8: Example Integration Function from Octave prototype



Figure 3.9: Capture of riding mower integrated with the function shown in Fig. 3.8

In the first Octave-based prototype implementation the integration gain function is represented as a composite spline. Users familiar with image editing will, whether they know it by that name or not, possess at least a passing familiarity with composite Bezier curves, used for drawing arbitrary lines in a wide variety of image editing applications, or (Centripetal) Catmull-Rom splines [49], also used in image editing for specifying color curves in many photographic editing tools, and modeling camera motion in video processing. Initially, Centripetal Catmull-Rom splines seemed particularly appealing because they are straightforward both to visually manipulate, and to compute the value of at arbitrary position, and already widely used in imaging applications. Furthermore, Centripetal Catmull-Rom are inherently smooth and non-looping (mathematically; twice differentiable), making them immune to ambiguities or discontinuities. Unfortunately, a single Centripetal Catmull-Rom spline can represent only a very limited family of functions, which does not include many trivially-interesting cases.

A more general representation of temporal gain functions is therefore required; the method in this phase of experiments used normal cubic splines [50] as a highly-flexible representation which retains the desirable property of always being twice differentiable. Using this scheme, each the integration gain function is specified as a series of control points. To use the integration gain function, the domain of the specified control points is mapped to the interval of recorded light (allowing for arbitrary granularity), such that the gain to be applied to the incident light at time $t_{current}$ into the sampled interval is the value of the normal cubic interpolation at $t_{current}/t_{max}$.

While the natural behavior for a computer scientist is to specify the temporal

integration gain function as an equation or series of control points, perhaps over a unit interval, for most users this will be extremely awkward. An elegant interface would present the user with an initially horizontal line that they can interactively modify by clicking and dragging to add and modify control points. The integration scale factor for each instant is then the height under the curve at that distance into the interval, which is mathematically straightforward, readily visually representable, and leverages existing mental models likely to be available to those accustomed to image editing tools. The horizontal (x) axis of this function represents time, to be stretched over whatever integration interval is selected. The vertical (y) axis of this function represents the instantaneous gain to be applied to the incident light at time $(t/interval) * fn_{max}$.

3.8 shows an integration gain function specified with this method representing a double exposure, with the first exposure ramping very quickly to very high gain then somewhat more slowly tapering, and the second very quickly flicking on and off to a smaller maximum gain. 3.9 shows the result of applying that integration function to a capture of a passing riding lawn mower, rendered from 30FPS video. Note that the resulting image contains two displaced images of the mower. The first mower image corresponds to the first spike in the integration gain function. It is mostly opaque, picks up suddenly with a sharp leading edge, then slowly fades away in a smear as though it were moving quickly relative to the shutter speed. The relative opacity is because the majority of the light energy integrated at those locations in the frame come from the first spike, while the sudden appearance and slow taper are the result of the shape of that first spike. The second mower image, further down the row, corresponds to the second spike. It is relatively sharp and un-smearred because the width of the spike is short compared to the speed the mower was moving. However, it appears relatively translucent because the majority of the light energy integrated at its location was contributed by the background in the earlier portion of the exposure, rather than the time when the mower was at that position.

One interesting detail of arbitrary integration functions is that it is perfectly possible to specify *negative* gain for some portions of the interval. This behavior would be physically analogous to the sensor subtracting the contribution of incident light during portions of the exposure, rather than adding it. This is not something that is physically realizable in a conventional camera, but is very useful creatively for tasks such as subtracting static features from a scene. Partially negative gain functions also provide a ready way to provide even average brightness for differently-integrated parts of the scene to compensate for intervals with particularly high gain applied.

3.10 Non-Uniform Over Space

Non-uniform integration over space is analogous to creating a scene-specific piece of film whose sensitivity to light varies across its surface, or the practice or selectively lightening or darkening portions of a scene in post-processing. While applying different gains to different portions of the scene in order to properly expose each is obvious, specifying the spatial regions on which to apply the different gains is

somewhat mechanically awkward. Extended discussions on the matter resulted in several unappealing options - specifying by mathematical function (awkward for the user), specifying by rectangular region (restrictive), specifying by arbitrary polygons (complicated and restrictive), or specifying by bucket-fill algorithm (computationally difficult, self feedback problems) - and one promising avenue.

The promising method is to use a mask, drawn as a bitmap of the same resolution as the capture source, colored with a different pixel value for each region to be processed. This covers all the functionality of arbitrary geometry or function-determined regions by offering users a simple, portable, well-known format to generate their complex masks in, while allowing straightforward use cases to simply draw their desires in a basic image editor. A bitmap mask for region definition also allows for straightforward batch processing, either by applying the same generated or otherwise pre-prepared mask for multiple exposures, or enabling the use of an external tool to perform higher-level per-frame functions, such as object tracking, to generate sequential video frames from a TDCI stream with specific exposure properties for different objects in the scene.

The format currently being used to express these spatial exposure masks is a 8-bit P2 PGM with the same spatial size as the TDCI stream to be exposed. Each of the 255 gray levels possible in the format represents a distinct region, and the value of each pixel in the mask PGM specifies which exposure region to apply to the corresponding pixel in the input stream. This way, a simple gray-scale mask can be generated where each pixel in the mask is tagged with the encoded value of the gray level. Each gray level is then assigned a particular integration function. This provides a number of regions far in excess of any easily-conceived practical application, avoids forcing users to deal with any specialty tools or mathematical specifications, and is extremely straightforward for software to both generate and ingest. Each numbered region is then assigned an integration function with which to "expose" that portion of the image.

This technique is quite general. It is possible to not only vary the integration parameters for portions of the scene, analogous to existing HDR techniques, but to directly produce temporally composite exposures. In such an exposure, the output image is generated from sections which spatial sections of the image are integrated from temporally differently-centered and possibly non-overlapping sub-sections of the sampling interval, opening a wide range of options. One simple application for this combined case might be selecting independent intervals for each face in a group picture to give each pictured individual open eyes and pleasing expressions, even though though they did not happen at the same time. Another application could be masking a moving object from the background in a scene, and integrating the moving part with a short, sharp-edged, high-gain integration function, and the background with a longer, shallower, lower-gain integration function on the same center, yielding an image with a sharp object with a minimum of motion blur on an apparently well-lit, detailed background.

Including a simple editor which would provide a transparent overlay of a frame preview and some basic drawing tools to generate region mask bitmaps inside the TDCI exposure tool is an obvious nice-to-have, but is not in the critical path for

demonstrating the technological features. This is especially reasonable as most users likely to be using complicated exposure behaviors are likely to already have a deep familiarity and established work-flow with their image editing tool of choice, and staying out of their way may even be the better choice in general.

To provide a minimal illustration for the effects possible with this mechanism, 3.11 contains a simple top/bottom split mask, specifying the two regions on which to apply the two integration functions in 3.10. This mask and function are then applied to a 240FPS video of a foam penguin and foam rock swinging like a pendulum while attached to the same string, resulting in 3.12. Note that the penguin, integrated with the function with two wider peaks, appears in two places, with a relatively large amount of motion blur indicating the two longer intervals of integration, while the rock, integrated with the single very narrow peak, appears only once, and relatively sharp-edged, corresponding to the single narrow peak. Also note that the offsets between the peaks and the appearance of blurring in the image provide a tell that the images of the penguin appear from light contribution during the right-to-left traversal, while the light contribution from which the rock is taken is from the left-to-right return trip, despite appearing “between” the two images of the penguin.

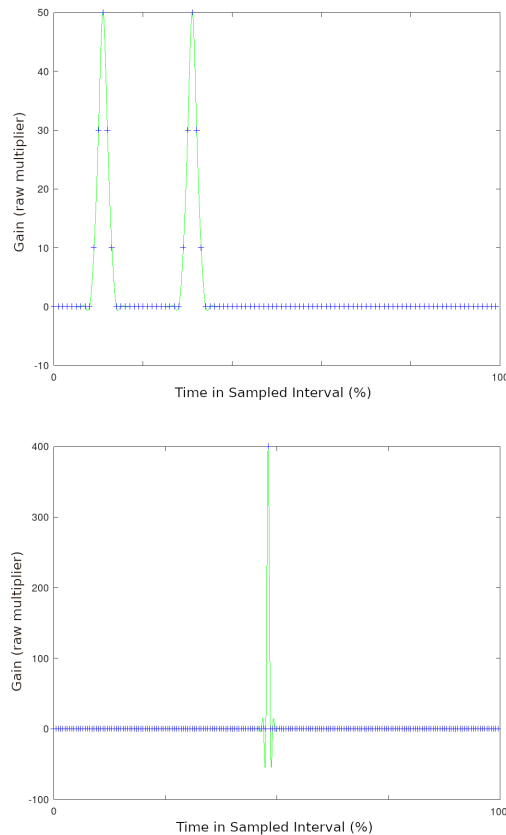


Figure 3.10: Two integration functions



Figure 3.11: Mask specifying two areas of the scene to integrate with different functions.

3.11 The Octave Prototype

The proof-of-concept implementation presented in a paper “Non-Uniform Integration of TDCI Captures” at EI2020 [51] is in the form of an Octave script A which can ingest a sequence of video frames to simulate continuously sampled incident light, and apply user-specified spatial and temporal non-uniformities to the integration of that light. This proof-of-concept implementation serves primarily as a testbed for algorithms and representations, as well as an easy way to experiment with the effects which can be produced, and is not tuned to be particularly fast or high quality.

In this prototype, spatial non-uniformity is specified by an 8-bit PGM mask as proposed above. Each region to be integrated is assigned a unique gray value, and each gray value is mapped to a corresponding temporal gain function by a simple table of gray value:function index correspondences. Directly encoding the index of the gain function to be used as the gray value was rejected, as numerically adjacent gray values are indistinguishable to a human observer, and storing the control point vectors in a sparse representation adds more complexity to the prototype than simply re-mapping the indexing.

Likewise, in this prototype, integration gain functions for temporal non-uniformity are specified by a series of p user-supplied control points per function. These control points are interpolated with a normal cubic spline to give the gain to be applied at time t into a sampled interval of length t_{max} by evaluating the interpolation at $(t/t_{max}) * p$. This means every integration gain function is mapped to the entire input interval, so the granularity of the function can be increased by inputting a

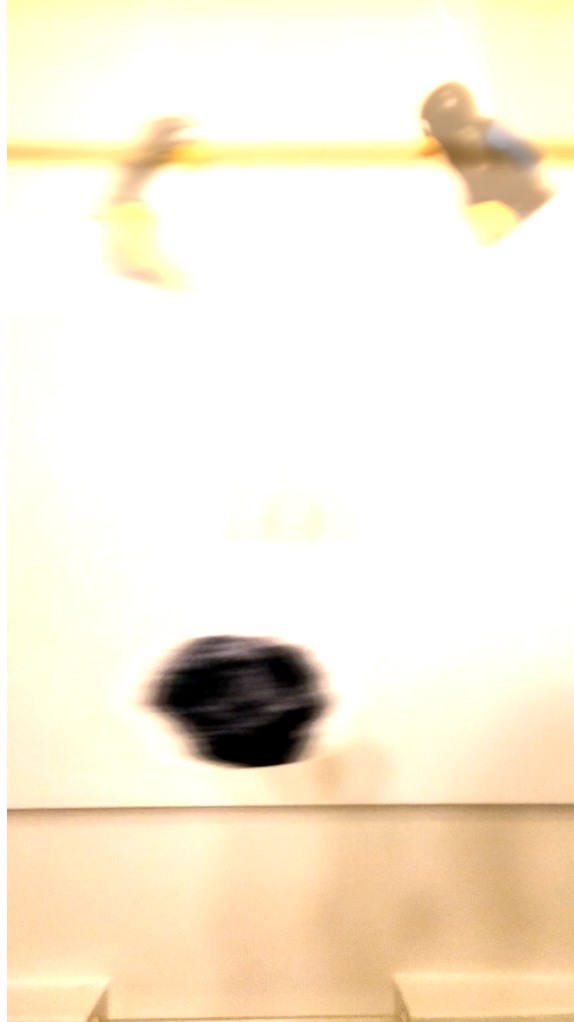


Figure 3.12: Capture of a single pendulum carrying a foam penguin and rock, exposed with the mask and functions from fig. 3.10 and 3.11

larger number of control points, and the position inside the sampled interval can be accomplished by zero padding, without the addition of any other constructs. An arbitrary number of control points can be specified to produce an approximation of any desired integration function, and the multiple functions specified for multiple regions are not required to contain the same number of control points.

The approximation to incident light to be integrated is generated by extracting successive from a video sequence, and treating each as an interval of contributed light for $1/\text{framerate}$ seconds. Integration is performed by summing the contribution of each input frame, multiplied by the average value of the mask-specified gain function for the interval represented by the frame, and subsequently dividing this weighted sum image by the number of frames integrated over to normalize the exposure.

This initial prototype does not attempt to interpolate between samples, as was done in the TIK TDCI testbed [3], but a version built on top of TIK is currently under development based on the algorithms demonstrated in this work, and should

result in higher-quality output with less dependency on the frame-rate of the video input, and much better performance.

3.12 Findings from the Octave Prototype

This proof-of-concept implementation has demonstrated the feasibility of using the TDCI paradigm to generate virtual exposures with physically impractical exposure parameters. This mechanism shows promise both for a variety of creative applications, as well as potential for use in scientific applications. One simple example is using this technique to perform HDR stacking with different exposure parameters for different parts of the scene, all centered on the same instant in time allows a photographer to (iteratively) develop the dynamics of an exposure without the common problems of stitching errors from scene motion or incorrectly pre-parameterized exposure settings. In another, the function-driven integration can be used as a more flexible alternative to stroboscopic photography for capturing and analyzing motion, by sampling a scene then imposing a pulse train exposure function until the desired effect is achieved.

Visualizing the effects achieved by these methods, much less their compelling applications, is still rather difficult, since many of them are not achievable with any physically realized camera. So far, the most effective way of visualizing the tool's behavior is to imagine a camera with a focal-plane shutter consisting of an extremely transmissive, extremely fast, LCD of resolution high enough that its dot size is not the limiting factor in the optical path. One can then think of displaying the imposed spatial and temporal functions on this screen in the optical path and - more or less - predict the properties of the resulting image.

This experiment was also valuable in terms of lessons learned while taking an initial foray into the design space. One of the most immediate lessons is that the idea of exposure intervals being continuous smooth functions represented by sophisticated splines was a bad move. Conventional exposures time properties look like slightly slew-limited boxcar functions; roughly 0 except during the exposure interval, which starts and stops abruptly. As indicated by the earlier study of shutter artifacts, they aren't perfectly square, the blades of a mechanical shutter are neither perfectly in the image plane nor capable of traveling infinitely quickly. This secured the idea that the next prototype should make the common case easy; linear interpolation between control points makes it straightforward to represent boxcar type functions,

It also exposed some extra considerations with the concept of negative gains; while negative gain is quite useful for subtracting some incident light for feature isolation, it leaves a risk of negative output, something that no reasonable image format supports.

This is not a completely unprecedented problem; it's perfectly reasonable to read two images in code or an image editor and subtract one from the other to obtain the difference. The matrix-math interpretation is straightforward, and most of the image interpretation follows, but the issue of negative values is already present - what exactly does a Red value of -6 represent when the range of no-red to as-red-as-possible is mapped to $0 - 255$?

This is generally treated as a normalization problem; if the output of integration produced negative, saturated, or otherwise unrepresentable values, there is a choice on

how to handle the case. A later prototype follows the behavior of most image processing software and libraries and explicitly saturates output at 0 and the maximum representable value in its output format as it seemed to produce the least surprising behavior, but is not the only conceptually reasonable option. In this interpretation our -6 red from before simply becomes 0. This saturation method is also the default behavior in many image processing tools, including the OpenCV library [52] used in the construction of later prototypes in this work.

Other options include treating negative values in one color channel as additions to its compliment(s), perhaps scaled by some factor, which is somewhat analogous to color perception models. In this scheme, our -6 red would turn into, say, $+3$ in each of the blue and green channels. This scheme would be both rather computationally inconvenient, and is extremely likely to produce surprising behavior.

Similarly, out of range values could be treated as a tone-mapping problem similar to methods for mapping between image formats with different dynamic range; the output image minimum value could be mapped to the lowest (most negative) value in the integration result, the maximum result of integration to the maximum output value, and the remaining output mapped - presumably linearly though an argument could be made for log or other functions - between those values. In this interpretation, the output mapping of our -6 red depends on the range of result values and would be the position of -6 relative to the least and most result values. This is both more computationally straightforward to implement and holds a better analogy to an existing practice than in inverse-color interpretation, but was also rejected for being likely to produce surprising results.

3.13 Camera Hackin’

One of the major desires in this work was to build a top-to-bottom TDCI toolchain which would generate exposures from captures generated on a prosumer-grade camera. Modern digital cameras contain sophisticated computer systems, comprising a CPU, a sensor with typically many ADC channels for readout, a relatively large RAM, one or more storage devices, various special hardware function units such as encoders for specific image formats, and the bussing and DMA (Direct Memory Access) devices to move data between the parts. These cameras, therefore, function as cameras by virtue of the software loaded into them.

A number of options for cameras which could be modified to support in-body TDCI were explored in some depth, and each one hit a showstopping limitation. The technical reasons and apparent motivations for those limitations is an interesting topic in its own right, and will be discussed after

Sony a6000

The first and most desirable platform explored was a Sony Alpha mirrorless body. The sensors are excellent, mirrorless cameras are designed to run the sensor more or less continuously exposed to incident light, and because Sony publishes compliance sources for the various open-source software running in their devices [33], we know

that devices in that family run a Linux + BusyBox operating system. A number of older Sony Mirrorless bodies also support the PlayMemories Camera Apps [53] ecosystem for loadable software, an Android-like development environment for limited application development of software to run in-body. The PMCA environment is too restricted to even attempt to develop a TDCI-like capture mode in, during the same period of time this work has taken place over, is being discontinued entirely [54].

However, a series of hackers have investigated the firmware update format and PlayMemories API which lead to possibilities to run unrestricted user code in-body. The first of these project was NEX-HACK [55], a project to reverse engineer the Sony Alpha firmware, which resulted in a large amount of approximate documentation, and a tool to unpack, repack, and forge signatures on user-modified firmware updates for Sony Alpha cameras. This initial firmware repacking tool was superseded `fwtool.py` by `malco` [56], a more complete and polished tool for similar manipulation.

Malco also worked from the reverse-engineered documentation to generate a development environment called OpenMemories [57], to enable the development and loading of PlayMemories programs outside of Sony’s tools and approval process. One of the reference applications is [58], a suite of tools for hackers to play with the camera, which includes some , and critically, a telnet server allowing a user to connect over WiFi to a root shell and inspect the state of the live system.

Given this access, an exploration of a specific test device, a Sony α 6000 (aka ILCE-6000) revealed a number of interesting details, the first of which is that it really is a fairly standard embedded Linux system internally: `uname` returns `Linux localhost 3.0.27_n1-rt106 #1 SMP PREEMPT RT Thu Feb 18 09:45:24 JST 2016 armv7l unknown`, showing the system is based on a customized 3.0 series Linux kernel with Real Time extensions, and basic POSIX interfaces are supplied by a BusyBox binary, as expected from the compliance sources. Exploration with standard Unix utilities reveals 200MB of main memory (there are likely also inaccessible buffers internal to the image capture system), and a four core ARM V7l processor. Inspecting the process table with `ps` shows a Zygote process - the same process manager used by Google’s Android operating system, consistent with the PlayMemories interfaces resembling Android. Checking loaded kernel modules with `lsmod` shows a large number of expected main-line features like `mmcio` and `nand` storage interfaces, an 802.11 wireless stack based on the `cfg80211` interface featuring an `ath6kl` chipset attached via `sdio`, modules to support the built in HDMI with CEC port, and that the kernel is tainted with some proprietary modules. The set of proprietary modules is quite extensive, and includes a set of modules prefixed with the string “osal” (`osal_utm`, `osal_uipc`, `osal_uologio`) which are not publicly documented but the names suggest an operating system abstraction layer to ease porting of some software components, maybe from another RTOS, and a set of modules `dmac` (speculatively, the interface to a programmable dma controller), `sircs` (whose name strongly suggests it implements a version of the Sony IR Remote Protocol [59] as a bespoke module rather than via the open source LIRC interfaces), a pair of modules `lld` and `ldec` (possibly “load” and “decode”). There is also a module `liro` which is a dependency for a number of the other proprietary modules, which spawns over a hundred kernel threads visible with `ps`.

Going a level deeper, pointing basic binary inspection tools like `objdump`, `strings`,

and `binwalk` at some of the proprietary modules - whose interfaces must be at least moderately exposed to allow communication through the kernel module interface boundary - reveals a number of interesting (but not helpful) details. The ideal finding would have been a set of descriptively-named functions to control the sensor readout, but One major observation from comparing the stubs, there is an enormous amount of communication among `liro` and various `osal` modules, as they each make large numbers of calls to functions exposed by the others. This observation does not bode well static analysis. Another observation is that the `liro` module appears to embed a partially-encrypted firmware image for a separate computer within the camera; there is a boot header, a small un-encrypted binary, and an encrypted blob, as shown in 3.13. This implies that, in addition to many intercommunicating blackbox parts running on the main Linux system, there is a secondary attached processor involved in the device specific low-level functions.

```
$binwalk liro.ko

DECIMAL          HEXADECIMAL      DESCRIPTION
-----
0                0x0              ELF, 32-bit LSB relocatable, ARM,
  version 1 (SYSV)
35960            0x8C78           ESP Image (ESP32): segment count: 2,
  flash mode: QUIO, flash speed: 40MHz, flash size: 1MB, entry
  address: 0x0
36191            0x8D5F           mcrypt 2.2 encrypted data, algorithm:
  blowfish-448, mode: CBC, keymode: 8bit
57094            0xDF06           JBOOT STAG header, image id: 0,
  timestamp 0x391C0000, image size: 725352448 bytes, image JBOOT
  checksum: 0x0, header JBOOT checksum: 0x7C1C
```

Figure 3.13: Binwalk results for the `liro.ko` module on an a6000

Unfortunately, despite being easy to inspect up to this point, the conclusion from that inspection is that the interface to the sensor and image-handling pipeline are a set of black-box, undocumented, proprietary, binary kernel modules interacting with bespoke hardware and each other.

Reverse engineering those interfaces would be a high-risk project on the same scale as the intended product of this work, have limited reach since no models released after 2017 support PlayMemories, and would be necessary to make an in-camera TDCI implementation superior to the fall-back position of reprocessing captures externally, so this line of inquiry was largely dropped.

Canon

Canon’s entire product line shares a number of significant architectural similarities. The native software is built on a Canon developed RTOS (**R**ea**T**ime **O**perating **S**ystem referred to as “DryOS” [60] with various computer platform features and

camera-specific functionality implemented on top. DryOS appears to implement the μ ITRON RTOS kernel specification, and also exposes some POSIX and DOS-like interfaces - for example, when configured to boot from an external storage device, it attempts to launch a file named `autoexec.bin`, a fact which is very important when attempting to load your own code on a camera. DryOS has been used across the Canon line since around 2007. The CHDK (Canon Hack Development Kit) [32] project targeting Canon's fixed-lens cameras is based around reverse engineering of Canon's interfaces, though CHDK generally limits itself to calling Canon functions.

I have been involved in a number of prior projects implemented by reprogramming Canon compact cameras using the CHDK [32] framework, including a number of multi-camera array designs [42], the ISO-invariance project [45] discussed in Section 3.1, providing support for a project which developed a CHDK-based photoplethysmography system [61], and other applications. As described among the earlier work in the introduction 2.1, Canon compacts hacked with CHDK were the platform for an early, primitive in-camera TDCI product [5]. Canon's prosumer EOS cameras with interchangeable lenses are (generally) not supported by the CHDK project.

Magic Lantern

However, a sister project, Magic Lantern [62] has developed around Canon EOS bodies, and provides even deeper hooks into the camera. Though the sensors and on-board computational resources are not quite as impressive as those in the Sony mirrorless bodies, this experience makes the Canon EOS prosumer cameras an attractive potential target. For the same designed-for-continuous-exposure reasons as the Sony body selection, the most promising of the Canon options are the mirrorless bodies, so the exploration on this front took place on a Canon EOS M body. ML focuses on higher-end interchangeable-lens cameras, and directly manipulates hardware configuration registers. In fact, though they are independent projects with entirely separate code bases, Magic Lantern originally derives from the reverse engineered documentation of the CHDK project, and they continue to share information. Magic Lantern operates as a program that runs along side the vendor software; the only modification made to the original system is setting the `BOOTDISK` flag in the onboard Flash, so the camera will attempt to load code from `autoexec.bin` in the root of the CF or SD card.

The Magic Lantern project [62] is a community developed, Open Source (GPL Licensed) project which has developed a development framework and extensive collection of software which is loaded into the camera by the aforementioned process to load user code from attached storage. The Magic Lantern community is chiefly focused on adding video recording features and capabilities to available cameras. Specifically, the project was initiated by Trammell Hudson in 2009 to add extended video features to the 5D Mark II, and management of the project transitioned to Alex in late 2010. As the understanding of the camera internals, set of supported cameras, and community expanded, it has also extended camera capabilities for general shooting like focus peaking, zebra highlights, and live histograms, added useful shooting modes like intervalometer, motion detect, and automatic exposure bracketing, and a wide

variety of other features. Magic Lantern also provides a set of sophisticated developer tools for inspecting camera behavior, and several methods to run custom code on the camera including a scripting interface in the Lua programming language, and a module system to load custom compiled code.

Magic Lantern is academically interesting for several reasons. The first source of academic interest in Magic Lantern is quite similar to the main ML community interest; the possibility of modifying a (relatively) capable commercial camera to behave in new ways to construct research prototypes. Because of the exposed internal memory structures and full programming environment, the functional units of the camera can be freely reconfigured up to the limits of the reverse-engineered understanding and/or capabilities of the hardware.

A second interest for research applications is the sophisticated scripting interface exposed by Magic Lantern. The aforementioned Lua scripting and loadable compiled module interfaces allow researchers to both arrange programmatic capture to use the camera as an apparatus for experiments, and also programmatically operate the camera to study its properties. Simple applications of custom code may include programmed timelapses, motion detection, exposure stacking for focus or dynamic range, etc. but as it is a complete programming environment, the possible functionality is limited only by the resources present in the device.

Another other major academic interest for MagicLantern is the insight it provides into the internal design of a (relatively) modern camera system. Camera manufacturers do not generally intentionally provide low-level access to the camera or its' embedded computer system, or even document its features, over concerns about licensing and competition. The reverse engineering efforts required to create community modifications like Magic Lantern expose that information. Close knowledge of the workings of widely available camera systems allow researchers and photographers alike to reason about both the resulting images and the potential capabilities of a camera in ways that a black-box treatment does not, even if they are not aiming to expand or alter the functionality.

The ML software also allows an enormous degree of live instrumentation into the running camera. For example, a built-in feature allows one to view the memory map and utilization, the process tables of both ML and Canon's native software, as in Fig. 3.14, and a wide variety of other logging and monitoring, several of which are applied later in this work.

In the specific case of the EOS M used as an example in this work, the embedded computer is a Canon DIGIC5 chipset. A rough diagram of the relevant architecture is shown in Fig. 3.15. On the computer front, two processor cores are ARM5TE 32-bit processors, and total RAM is approximately 256MB. The "Image Preprocess" and "JPCORE" blocks represent memory-mapped fixed-function hardware for RAW processing and JPEG en/de coding (names derived from firmware strings), the SD-CON/SD Card blocks represent the interface to the SD card, and the EDMAC is a sophisticated DMA engine which will be discussed in its own section below. Some devices - such as the onboard FlashROM that contains the built-in software, and the various IO devices for reading buttons, blinking LEDs, and interfacing lens mechanics are not included in this diagram, though they are also memory-mapped devices.

Canon tasks				[101/104]					
01	sd1c	u=40	n=0x0	45	MoviePlay	p=16	u=4	n=0x1	
02	PowerMgr	p=20	u=40	n=10x0	46	WVReader	p=17	u=2	n=0x1
03	ChngMgr	p=19	u=4	n=10x1	47	MovieReader	p=17	u=4	n=0x1
04	ChngMgr	p=19	u=4	n=10x1	48	LVC_DRV	p=14	u=4	n=0x1
05	ChngMgr	p=14	u=4	n=20x1	49	LVC_FACE	p=17	u=4	n=10x1
10	HotPlug	p=16	u=4	n=6x0	50	Cal	p=14	u=4	n=40x1
11	FileMgr	p=19	u=4	n=45x1	51	Exp	p=1	u=4	n=70x1
12	FileMgr	p=19	u=4	n=45x1	52	Exp	p=10	u=4	n=70x1
13	FileMgr	p=19	u=4	n=45x1	53	LVFACE	p=14	u=4	n=7x1
14	FileMgr	p=12	u=4	n=10x1	54	LVICY	p=13	u=4	n=10x1
15	ShotCapture	p=12	u=4	n=10x1	55	CLC_CALC	p=16	u=4	n=4x1
16	ShotLock	p=19	u=4	n=0x1	56	News	p=13	u=4	n=20x1
17	ShotPreDevelop	p=16	u=4	n=0x1	57	GalSB80Drv	p=19	u=4	n=0x1
18	SystemTask	p=14	u=4	n=0x1	58	USBTrns	p=19	u=4	n=0x1
19	SAR	p=14	u=4	n=24x1	59	SDIOTrns	p=19	u=4	n=0x1
20	SR_CROSSSTALK	p=19	u=4	n=0x1	60	PPRevisionTASK	p=19	u=4	n=0x1
21	IOMgr	p=19	u=4	n=0x1	61	PtpDps	p=19	u=4	n=16x1
22	Estimate	p=19	u=4	n=0x1	62	Ceres	p=19	u=4	n=10x1
23	MainCtrl	p=11	u=4	n=10x1	63	create	p=19	u=4	n=0x1
24	AudioJudge	p=19	u=4	n=0x1	64	create	p=19	u=4	n=0x1
25	AudioJudge	p=19	u=4	n=0x1	65	Read	p=19	u=4	n=0x1
26	AudioJudge	p=19	u=4	n=0x1	66	Read	p=19	u=4	n=0x1
27	AudioJudge	p=19	u=4	n=0x1	67	Write	p=12	u=4	n=0x1
28	AudioJudge	p=19	u=4	n=0x1	68	Voice	p=19	u=4	n=0x1
29	AudioJudge	p=19	u=4	n=0x1	69	Sound	p=19	u=4	n=0x1
30	FrontShdDevelop	p=14	u=4	n=0x1	70	WVReader	p=19	u=4	n=0x1
31	DianaFrontShdDevelop	p=14	u=4	n=0x1	71	SpS	p=19	u=4	n=0x1
32	RearShdDevelop	p=14	u=4	n=0x1	72	Brk	p=19	u=4	n=0x1
33	DianaRearShdDevelop	p=14	u=4	n=0x1	73	reDevelop	p=19	u=4	n=0x1
34	ShotsDevelop	p=14	u=4	n=0x1	74	ppMgr	p=19	u=4	n=0x1
35	ShotsDevelop	p=15	u=4	n=0x1	75	OpSReceptiveTask	p=19	u=4	n=0x1
36	GuiLockTask	p=17	u=4	n=11x1	76	OpSReceptiveTask	p=19	u=4	n=0x1
37	AS1	p=17	u=4	n=0x1	77	OpSReceptiveTask	p=19	u=4	n=0x1
38	AudioCtrl	p=17	u=4	n=0x1	78	InnerDevelopMgr	p=19	u=4	n=0x1
39	SoundDevice	p=19	u=4	n=0x1	79	ShutterFilter	p=15	u=4	n=0x1
40	AudioDevice	p=19	u=4	n=0x1	80	TouchMgr	p=17	u=4	n=9x1
41	SoundEffect	p=16	u=4	n=0x1	81	DisplayMgr	p=12	u=4	n=11x1
42	MovieTr	p=19	u=4	n=0x1	82	GuiMainTask	p=17	u=4	n=20x1
43	MovieRecorder	p=11	u=4	n=0x1	83	CtrlSrv	p=19	u=2	n=24x1
44	Test6ero	p=19	u=2	n=0x1					

Figure 3.14: Process table of Canon native processes

Strings internal to the firmware refer to those IO devices as the “MPU” and “LPU” for the medium and low speed devices, respectively.

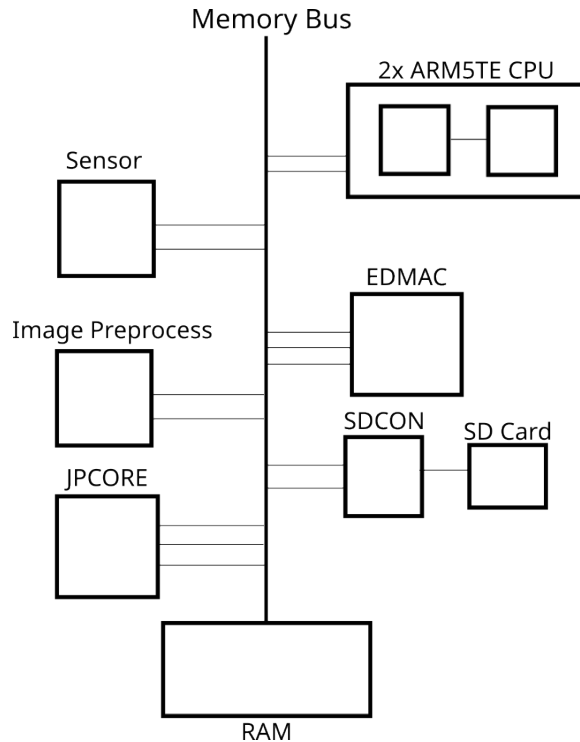


Figure 3.15: Rough layout of DIGIC 5 SoC

Another relevant detail of the low-level memory behavior of Canon cameras is that the native RAW pixel format for 14-bit Canon cameras is packed in a somewhat convoluted way, shown in figure 3.16. This means efficient processing of the native format involves working on 224-bit (least common multiple of 14 and 32) blocks, necessitating some interesting bit-twiddling and/or specific hardware support, some of which is accomplished by the aforementioned Image Preprocessing hardware, but much of which is managed by the EDMAC discussed in the following section.

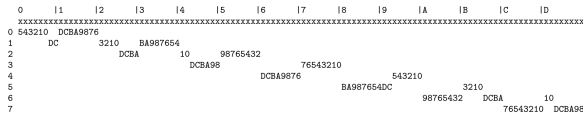


Figure 3.16: The packed layout of Canon 14-bit RAW encoding

EDMAC

One of the major accomplishments of the ML project has been the reverse engineering of the EDMAC "Engine DMA Controller", where "DMA" in turn means "Direct Memory Access", device present in Canon Digic SoCs. This functionality was not available for the first several years of the project, but even a partial understanding of it has enabled a great deal of the functionality now supported by ML.

The initial reverse engineering work was performed by alex in late 2016 [63]. Shortly after the initial behavior and strings were documented, it was back-matched to a patent, [64] initially filed by Canon in 2003. The EDMAC name and much of the related terminology in the reverse-engineered documentation is derived directly from strings in the firmware, and later more terms were matched to the patent, so unlike many systems whose public understanding is based on reverse engineering, the terminology more-or-less lines up between Canon published documentation and public reverse engineering.

The EDMAC is a sophisticated point-to-point data transfer engine, which can be programmed to move data not only between memory regions, but also to and from various hardware devices. For example, on many camera models EDMAC channel 0 is connected to the raw read-out of the sensor [65], while channel 3 is connected to a hardware JPEG encoder/decoder.

The ML project now contains a loadable module which contains a great deal of live and logging instrumentation for the running EDMAC; it can provide a live view of current EDMAC activity as in Figure 3.17, logging at regular intervals to allow study of EDMAC activity during specific operations, and automatically identify unused EDMAC channels which can potentially be repurposed.

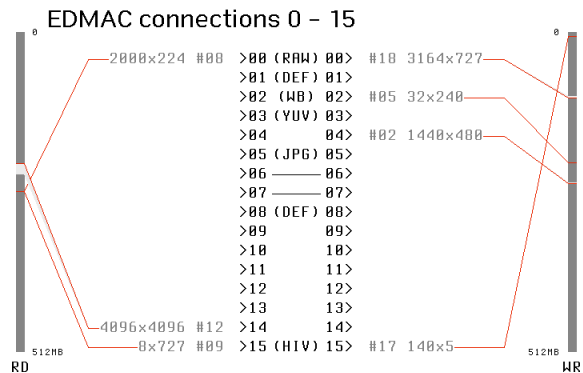


Figure 3.17: First screen of EDMAC live monitoring

The specification of the memory regions to read or write from in the EDMAC is also quite sophisticated; it supports x and y block size, stride, count, and offset argu-

ments, special sizes for last blocks in sequences, and it supports these specifications for both the source and the destination region, allowing it to transfer and transform memory regions of complicated shape and size with minimal CPU involvement. A variety of useful camera behaviors - like cropped sensor readout - are performed using this mechanism. The EDMAC DMA transfer behavior can be described in C as shown in Fig. 3.18, taken directly from the QEMU-based development tools built by the ML project.

```

for (int jn = 0; jn <= yn; jn++)
{
    int y      = (jn < yn) ? ya      : yb;
    int off2   = (jn < yn) ? off2a   : off2b;
    for (int in = 0; in <= xn; in++)
    {
        int x      = (in < xn) ? xa      : xb;
        int off1   = (in < xn) ? off1a   : off1b;
        int off23  = (in < xn) ? off2    : off3;
        for (int j = 0; j <= y; j++)
        {
            int off = (j < y) ? off1 : off23;
            cpu_physical_memory_write(dst, src, x);
            src += x;
            dst += x + off;
        }
    }
}

```

Figure 3.18: EDMAC DMA Transfer Behavior

Visually, this produces access patterns like those in Fig. 3.19 illustrating an access pattern with $xn = 3$, $yn = 2$, $xb \neq xa$, $yb \neq ya$, and differing positive values for $off1a$ and $off1b$ which affect the stride in the X direction. Negative offsets are also legal; it would cause the tiles to overlap rather than skip.

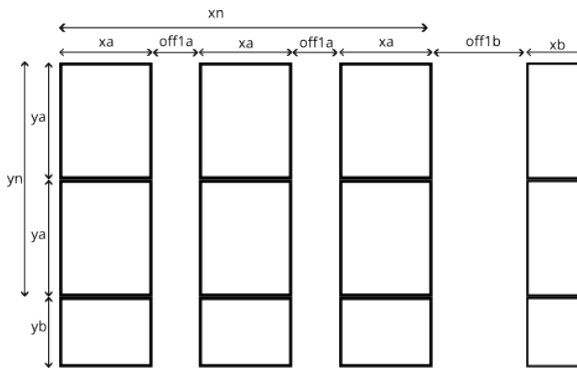


Figure 3.19: EDMAC Memory Layout, with Offsets

MLV

Another relevant accomplishment of the Magic Lantern project has been the creation of the MLV (Magic Lantern Video) format and associated tooling. The MLV format

is, essentially, a container for sequences of raw frame data read directly from the sensor, as well as standardized ways of writing out supporting metadata, and optionally synchronized audio blocks. The format is specified as a roughly 200-line LGPL licensed header `mlv_structure.h`.

The initial “RAWv1.0” design was chiefly experimental. The more widely used specification, implemented by the `MLV_Rec` and `MLV_Lite` modules and all the major post-processing tooling is considered internally to be “RAWv2.0.” Later developments have not altered the on-disc format, but have focused on optimizing the implementation, maximizing utilization of the camera hardware to extract as much data as possible within the available sensor, memory, and (critically) storage bandwidth. Most camera-side development has been focused on the `MLV_Lite` module since it was forked by David Milligan around 2016 [66].

On the EOS M used for testing, the SD bandwidth has an empirical limit of around 60MB/s, which means - best case - full 14-bit RAW MLVs can be captured for longer than the handful of seconds it takes to fill the camera’s internal buffers at a resolution of roughly 1728x692 at 30FPS, and then only if one finds an SD card that happens to sustain the maximum observed speed. This resolution is not *terribly* impressive by modern standards, but an 14-bit RAW video from a ultra-compact body released in 2012 is quite an accomplishment. Unfortunately, the SD standards are not particularly uniformly implemented, so finding a card that will negotiate to the proper mode involves either locating an exact match to a card verified to do so by another user, or extensive trial-and-error.

The chief optimization of the on-camera MLV tooling is that it uses the EDMAC (above) to perform all the data motion; the sensor read-out is DMA on the EDMAC. The SD card write out is DMA on the EDMAC. The cropping is DMA on the EDMAC. The MLV capture tooling also works around various platform limitations, such as the 4GB file size limit on the FAT32 format volumes used on the SD cards in (most) cameras with integrated support for multi-file encoding.

An ecosystem of processing and conversion tools have formed around the MLV specification. Examples include `MLVApp` [67], a MLV processing tool initiated by `ilia3101` (Ilia Sibiriyakov), a sophisticated, open-source, community-built tool for processing the resulting MLV files. `MLVApp` supports the native formats produced by the various ML supported camera models, and allows a user to post-process and manipulate the RAW video in various desirable ways; sophisticated Demosaicing, highly parameterized exposure analysis and manipulation for toning and look, various forms of RAW correction for dead pixels and noise reduction, and conversion to a wide variety of conventional output video formats. It is distributed under a GPL3 license, and is built chiefly in C++ using the Qt toolkit. Many of its features are the result of community members adding specific functionality they desired, and/or hooking code from other open source developments, such as the `librtprocess` [68] tools derived from the open source RAW still processing software `RawTherapee`.

Another approach to accessing MLV data is `MLVFS` [69], also initiated by David Milligan of `MLV_Lite`. It mounts a MLV file as a virtual file system using the FUSE (File System in UserSpace) facility on UNIX-like systems, which allows the individual frames of the MLV stream to be accessed as though they area directory of DNG format

RAWs, and consumed by any software which can operate on DNGs.

Limitations

The current list of camera models supported by Magic Lantern are the Canon 5D Mark III, 5D Mark II , 6D , 7D, 60D, 60Da , 50D, 700D / Rebel T5i , 650D / Rebel T4i , 600D / Rebel T3i , 550D / Rebel T2i, 500D / Rebel T1i, 1100D / Rebel T3 and EOS M, as enumerated on the current builds page at <https://builds.magiclantern.fm/>, with a few ports in progress. The newest of these cameras came out in 2012-2013, as platforms after the DIGIC5+ generation have not yet been adequately reverse engineered to build a working port.

Even those cameras which are supported will have features which are not fully exploitable. As an example of attempting to make use of a not-fully-understood feature, the original application that lead to this work was an interest in using the subtraction channel apparently available the EDMAC to perform on-the-fly frame diffing, for use in ongoing research projects. It can be experimentally verified, using the extensive introspection tools included in ML, that the EDMAC has some sort of subtraction mechanism. This mechanism is exposed in the camera UI for “Long Exposure Noise Reduction.”

Actually making use of the subtraction mechanism presents two issues: the setup for two-reader one-writer EDMAC operations - like subtract - is not publicly documented, and the location of the subtraction engine in a particular camera is not stubbed into the ML code.

The second problem is relatively straightforward; a camera with ML active can log EDMAC activity at user-controlled intervals, and on the EOS M a comparison of the logs from a series of otherwise identical exposures, with “Long Exposure Noise Reduction” active and without reveals that EDMAC channel 20 is activated only when the subtraction mechanism is active.

The first problem, however, proved to be beyond reasonable effort for the experiment at hand. Though two-reader-one-writer EDMAC functions are visible in the logs, the existing ML code calling EDMAC functions primarily uses it to implement a fast `memcpy()`, or other one-reader-one-writer functions. When an EDMAC operation is configured, there are calls to `StartEDmac(ChanN, 0)`; to configure a channel for writing and `StartEDmac(chanN, 2)`; to configure a channel for reading. This leads to the natural conclusion that calling `StartEDmac(ChanN, 1)`; might plumb a second reader, but making calls of that form doesn’t appear to do anything other than hang the camera.

The limited successes of this exploration were presented at Electronic Imaging 2024 as “Magic Lantern as a Platform for Digital Photography Research” [70].

Magic Lantern for TDCI

There is a tradeoff in this project between the desire to perform the TDCI encoding as close to the sensor as possible, in order to maximize the number TDCI’s attractive features which can be directly demonstrated, and the extra development challenges as

- developing software on a conventional computer over documented interfaces is much easier than working in-camera where computational resources (CPU cycles, RAM, storage bandwidth) are scarce, interfaces are poorly or undocumented. With this in mind, several approaches to leveraging the access afforded to a prosumer camera by the Magic Lantern project to create TDCI tooling were considered, guiding which details of the Magic Lantern ecosystem were explored in depth.

First and most potentially compelling was building a TDCI capture mechanism by directly in-body by manipulating the EDMAC engine. The attention above to the APIs for sophisticated patterned readout and two-reader-one-writer operations in the EDMAC was in the service of generating a TDCI stream. While the computer in the EOS M is dramatically too slow and memory starved directly maintain a TDCI scene model, leveraging the apparently-present memory region subtraction feature inside the EDMAC to execute on-the-fly frame differencing looked like an avenue to approach in-body TDCI. Because the `textttmlv_lite` code successfully maintains several frames in memory, stealing a few of those frames for manipulation appears potentially feasible. These memory regions could then be used to maintain a current expected value frame, and series of successive differences between the expected and most recent frame, and that diff and the prior diff, to produce an approximation of the discrete time second-derivative for use in a TDCI model. This case is extremely ambitious on both memory use and arithmetic intensity, which gave it the additional downside of likely requiring a small crop area and slow sample rate. As a fallback, writing out the diff frames rather than the raw data should allow very simple compression schemes - such as run-length encoding, to dramatically improve the speed with which scene data can be written out by eliminating redundancy. This becomes even more effective if the diffs are thresholded based on a noise model of the camera to eliminate changes below significance - the notion of analytically distinguishing scene change from capture noise appears repeatedly in the larger body of TDCI work. This claim is based on the same scene constancy assumptions that underlie most video compression and TDCI bandwidth claims - the differences of adjacent frames should be small compared to the total scene content. Because raw video capture on the target camera is deeply SD write speed limited, this would make an excellent demonstration of the possibility and value of the redundant-data-stripping features of TDCI style capture. However, since the operation of two reader one writer EDMAC operations has proven elusive, and it is even unclear if the subtraction mechanism is truly general or specifically optimized for the sparse case of dead pixel elimination, further exploration along this line was not tractable.

Another possible avenue to leverage the Magic Lantern tooling in pursuit of a more sophisticated TDCI implementation is to reprocess an MLV video stream generated by the camera on a host computer, in the same fashion as previous experiments with TIK. The benefits of such a scheme

However, the experimental limit on the EOS M under test of RAW video at 1728x692 at 30FPS is not compelling. The limited resolution, particularly temporal resolution, of MLV streams makes the effort-to-reward for pursuing that avenue for TDCI reprocessing less than promising. As a standalone experiment, the MLV container format and reprocessing tools in MLVApp would make a reasonable platform

for exploring temporal demosaicing, but a narrow experiment on that front was not compelling given decades of existing work on frame oriented (inter-frame) temporal demosaicing techniques [17].

Other Platforms and Adjacent Experiments

A number of other camera devices came up in adjacent projects, and some of them bear mentioning in the context of the larger work. Several precursor projects relied on Canon point-and-shoot cameras programmed under the CHDK environment, as discussed earlier when introducing the Canon programming environments 3.13 and in discussions of various sub-projects which use them, such as the early in-camera TDCI implementation 2.1 and parts of the IOSLess 3.1 experiments that largely inspired the rest of this work. Unfortunately, the lack of onboard compute resources - both CPU and RAM - on these devices, the lack of access to the sensor data and configuration at levels below the standard Canon firmware APIs exposed by CHDK, and the mediocre sensors do not make them suitable targets for further development.

Yet a different group of related projects were built using devices which are more embedded development platforms with small image sensors attached, rather than dedicated camera systems. Most prominently the AI-Thinker ESP32Cam product [71]. This board combines an ESP32 microcontroller development system, and an Omnivision ov2640 camera module. The camera captures up to 2MP (1632x1232) color images at up to 15FPS, and is connected over the SCCB bus allowing a great degree of low-level control. The ESP32 module provides a dual core 32Bit Xtensa LX7 processor clocked at around 240MHz - a relatively capable processor among the camera devices explored - but only 520kb of SRAM and 8MB of PSRAM which is extraordinarily restrictive in an imaging device. It also provides a capable wireless stack, and, perhaps most importantly, a vendor-supported development environment intentionally design designed for user reprogramming, unlike the hostile development environments afforded by nearly other every device in the space.

One project involved a much slower scene-constancy and non-uniform sampling based incremental imaging device called Lafodis160, described in “An Ultra-Low-Cost Large-Format Wireless IoT Camera” [72]. This project essentially constructs a 2D polar robot, shown in 3.20 that can locate the sensor of an ESP32 anywhere within the image circle of a large-format lens, allowing one to (extremely slowly) programmatically sample any or all of the 160mm diameter image circle projected by the lens, by physically placing the ESP32-CAM’s sensor at the location - sampling a square 1.534mm on a side into 1600x1200 pixels of input at a time. My work on the LAFODIS touched on the electronics and motion system, but owing to pandemic-era difficulties in collaborating on hardware, was largely in generating control software to plan and visualize motion patterns; the relation to the larger body largely being that LAFODIS allows (and requires) the image to be constructed by a series of potentially-uncorrelated samples of sections of the scene - the output of a script which generates both a visualization of the sensor pattern (blue square per exposure) and the commands for the motion system is shown in the midst of a naive full-coverage incremental sweep in 3.21. This bears significant commonality to one of

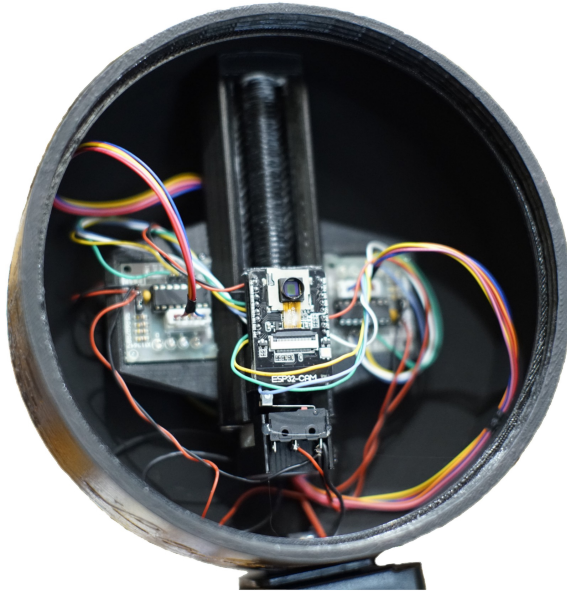


Figure 3.20: The LAFODIS160 polar slow-scan camera

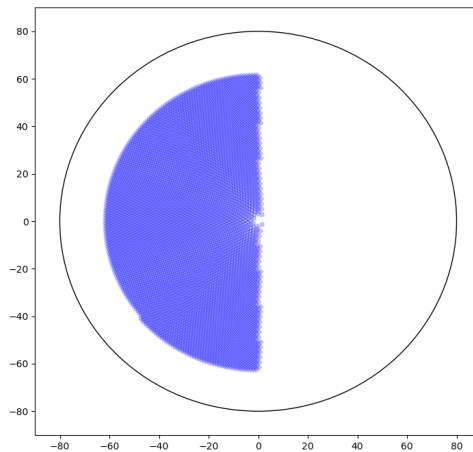


Figure 3.21: An in-progress full-coverage scan for LAFODIS160

the arguments for non-uniform capture behavior; that exposure parameters can be set appropriately for the area of the scene, and areas of the scene with a history of faster-changing content to be recorded more frequently as a way to reduce data rate while maintaining a relatively sound scene model.

Much of the ESP32-CAM work was in collaboration with a series of undergraduate researchers, which resulted in, among other products, a publication “ESP32-CAM as a programmable camera research platform” [73].

Unfortunately, restrictions like the limited memory and slow low-resolution sensor make the ESP32-CAM module entirely unsuitable for anything to do with implementing TDCI or other decoupled capture and integration imaging systems, but they do

enable a wide variety of interesting experimentation on camera systems.

3.14 NUTIK

Based on the relative promise of the early non-uniform model and the greater-than-anticipated distance to an end-to-end testbed, the next research objective turned to integrating the lessons from the Octave-based non-uniform integration prototype 3.11 into the TIK tooling 2.1. This effort is an opportunity to refine ideas developed, improve both the quality and performance of the synthesis process, and generally offer a closer approximation to the proposed functionality.

To this end, a later more sophisticated prototype of a non-uniform exposure system was constructed by attaching an improved port of implementation of the gain masking and function specification system to the rendering code of a version of the TIK Sources, which were cleaned up and adapted to use some OpenCV library code in mid-2022.

This prototype has been termed NUTIK (Non Uniform TIK), and adds support for arguments specifying masks to separate regions for different integration functions, function spec files to specify lists of integration functions mapped to the mask values, and a considerable amount of internal machinery in the rendering process to apply the new features.

These new features are activated with added command line flags; Mask files are specified to nutik with the command line option `-mMaskFile.pgm` and Function files are specified to nutik with the command line option `-kFnFile.fn`, in edits to the front-end code shown in appendix B.

The mask specification has remained more or less stable through all the different iterations of the non-uniform exposure code: an 8-bit PGM image (as PGM reading has been deferred to libraries, ASCII encoded P2 or a binary encoded P5 are both fine), where each gray level is associated with a different function. This allows for up to 256 unique functions to be specified for different portions of the frame. This mask must be of the same spatial resolution as the input steam such that each site has a clearly defined gain. The mask can be created - essentially- by drawing an image with the same spatial resolution as an exposed frame in a conventional image editor. A rendered frame from the source can even be used to to isolate desired correctly exposed features, filling regions with a gray level for each area a different exposure is desired in.

The function specification in this version uses both a different scheme for representing the functions and a different syntax for encoding them. After some experimentation with the original Octave prototype, one of the lessons is that sophisticated functions are not particularly desirable - the simple case is camera-like exposures specified by boxcar functions whose length in X is the duration of the exposure and height in Y is the gain. The decision to use sophisticated interpolation through a series of control points in the first version makes representing boxcar functions difficult, as near-vertical features in higher-order functions or splines tends to produce overshoot, undershoot, and rolled over corners. Therefore, this version performs simple linear interpolation between points, optimizing for the simple case of roughly boxcar

functions, and allowing more complicated functions to be described with more points, potentially by generating them in other software. This is also rather easier to write standalone code for.

The encoding used in this version specifies one function per line, in the format: `Mnn[t0:g0],[t1:g1],...,[tn:gn]` where `nn` is a value 0-255 for the corresponding mask value, each `tn` is a time in ns from the start of the capture, and each `gn` is a gain to be applied at that point, both expressed as a floating point number. Lines not starting with an `M` are discarded as comments.

The points *must* be specified in increasing order by time, such that they describe a function - consideration was given to sorting in software, but even early experiments made it clear that it is better to make mistakes obvious rather than potentially surprising behavior. A simple example of a problem that is easy to make a specification file that will result in unexpected behavior is a missing digit - as times are in ns, it is easy for a human to miss a trailing 0 and place a control point a power of ten earlier than intended, resulting in an unwanted long exposure. It is preferable that this be an error than an unexpected early control point that wildly changes the function. One convenience feature which was added to the NUTIK implementation is that times before the first or after the last control point are assumed to have the value of the first or last control point. This is again an optimization for the common case in which there are only contributions integrated from relatively brief windows, surrounded by extended regions of no contribution before and after.

An EBNF grammar for the specification format is supplied in listing 3.22.

```
/* A cruddy little EBNF grammar to describe my exposure function
   spec files in a formal way*/
/* I intend that any line not starting "M" is a comment, but most
   grammars seem to just ...punt comments to the lexer?*/
Digit ::= '0' | '1' | '2' | '3' | '4' | '5' | '6' | '7' | '8' | '9'
Uint  ::= Digit+
Int   ::= '-' Uint | Uint
Float ::= Int | Int '.' Uint
Tuple ::= '[' Float ',' Float ']'
Fn    ::= 'M' Int '{' Tuple+ '}'
Specfile ::= Fn NEWLINE +
```

Figure 3.22: EBNF grammar of the internally developed language for specifying exposure functions

This format is relatively simple to hand-write, simple to parse, and those same properties also make it relatively straightforward to programmatically generate, with an eye toward using it as an interface for potential future interaction with higher level software.

There are two implementations of this exposure function specification file format, one integrated into the NUTIK codebase for generating exposures as `maskgain.[h,cpp]`, shown in appendices B and B, and another in a support tool for plotting functions.

`FnPlotter.py`, listed in appendix B is a relatively simple Python script which plots all the functions specified in the file as a set of stacked graphs. This is ac-

complished by parsing exposure function spec files into a data structure compatible with the Matplotlib [74] plotting library, then generating a subplot for each specified function. This support tool allows for easy visualization of described functions in a human-readable form.

Another feature considered but rejected for this prototype is the design of an integrated format that contains both an exposure mask, the function specifications, and perhaps even the scene data to be rendered from in a single file. The idea of an integrated format seems appealing as an interchange format and operator convenience, but this argument doesn't seem to hold much weight at this time. There is not a great deal of value in being able to easily move and handle exposure specifications; generally those are expected to working intermediate data - in the sense that a Photoshop psd or GIMP xcf file is typically not the final product for easy exchange, but a format for intermediate work before a final image is rendered. Conversely, sticking to plaintext and pgm images enables easy manipulation of the files with existing tools during experimentation is desirable. The utility of directly handling the native formats in existing text editors, image editors, scripts, and other established software, and leveraging existing user knowledge of that software is quite high.

The bulk of the development in this prototype is dedicated to adjusting the rendering code to follow the function specifications.

NUTIK uses the existing tik infrastructure to render a `.tik` file from an input video stream, then performs function-controlled rendering of output frames from that `.tik` file. This is a command-line conversion tool, called like `./tik Clipname.mp4 ClipName.tik` to generate a tik encoded stream `ClipName.tik` from an input video in any of a wide variety of OpenCV-supported video formats. For metadata inconsistency reasons, the frame-rate and shutter angle of the input can be explicitly specified, as in `./tik -f120 -a180 ClipName.mp4 ClipName.tik`, specifying a frame-rate of 120fps (`-f120`) and a shutter angle of 180deg (`-f180`).

The tik tool is then called again with exposure parameters to generate a frame, eg. `./tik -mMask.pgm -kFnFile.fn -b1 -t0.005 ClipName.tik`. `-mMask.pgm` designates a mask file as described above to spatially map exposure functions, and `-kFnFile.fn` designates an exposure function specification file to temporally map exposure behavior. Currently, the `-b` and `-t` options specifying the start and duration of integration are required. NUTIK *absolutely* should default to only integrating from the input stream for the interval defined by the control point before and after the first non-zero control point in any function in the supplied exposure function spec file. However, both for reasons of enabling experimentation with forcing different overall intervals, and to avoid interactions with other features in the front-end code, the code to do so is currently disabled and the `-b` and `-t` options are still required. The NUTIK branch does print a helpful message `"Control Function live range from [ts,te] expose -bTs -tTe"`, where the `ts,te` are the start and end time in nanoseconds, as in the function specification format, and `Ts,Te` specify the start time and duration of exposure in seconds, as the command line parser expects, to simplify the common cases for different modes.

During this non-uniform integration step, the tik rendering mechanism implemented in `render.cpp`, shown in appendix B adds a number of calls to functions in

`maskgain. [h, cpp]` to determine the appropriate weight to be applied to each output site from the input samples encoded in the tik file.

Contributions from the input tik stream before the changes made to support non-uniform exposure are segmented on the temporal edges of input data, and the output interval. The non-uniform exposure code adds segmentation on the control points specified in the input functions, and those contributions are, and added to the output image weighted by the length of the contribution interval and the average function-specified gain during that interval.

The list of edges on which contributions to an output are segmented is: beginning of output interval, end of output interval, beginning of sample interval, end of sample interval, beginning of gap between samples, end of gap between samples, and integration function control point. Sample intervals and gap intervals can be interrupted by control points in the gain function, and are split on any control point, then handled as two or more intervals with different average gain.

Because non-uniform exposure is not a concept to which a great deal of existing intuition applies, designing input functions and anticipating results is “challenging.” A great deal of diagnostic output, (enabled with the pre-processor directive `#define CHATTY` is present in the non-uniform exposure code to inspect the behavior, and trace the exposure at a specified site in the output frame. This extra output is largely to verify that surprising results are the result of intended behavior rather than any sort of software malfunction.

This provides a tool which can, with extreme flexibility but abysmal usability, expose a frame with up to 256 spatial regions and temporally with a function specified in 256 control points per region from an input scene model captured with a conventional camera. Execution time is generally measured in seconds and scales with the resolution of the image and the duration of the live interval; around 6s for a 640x480 image covering a few tens of input samples. Ideal input is in the form of high frame-rate video, to extract as much temporal resolution as possible into the scene model.

Samples from NUTIK

!!! These examples must be improved, but presenting one to show that this awful thing works!!! With the NUTIK tool in hand, we present a number of examples to illustrate both the functionality of the tooling and new abilities presented by the post-capture synthesis of images using manipulable integration functions.

Shared Center for Sharp Margins

An ideal scene for which a non-uniform exposure tool has a straightforward and desirable property not obtained by any existing practice is as follows. The subject of the photograph is a dancer on a stage doing a solo, with other dancers still moving in minor roles on stage behind them. The subject is spot-lit, and the rest of the stage is relatively dark. This situation is absolutely pathological for existing photographic practices.

Taking a short-interval, moderate-gain image to properly expose the soloist and get a sharp image with little motion blur/artifact, the background will be *irrecoverably* dark and likely noisy. Even if you're willing to digitally manipulate in post, some areas in the background will have received an amount of light below the noise level of the sensor, so no real detail can be recovered. Taking a longer-interval exposure to get detail in the background is problematic because the dancers are all moving and will blur. Taking a higher-gain exposure to get detail in the background is problematic because the soloist will be *irrecoverably* blown out. In many circumstances it's now possible to "cheat" with burst shooting and stacking - but the moving figures will create artifacts when composited, because the center time of the different frames will be non-overlapping. The proposed non-uniform integration method suggests sampling the scene for a period around the desired image, then computationally integrating different areas *independently* with different time and gain to allow features. Because the intervals are set computationally after the fact, they can overlap, preventing edge artifacts. Each area of the image (as dictated by a user-generated map) can be exposed optimally, rather than having to select a compromise parameter for the whole scene or stitch from a range of pre-set guesses.

This lurid dinosaur being shaken violently in front of the lab machine room window will temporarily stand in for this case. (!!!THIS IS UNSUITABLE BUT JUST FILLING IN AN EXAMPLE EXAMPLE, ALSO NOT ALL THE PIECES HERE MATCH!!!).

Capture using the 120FPS high speed video of a Nikon Z6 III, then cropped to 640x480 to center the subject before tik encoding. Tik encoding via `./tik -v OrangeDinoCropTrim.mp4 orange.tik`, then exposure via `./tik -m./Half.pgm -k./HalfFn.fn -b7.415 -t0.005 orange.tik`

The supplied exposure function specification file `HalfSharpFn2.fn` is shown in figure 3.23, also shown graphically in figure 3.24. Note that both of these functions are boxcars, they are centered on the same time, and are roughly reciprocal: one is twice as high, and one is twice as wide (!!!they aren't and it isn't!!!). The two defined regions of the image to be exposed with the specified functions are defined by 3.25.

The resulting exposed frame is shown in figure 3.26. The shorter, higher gain function produces a sharper

```

M0
  {[0:0],[1904999999:0],[1905000000:1],[1925000000:1],
    [1925000001:0],[3000000001:0]}
M128
  {[0:0],[1899999999:0],[1900000000:0.75],[1950000000:0.75],
    [1950000001:0],[3000000001:0]}

```

Figure 3.23: HalfSharpFn2.fn

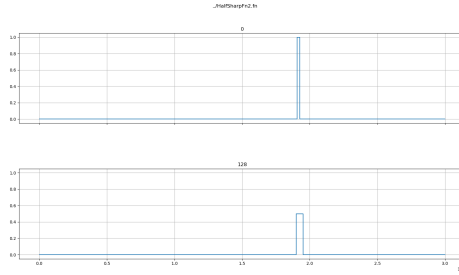


Figure 3.24: Visualization of HalfSharpFn2.fn



Figure 3.25: Half Mask



Figure 3.26: Rendered Frame

A Negative Gain

!!! Surely I can contrive a better sample, but I rendered placeholders with the desired functions from an on-hand tik file !!! As an example of negative gain's utility for feature extraction, consider this exposure rendered from the same input as the previous exposure, using only a single function which makes a positive $1/30s$ exposure with gain 1 surrounded by $1/60s$ exposure with gain -0.5 to either side, all occurring

1.5 seconds into the sampled interval. This exposure is described by 3.27, which is visualized as a graph in 3.28. This single function is tagged 0, so a black frame of matching resolution is supplied as the mask, to indicate it should be applied to the entire scene. The negative intervals to either side of the positive interval *remove* the light contributions from those intervals, magnifying the specific differences at the exposed instant from its surroundings.

This function is then exposed by calling NUTIK as follows: `./tik -m../AllZero.pgm -k../FeatureExtraction.fn -b1.500000 -t0.083331 OrangeFast.tik`, resulting in the “diff” frame shown in 3.29. While the total subtracted interval is less than the added interval, the gain is slightly lower, leaving a desaturated image of the static features, but strongly exaggerating the changed regions.

```
MO{[0:0.0],[1500000000:0.0],[1500000001:-0.5],
    [1516666000:-0.5],[1533332000:1],
    [1566665000:1],[1566665001:-0.5],
    [1583331000:-0.5],[1583331001:0.0],
    [3000000000:0.0]}
```

Figure 3.27: FeatureExtraction.fn

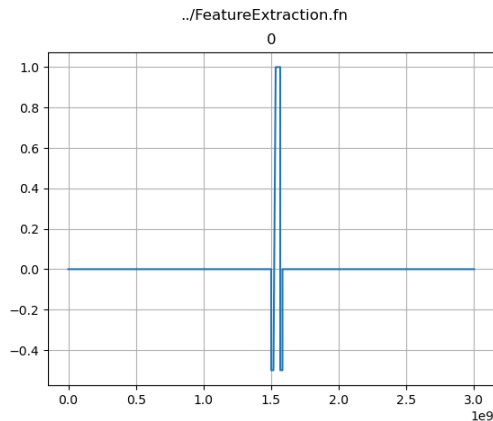


Figure 3.28: Visualization of FeatureExtraction.fn

A Time-Varying Gain

!!! One more "Do a trick", filler from an image on hand pending composing a nicer demo!!!

To demonstrate a behavior which is wildly unrealizable in conventional cameras, a frame in which the top and bottom halves have their gain ramped in opposite directions during the exposure interval. The function in 3.30 describes a 2/30 second exposure starting four and one third seconds into the interval. For the top half of the frame, gain is ramped from -0.75 to 2.5 , while the bottom half ramps from 2.5 to -0.75 over the same interval. The function is shown graphically in figure

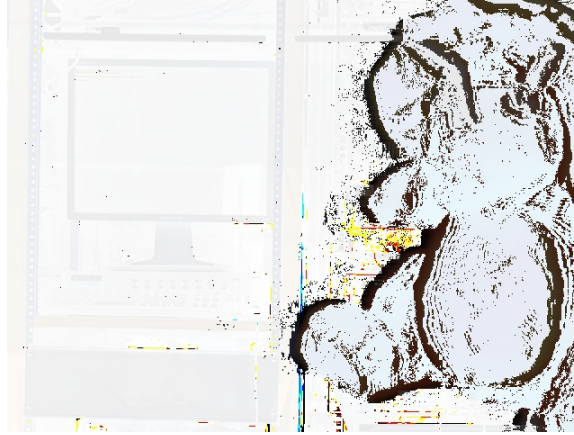


Figure 3.29: Rendered Frame showing exaggerated differences

3.31, the split halves in figure 3.32. NUTIK is called with `./tik -m../VHalf.pgm -k../RampFn2.fn -b4.03 -t0.06666 OrangeFast.tik` to render the image in figure 3.33.

This essentially describes splitting the sensed area in half and dynamically changing the ISO setting for the two halves during the period of exposure. It is wildly unlikely this exact behavior would ever be desired, but it serves to demonstrate the generality of the method.

```
M0{[4000000000:0] , [4033333332:0] ,
    [4033333333:-0.75] , [4099999999:2.5] ,
    [4100000000:0] , [5000000000:0]}
M128{[4000000000:0] , [4033333332:0] ,
      [4033333333:2.5] , [4099999999:-0.75] ,
      [4100000000:0] , [4500000000:0]}
```

Figure 3.30: RampFn2.fn

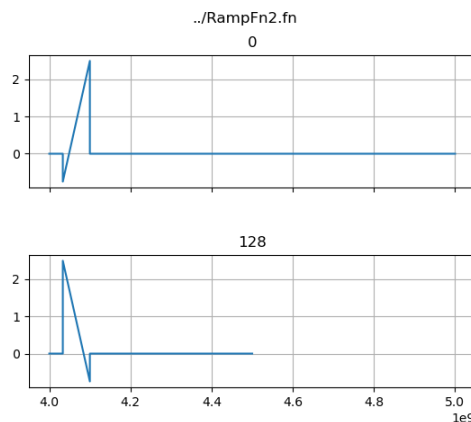


Figure 3.31: Visualization of RampFn2.fn



Figure 3.32: Vertical Half Mask

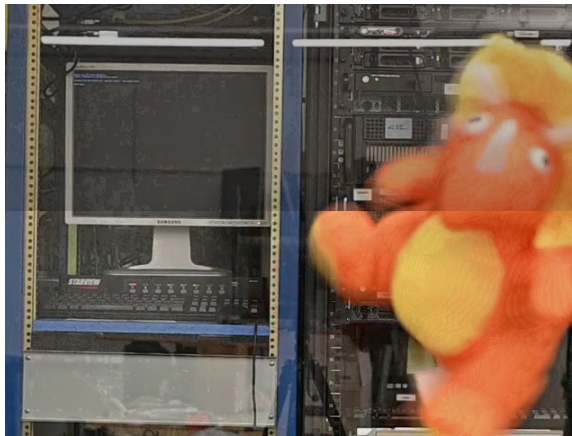


Figure 3.33: Rendered Frame showing the effect of ramp functions

Improvements for NUTIK

Quite a number of improvements to further enhance the NUTIK prototype present themselves.

The major category is helper utilities to ease the creation of suitable masks and exposure functions. These tasks are currently quite laborious. Exposure functions in particular are also rather mentally taxing to design, as they represent a degree of freedom for which there is no analog in other practices.

The addition of helper utilities to allow graphical click-and-drag creation of function specification files would improve the user experience and lower the barrier to entry to setting up a development. Supplanting a visual tool with a library of examples to help tie functions with useful - or at least aesthetically interesting - effects would further improve the utility of visual representations of functions.

Helpers for generating useful masks could also be constructed relying on contemporary imaging technology. The same foreground-isolation methods used for features that typically carry names like “blur background” or “portriat mode” could instead be used to generate a mask separating foreground and background features, allowing

selected foreground objects to be easily exposed differently than their surroundings.

On the programming front, the NUTIK code was developed to with the principle of not introducing any inessential complexity to the prototype, and this carries a variety of potential performance implications.

Determination of the weighting of each sample contribution involves a chain of dependent memory lookups; the gain depends on the ending control point in the function, which depends on the beginning control point in the function, which depends on the mask value for the location. Dependent memory fetches are potentially extremely slow on most computers, but the size of the data structures in question is such that architectural caches should largely hide the problem. Smaller less sophisticated host processors as found in embedded systems tend to feature memories which are faster *relative to the processor*, so these concerns would not be exaggerated in embedded implementations, as onboard a camera. Adjacent output locations tend to be exposed by the same function, so adding simple caching to the **weightherebetween** and/or **gainherenow** may offer some low-hanging performance gains. Each of the lookups above are also currently implemented as forward linear searches; switching to a more efficient search algorithm is, in principle, a drop-in local change with no inter-function implications.

Fortunately, empirically the non-uniform exposure changes add less than 2% to the execution time of earlier tik versions supporting only uniform exposure, making these performance concerns not a pressing issue.

Improving the performance of the base TDCI processing in TIK should also be relatively straightforward; like most image processing problems, rendering an output image from input samples is embarrassingly parallel across the spatial dimensions and color channels of the output image, and easily decoupled across time dimensions. This means that, if someone were foolish enough to try, it should be as straightforward as any parallelization ever is to map the loops that walk the image locations and color channels to parallel-for type constructs which would execute efficiently in stripes or patches across a large number of independent cores or even - as the operations for each site or channel chiefly only differ by data - SIMD hardware.

Temporal resolution of the NUTIK tool could be improved by incorporating the temporal super-resolution from shutter behavior techniques proposed in 2017 in “Temporal super-resolution for time domain continuous imaging” ??, but this would substantially complicate the computation of both sample contributions and gains.

Chapter 4 Discussion

!!! Citation for the market slide from film to digital!!!

Much of this work has been an exercise in exploring the degree to which digital cameras are *simulacra* of film cameras. Though the super-majority of the photographic and cinematographic market has shifted from film to digital sensors, storage, and processing, the devices, practices, and tools have remained firmly anchored in practices derived from film cameras. Rather than being superseded by digital cameras designed *as digital cameras*, film cameras have been supplanted by digital cameras and tools that go out of their way to simulate their film predecessors.

4.1 A Better Way To Use a Digital Camera

Crutches like the “Sunny 16 Rule” - an alliteratively convenient aphorism whose origins appear lost to time stating that “On a sunny day set aperture to f/16 and shutter speed to the reciprocal of the film speed for a subject in direct sunlight.” - are effective for allowing a human to quickly estimate a reasonable exposure given a few fixed parameters for an entire scene at time of capture, but that is not the circumstance under which modern photography occurs.

For much of their history cameras have been increasingly automated. Photoelectric light meters integrated into the camera body and coupled to the exposure mechanism became common by the 1930s, with cameras like the Contaflex (1935) and Super Kodak Six-20 (1938). These devices are simple averaged-intensity meters with simple couplings to the operation of the camera, but allowed the operator to at least partially defer to automation. Microprocessors appeared in consumer cameras long before digital sensors - in the mid 1970s products like the Canon AE-1 (1976) [75] consolidated some of the profusion analog electronic and clockwork mechanisms for camera automation into a single IC as one of the early applications of microcontrollers. Within a few years, the now familiar so-called “PASM” (Program, Aperture Priority, Shutter Priority, Manual) [76] control scheme for expressing user priorities to a computer agent emerge with the Canon A-1 (1978) and have remained more or less remained a constant in the “more serious” camera market segments since.

Not only are most cameras equipped with some form of integrated sensors and computer controls which combine the sensor data with some indication of user intent to actually drive the camera mechanism, modern digital photography almost always has an embarrassingly powerful computer in the loop with the main sensor data which can easily make specific, localized decisions about exposure. In particular, modern mirrorless cameras are continuously sampling and processing the output of the sensor - the screen or EVF (**E**lectronic **V**iew **F**inder) is sampled, processed, automatically exposure controlled stream. Furthermore, the gain of the captured image is not a static feature. Where with photosensitive emulsion film the gain is set for the entire scene long before the exposure when the film is loaded into the camera, in a digital camera the gain can not only be altered on the fly, it can be altered - at least to a

degree - *after the fact* with no apparent loss of image quality, and in principle set differently for different parts of the frame, though few cameras expose much control on that front. Thus a key lesson from this work is that photographers should consider a different paradigm for setting exposure, aiming to expose to *capture the maximum amount of scene data* rather than to capture a pleasing image, then generate the desired integrated frame after the fact by applying digital processing to the gathered scene data. The feature to optimize on in this paradigm is to minimize the number of sensels which are out of range in the scene - the scene information gathered from a sensel which is (within noise level of) saturated or (within noise level of) black is much lower than information from a sensel which is anywhere within its range, no matter how badly exposed.

4.2 Capture, Then Integrate

A major suggestion from this work, like previous studies into TDCI, is that there should be a decoupling of capture and integration. In film photography, the gathering of incident light and because the process by which the scene information is absorbed is the same photochemical reaction that renders at least an intermediate image (a film negative). Digital cameras are currently operated under the same regime, but the capture and integration processes are not inherently linked. Deferring integration

The main challenge to separating the capture of a scene model or record of incident light for each point in the scene is managing the data-rate. More sophisticated sensor readout schemes with faster, more numerous ADCs to read out the sensor, and faster, larger memories in cameras all contribute to the feasibility of such a system, but do not solve the problem entirely. Emerging alternative read-out regimes, like most event cameras, tend to suffer from information loss due to “swamping” in the event of correlated motion producing events exceeding their readout bandwidth. The TDCI method of recording second derivatives - changes to the rate of change - of incident light, clipped by a noise-model-aware threshold is extremely promising, but still far from credible hardware implementations. Fortunately, the specific details of how the data-rate to support capturing a continuous scene model are independent of the idea that that separation brings benefits.

The benefits of this separation are substantial. Recording a scene model defers the decision about exposure parameters until after the time of capture. Many photographs are spoiled by failing to correctly estimate the correct timing, duration, and gain for exposure under particular lighting conditions. In a simple example, trying to photograph a young child running presents the photographer and/or their computer agent in the camera with an array of parameters that separate a delightful image from something unusable. A small change to exposure time separates a delightful picture of a child running from a tragic picture of the child falling to the ground. A small change to exposure interval or sensitivity separates clear rendering from a blown-out or dark and grainy frame. Conventionally, all these decisions must be estimated at least approximately correctly before the instant to be photographed.

Deferring those choices allows the photographer to not only carefully select parameters at their leisure, it allows them to virtually re-expose the same scene an

arbitrary number of times and examine the results until the desired result or results is obtained. Furthermore, the gain and interval of integration is not constrained to a single value for the entire frame; portions of the frame can be arbitrarily exposed with different times and effective sensitivity to obtain desired results which may be out of reach of the dynamic range of the recording sensor device.

As an example a scene with a dim field and a fast-moving but more brightly lit subject presents a problem for traditional photographic practice. This is not an uncommon situation; for example, a moving performer under a spotlight presents exactly this situation. ISO and exposure interval set to properly expose the subject will not only underexpose the background, there will be visible noise in the below-noise exposure. ISO and exposure interval set to avoid a dark, grainy background will leave an excessively bright subject with significant motion blur.

In a decoupled, non-uniform exposure scene, instead of attempting to produce an appropriate image on the fly, the photographer instead captures the incident light during the desired interval. Later, they can use the record of incident light to assemble - for example setting the interval of integration such that the subject is properly exposed with the desired amount of motion blur. They can also *independently* determine a set of exposure parameters which will expose the background properly with a minimum of noise. Finally, they can mask off the regions of the image and generate an exposure using the two functions for different areas, but using the records of incident light centered on the same instant.

A similar trick can almost be performed to a degree with burst shooting, but that doesn't allow the intervals for the differently integrated regions to overlap in time - a serious problem if, for example, the subject is moving.

Even stranger things are possible; the gain doesn't have to be positive - it's perfectly possible to subtract the light gathered during an interval from the light gathered in another. Subtraction is useful for isolating features - particularly differences from the average of a period.

4.3 Violating Assumptions Makes Everything Harder

This work violates a number of deeply-held assumptions across a number of concepts, and many of the challenges derive from the tendency that the more foreign something is, the more difficult it is to integrate with existing technology. The *variety* and *magnitude* of those violation was not clear until a deeper investigation, and a direct discussion of some of those assumptions and how they became rooted is worth having.

The first, most obvious, and deepest violation is that the vast majority of other imaging technologies are frame-oriented, while this work treats time (and gain) as continuous dimensions. In the discussion of mechanical shutters and emulsion photography, it's clear where photographers obtained that assumption: the use of APEX shutter and film speed graduated by doubling and halving in order to make exposure calculations tractable for a human operator impose a consistent, discrete scale on both, and that assumption is deeply ingrained into professional practitioners. Likewise, mechanical movie cameras operate on series of frames of film exposed for

consistent pre-determined intervals - the entire concept of shutter angle is premised on a mechanical method for discretizing frame rate and exposure intervals.

Early digital photography carries over many of those assumptions simply as a matter of practice and technique, and those assumptions were baked into software tools for manipulation of digital images. Interestingly, digital *video* encoding tends to have a continuous-time component; motion compensation is applied as a form of compression to allow many frames to be derived from a single complete reference/key frame by recording changes from the reference rather than complete frames, an offshoot of ideas about Scene Constancy and Optical Flow discussed earlier 2.5. This would seem to imply a degree of non-frame-oriented fundamentals in digital video, but, as a historical quirk, those properties are blackboxed to the greatest degree possible.

The H.261 [77] video encoding standard which evolved into MPEG-1 video encoding in 1992 [78] was the first practical, widely deployed video encoding standard relied, as most compressed video formats do, on a mixture of discrete cosine transforms and motion compensation for compression. General purpose computers at the time of its adoption were incapable of real-time encoding or decoding of compressed video, and lacked the working memory to operate on more than a few frames at a time, so the entire encoding/decoding process was performed via offload to dedicated special-purpose hardware which returned frames. As a result, almost all tools built to work on video had not only the legacy inertia of film oriented thinking to make them frame-oriented, they also had an architectural constraint of their own that led to a similar design. This is no longer the case; video encoding/decoding is often done in software, on machines with plenty of RAM to operate on large segments at once, but the separation of the optical-flow storage format and frame-oriented exposed format persists. Given that almost all video formats operate in the optical-flow domain for storage and transmission, it would be nice to edit directly in that context instead of by decompressing a section into a frame then re-compressing - analogous to long-standing work in Homomorphic encoding.

In an even deeper, broader form, humans - at least culturally - don't tend to think of time as a continuous dimension. We talk about discretized time - seconds, nanoseconds, intervals - but don't even have language to discuss time as a continuous phenomena the way we discuss spectra for frequency ombré for color.

4.4 Changes in Cameras

Much of the content earlier in this thesis has been devoted to discussing changes in camera technology, and how various assumptions have persisted despite the decline of the technologies they were grounded in. Using the same lens, it makes sense to look at current trends in camera design, both to see which assumptions they might violate or reinforce, and to see how they might interact with the proposed design of cameras that operate on non frame-based capture and post-capture synthesis.

The Rise of MILCs

One change we are toward the end of which seems to be informed by an effort to transition from a film-oriented to sensor-and-computer oriented camera design is the gradual transition from SLR (Single Lens Reflex) digital cameras to MILC (Mirrorless interchangeable Lens Camera) designs.

The design of Digital SLRs were very much designed according to analogy to film - the separate optical path for the viewfinder and sensor accomplished by a mirror is logical when you have an optical viewfinder through which the operator sets up focus and exposure before exposing a photochemical surface, but makes little sense in a digital camera, where keeping the sensor and therefore the computer managing it in the loop to perform functions like automatic focus and automatic gain control is an obvious benefit. !!!Market Share Citation!!! In the last 15 or so years - counting from the introduction of the Micro Four Thirds ecosystem in 2008, the Sony E-mount and Nikon 1 systems in 2010, and a number of similar products from the other major camera vendors in the following years - the camera market made an exponential shift from SLRs to MILCs.

A number of other compromise technologies between the SLR and exposed-sensor designs have been attempted, most using a “pellicle mirror” which beam-splits the incident light. These are relevant mostly in that they indicate a preexisting desire for two features of the MILC design: operating sensors on the light projected by the main lens, and avoiding the delay and inertia introduced by a moving mirror in SLR designs. Pellicle mirrors were used in a number of pre-digital cameras to split the image projected by the lens for color-separation cameras, for use in a metering device (as in the Canon Pellix from 1965), or to keep the viewfinder lit during shooting and avoid the delay and inertial kick from mirror movement (as in later canon products like the EOS RT from the late 1980s).

In a digital context, around the same time as early MILCs, a competing technology was briefly attempted that took a more compromised approach to combining conventional SLR designs with keeping the main sensor in the loop by using a similar approach to the Pelix design: between 2010 and 2016 Sony released a dozen “SLT” (Single-lens translucent) cameras which used a partially-silvered mirror, splitting light between the main sensor and - rather than a viewfinder for the operator, which was instead provided by an electronic view finder fed by the main sensor - a set of dedicated phase-detect autofocus sensors. These appear to have died out as there are not currently any on the market, most likely because it became preferable to computationally infer the features the sensors were used to detect from the data stream of the main sensor, or to simply embed additional sensing elements in an MILC design.

Many early forays - like the Nikon 1 - attempted to position an MILC line with a small sensor as a “bridge camera” between small inexpensive consumer cameras and professional SLRs, which did not go particularly well. However, MILCs aimed higher in the market - such as the Sony EF and Nikon Z ecosystems with larger sensors and more sophisticated controls - have largely overtaken the former SLR market.

This is a clear example of a gradual transition from a Film-oriented philosophy to designing native digital cameras.

Upcoming Changes in Cameras

Some changes currently happening in the camera market have a significant bearing on the applicability of this kind of non-frame-oriented sample-then-integrate technology.

Several “exotic” camera technologies lend themselves extremely well to this paradigm. In the preliminary research for this work, QIS sensors were discussed as a related work to precursor TDCI designs. In the interim, several developments have made QUS an TDCI even better suited to each other. Experimental QIS sensors have scaled out to relatively resolutions, as with the 163 megapixel number-resolving (pixel counting) active pixel QIS sensor design from 2022 discussed in [79].

This sensor operates on exposure times of around $100\mu\text{S}$ to 1mS . This extremely short exposure is because the cells have a quantum efficiency of around 70% in the visible band, and each cell saturates in around 5000 e^- , making it largely limited by saturation. Also problematic, even with 66 400MSPS LVDS lanes to transfer data off-chip, the bandwidth of the readout system in the presented design limits the sensor to around 7.5FPS at full resolution - too low a frame rate, or more importantly shutter angle, to be directly useful for reprocessing with a tool like TIK.

A TDCI model, however, has several things to offer to this line of development. Adopting a TDCI model for the already sophisticated on-chip readout system would squash redundant samples unchanged from exposure to exposure, allowing for more efficient use of the off-chip bandwidth, and thus increase frame-rate in a frame-oriented readout mode. Because their readout scheme is already ramp-function driven and their saturation intervals are short, it would also be well suited even deeper application of a TDCI model with an uncorrelated read out mode that natively generated a TDCI model.

The function driven integration that is the focus of this thesis would also allow such a sensor to simulate exposures longer than saturation limits. Integrating at low gain would allow the rendering of long virtual exposures with characteristic visual effects suggesting motion from combinations of the very short saturation intervals, and doing so selectively would allow absurd linear dynamic range of hundreds of thousands to one.

Recent trends in more conventional camera designs also have bearing on the applicability of TDCI technology and the imaging model proposed in this work.

Using the Sony A9 III [80] as an example, the addition of ever-faster readout schemes with more independent ADCs and larger high-speed on-package memory are certainly advantageous to the construction of TDCI-like cameras.

The larger arrays of more ADCs should be helpful in implementing TDCI-like readout schemes as not relying on single ADCs for reading out large rectilinear sections of the frame comes closer to the requirements for performing non-correlated readout, though there is no indication that the firmware would be any more conducive to being driven in such a way.

For large, fast buffers, the A9 III in particular claims “1.6 seconds of 120fps photography at 14-bit Raw quality” and those are 24MP frames, implying approximately 7.5GBytes of buffer which can be filled as fast as it can be exposed and read out. This large buffer would provide plenty of room to store the several frame-sized intermedi-

ate components of a TDCI model, avoiding many of the memory-pressure concerns that pervaded the extensively studied cameras, and in particular the EOS M.

Another emerging feature typified by the A9 III is the addition of global shutters in cameras with competitive image quality has mixed implications for TDCI-like technology. On one hand, these global shutters lean in to the frame-oriented assumptions and make the presumed correlation of the readout even more true. This prevents the sort of structured shutter estimation that allows post-processed TDCI schemes to get finer time-granularity [18], but aren't as helpful for a naively non-frame-oriented camera readout scheme. On the other hand, global electronic shutter implies the ability to dump the entire sensor in parallel, apparently in analog form into a second diode used exclusively as a storage element [81], a hardware feature which would be conducive to implementing a TDCI-type continuous readout mode.

Without any changes inside the camera, the ability to generate extended high-quality high-framerate video makes excellent fodder for reprocessing by tools like tik.

Most Cameras are Phones

Cameras being wiped out in favor of phones, which are worse cameras with smaller sensors and limited optics... but better computers. TO make these devices more effective, the market is becoming quite comfortable with cameras that do a considerable amount of processing between the sensor and the resulting image. Many cell phones now support features like “portrait mode” which uses selective computationally applied blur to simulate shallower depth of field than achievable with little to no aperture control. Likewise, many consumer devices now synthesize their output from several cameras. The Light L16 [82] was an exercise in taking this technology to the illogical extreme, cramming 16 camera modules with different sensors and small lenses into a single device, then controlling them in concert and merging the output to allow computational alterations to zoom and exposure. Though the Light L16 failed on the market, variations on the technology are present in most high end cellular phones for years, typically operating on a cluster of 2-4 cameras with optics of different focal length.

Manufacturers now even argue that there are “No Real Pictures” as Samsung’s Patrick Chomet recently claimed [83] in a press release, some time after Samsung was caught injecting artificial detail from training images into pictures of the moon [84]. Thus, many user-facing cameras are no longer operating in a genuinely frame-oriented mode, synthesizing image from assembled scene data across multiple sensors, times, and possibly just making probable content up from random image data in the tools’ training set, and there is a large amount of on-device compute available to facilitate these things. Working toward a cohesive paradigm for computationally driven, non-frame-oriented imaging that fully leverages its potential and allows for honest evaluations of veracity rather than constructing it piecemeal from hacks seems like a desirable end-goal.

In the Hands of Users?

An obvious question for work of the kind presented here is about if and how the findings might impact users. I do not have a crystal ball for how the market will proceed, particularly on matters of adopting technologies where technical merits rarely seem to be the deciding factor, but there are some reasonable guesses.

The first is that there will be a large number of partial solutions which move toward the the mode of operation suggested in this thesis while avoiding any fundamental changes to the stack or mindset.

Some of these are matters of technique. Without any additional technologies integrated into the software or hardware, sophisticated users will develop a better sense of what can and cannot be fixed in post processing in the output of digital cameras. For example, whether or not it is an explicit change to education or an observation from experience, photographers practices will likely shift toward preferring exposures that minimize clipping rather than produce aesthetically exposed images, as there is little to no quality penalty to making minor exposure adjustments in processing, but

Others are approximations that do not fully violate frame oriented assumptions. These include a variety of hacky alternatives already in use, like using relatively fast burst shooting under automatic computer control - as enabled by exposed sensors and large buffers - to perform exposure bracketing, exposing a set of images which are then composited - either automatically or under operator control -into a high dynamic range image, where the differently exposed scene elements are drawn from temporally distinct frames rather than generated from a shared sampling interval. In the limit, automatic exposure bracketing and HDR compositing is rather akin to TDCI - the slices of gathered light get infinitesimally fine, and the temporal alignment of the constituent parts becomes not only potentially exactly on the same instant, but arbitrarily controllable.

Other methods that integrate data from several frames - as with focus stacking, from elsewhere in the frame - as with healing tools, or simply synthesize features - as with "AI Enhancement" are also becoming rather common. One thing that could separate these techniques is that there is (or should be?) some kind of distinction between "substituting data from a different place or time in the same scene" and "Substituting random data from the internet" that does not seem to be widely drawn right now.

Secondly, it seems likely that most users interacting with digital-native cameras with extended ability to manipulate time and gain will never know that is what is happening internally. In the same way that most photography is done in some variety of "Intelligent Auto" for photographic parameters, and much of the software to manipulate the photographs performs "automatic enhancement" by tweaking levels, adjusting white balance, etc. the most likely widespread adoption of a camera system which samples light and synthesizes images will be hidden inside of an automatic tool of this sort, perhaps with limited, parameterized controls exposed to the user to hint the automation. A crude mock-up of such an interface is shown in 4.1

Finally, it is entirely plausible that we will eventually get fully-realized digital-native camera systems which operate more or less like the systems proposed here,



Figure 4.1: A mockup of a limited UI for re-timing a frame from a scene model

by sampling light then computationally constructing images from the samples with adjustable timing and gain under full user control. The timeline for the emergence of such devices, and whether anyone currently involved has their hands in it as more than an obscure footnote is an open question.

Continuing with the analogy to Ren Ng’s refocus-after-capture plenoptic digital camera technology alluded to elsewhere in this document, Ren Ng’s thesis did (with the advantage of a century of theoretical precedent and 20 years of more closely aligned prior work) for focus what this thesis is attempting to do for exposure. That technology was the basis for founding Lytro. \$140M of Venture Capitalist money, two commercial products, and a decade later they failed because the tech was offbeat and hence janky and weird, and photographers don’t like things that interfere with their long-established practices. Unlike plenoptic cameras, the TDCI-derived decoupled capture and integration methods discussed in this work do **not** inherently ask the user to accept a loss of spatial resolution in return for ability to repeatedly manipulate parameters post-capture.

Chapter 5 Conclusion

The most interesting observation in this work is about the enormous power of local optima. The last area I was working in was computer architecture, and that is a field completely dominated by a local optima: Von Neumann machines implemented as out of order superscalar designs, where all the local scheduling is accomplished by a little heuristic JIT executing microcode. There have been a few forays away from these designs, but principally, we're stuck.

Frame-based imaging is in an even deeper local optima that, essentially, no one outside academic curiosity has even taken a shot at moving away from. The frame-oriented practices around cameras have firm historical roots; in the context of photosensitive emulsion film there is little choice in the matter. Likewise, the exposure practices built around film in manually-operated cameras were necessary to make exposure computation practical for human operators with fixed-sensitivity film, and those practices were readily adapted to cameras containing sophisticated electronic automation.

As digital sensors began to replace photosensitive emulsions, the obvious method for designing cameras is to directly adapt the designs and practices established for film cameras. Even early digital video systems lean into the frame-oriented paradigm as those assumptions provide an easy way to separate computational concerns, offloading compression and decompression that the general purpose computers of the day were not fast enough to perform in real time onto special-purpose hardware, while allowing techniques developed for film cameras to be executed on individual frames.

However, in doing so, several desirable properties readily achievable with computer managed digital sensors were hidden. Some of these have been noted and slowly adopted, as with the move toward MILC cameras which continuously expose their sensor to allow the enormously powerful onboard computer to compute shooting parameters from the live data stream. Others, like the possibility of spatially or temporally non-uniform sensitivity and exposure, are still largely unattainable because of lock-in around those film-oriented assumptions.

The lock in remains *deep* because decades of operating under film-derived frame-oriented assumptions have specialized the design of cameras and software tools for that paradigm. Unfortunately, the depth of frame-oriented assumptions is such that *violating* those assumptions renders any tooling built without those assumptions incompatible, and turns such work into a vast exercise in perservation.

At the end of a several year exploration into the space, and despite the lack of a complete end-to-end prototype, this thesis hopefully provides a convincing argument that working out of the local optima toward digital native cameras with capture decoupled from flexible integration is both desirable and achievable in the current technological context.

Appendix A Non-Uniform Proof Of Concept: Matlab Prototype

Listing A.1: NonUniformPoC.m

```
# A simple tool for applying non-uniform gain to integrating a
series of image data
# Makes a normal cubic spline based on user-supplied control points
to model the gain function for each region
# Applies the average gain for the frame interval sampled from that
integration function
# Selects gain functions based on a set of regions specified as an
input-sized pgm with one gray per region/function.

#### This part is setup ####
#Image Input Setup
fr=(1/240); #framerate of input sequence, in seconds (not sensed,
video package broken on 5.x)
path="20190930_205109.mp4"; #Path to source file

#Read in an appropriate user-created mask
mask=imread('PenguinRockMask.pgm');
mask=cast(mask,'double');
#Mask values defined in the mask
# would be better to get from mask automatically,
# but I keep seeing border pixels w/ garbage
gray=[255,128];
fns=length(unique(gray));

#Integration Functions Setup
pts= [100, 200];
x=0:(max(pts)-1);
y=zeros(fns,max(pts));
y(1,1:pts(1))=y=[0 0 0 0 0 0 0 0 0 10 30 50 30 10 0 0 0 0 0 0 0 0 0
0 0 0 0 0 0 10 30 50 30 10 0 0 0 0 0 0 0 0 0 0 0 0 0 0 0
0 0 0 0 0 0 0 0 0 0 0 0 0 0 0 0 0 0 0 0 0 0 0 0 0 0 0 0
0 0 0 0 0 0 0 0 0 0 0 0 0 0 ];
y(2,1:pts(2))=[0 0 0 0 0 0 0 0 0 0 0 0 0 0 0 0 0 0 0 0 0 0 0 0 0
0 0 0 0 0 0 0 0 0 0 0 0 0 0 0 0 0 0 0 0 0 0 0 0 0 0 0
0 0 0 0 0 0 0 0 0 0 0 0 0 0 0 0 0 0 0 0 0 0 0 0 0 0 0 0
0 0 0 0 400 0 0 0 0 0 0 0 0 0 0 0 0 0 0 0 0 0 0 0 0 0 0 0
0 0 0 0 0 0 0 0 0 0 0 0 0 0 0 0 0 0 0 0 0 0 0 0 0 0 0 0
0 0 0 0 0 0 0 0 0 0 0 0 0 0 0 0 0 0 0 0 0 0 0 0 0 0 0 0
0 0 0 0 0 0 0 0 0 0 0 0 0 0];

#### End of configuration ####

#changem cribbed from,
# https://stackoverflow.com/questions/11952037/replace-values-in-
matrix-with-other-values
# because I'm not using a commercial toolbox for this
function mapout = changem(Z, newcode, oldcode)
```

```

% Identical to the Mapping Toolbox's changem
% Note the weird order: newcode, oldcode. I left it unchanged from
  Matlab.
  if numel(newcode) ~= numel(oldcode)
      error('newcode and oldcode must be equal length');
  end

  mapout = Z;

  for ii = 1:numel(oldcode)
      mapout(Z == oldcode(ii)) = newcode(ii);
  end
end

#Show the integration functions (comment to hide)
for dfs=1:fns
    figure(dfs);
    xspline=0:0.01:pts(dfs);
    yspline=spline(x(1:pts(dfs)),y(dfs,1:pts(dfs)),xspline);
    ylabel("gain");
    xlabel("fractional time");
    plot(xspline,yspline,"g-",x(1:pts(dfs)),y(dfs,1:pts(dfs)),"b+");
endfor

#Have ffmpeg process video for frames
# In a better world, I'd use the video package, but it's currently
  broken on 5.x
# https://savannah.gnu.org/bugs/?51344
# That would give automatic frame-rate extraction, but nooo
##ffmpegline=["ffmpeg -i ", path , " -vcodec ppm img%03d.ppm"]
##system(ffmpegline);

t=0; #time
fc=0; #number of frames ingested, maintained seperately because I'm
  lazy
sumimg=0;

#for each input image
files = dir('img*.ppm');
numimg = length(files);
texp = fr*numimg;
for file = files'
    #read in image
    img=imread(file.name);
    #Promote for range
    img= im2double(img);
    #compute gains for that frame
    for gfs=1:fns
        #Still don't quite touch the last control point
        gain(gfs)=( ...
            interp1(x(1:pts(gfs)),y(gfs,1:pts(gfs)),(t/texp)*(pts(gfs)
                -1.01),"spline") + ...
            interp1(x(1:pts(gfs)),y(gfs,1:pts(gfs)),((t+fr)/texp)*(pts

```

```

        (gfs)-1.01),"spline"))/2;
    #printf("Frame %d gain %d\n", fc, gain);
endfor
#apply to frame

gainmask=changen(mask,gain,gray);
imgmod=img.*gainmask;
#add frame to sum
sumimg=imgmod+sumimg;
fc=fc+1; #increment frame count
t=t+fr; #increment time
endfor

#Divide by number of frames
finalimg=sumimg/fc;
#cleanup
##delete img*.ppm;
#save and display rendered image
imwrite(finalimg,"result.ppm");
figure(gfs+1);
imshow(finalimg);

```

Appendix B NUTIK parts

Listing B.1: MaskGain.h

```
/* Header for adding temporally and spatially non uniform
   integration support to tik*/

#include <limits>

#define MAXLINE 1000
#define MAXPTS 20

typedef struct{
    double time;
    double gain;
}point;

extern point fns[256][MAXPTS]; //Points per function
extern int fnc[256];
extern Mat mask;

//Declare the functions

int readMask(char * maskfile);
int readGainFns(char * gainFnFile);

void dumpGainFns();

double nextControlTime(uint32_t where, double now);
double gainherenow(int where, double now);
double weightherebetween(uint32_t where, double start, double end);
double FirstLive();
double LastLive();
```

Listing B.2: MaskGain.h

```
/*Awful hacks to add approximate nonuniform integration to tik*/

#include "tik.h"

#define CHATTY 0

// These will usually be sparse, but the structure isn't large
   anyway
point fns[256][MAXPTS]; //Points per function
int fnc[256]={0};

Mat mask;
```

```

double gainherenow(int maskval, double now)
{
    int before = -1;
    int after = -1;

    if(fnc[maskval] == 0){
        fprintf(stderr, "No function defined for value %d\n", maskval);
        return 0;
    }

    //Find nearest points
    //Range check, take the end value if out of range
    if(now <= fns[maskval][0].time){
        //printf("Time %lu before first specified time %lu\n", now, fns[
            maskval][0].time);
        before = 0;
        after = 0;
    }
    if(now >= fns[maskval][fnc[maskval]-1].time)
    {
        //printf("Time %lf after last specified time %lf\n", now, fns[
            maskval][fnc[maskval]-1].time);
        before = fnc[maskval]-1;
        after = fnc[maskval]-1;
    }

    int i = 0;
    while(((before == -1) || (after == -1)) && (i < fnc[maskval]-1))
    {
        if(fns[maskval][i].time <= now && fns[maskval][i+1].time > now){
            //Find closest point before
            before = i;
        }

        if(fns[maskval][i].time < now && fns[maskval][i+1].time >= now){
            //Find closest point after
            after = i+1;
        }
        i++;
    }
    #if CHATTY
        printf("Matched time %lf in function %d with before = %d (%lf:%lf)
            after = %d (%lf:%lf)\n", now, maskval, before, fns[maskval][
                before].time, fns[maskval][before].gain, after, fns[maskval][
                    after].time, fns[maskval][after].gain);
    #endif
    // Compute gain at point
    if(before == after){ // We're on a defined point
        return fns[maskval][before].gain;
    }
    else{
        //Proportional linear interpolate between
        return (fns[maskval][before].gain*(fns[maskval][after].time -
            now)/(fns[maskval][after].time - fns[maskval][before].time))
    }
}

```

```

    + (fns[maskval][after].gain*(now - fns[maskval][before].time)/(
        fns[maskval][after].time - fns[maskval][before].time));
}
}

//Find the gain for a contribution over an interval at a point
//Tik keeps times in doubles, so I guess this takes times as doubles
?
// Weight for an interval contribution is the length times the
    average gain for that interval
// Makes gains as continuous as the input data.
double weightherebetween(uint32_t where, double start, double end){
    double len = end-start; // How long is the interval
    unsigned long center = (start+end)/2; // result to unsigned long
        ns for lookup
    //printf("Center Time is %lu\n",center);
    //Need to turn a location into a maskval; tik is full of raw
        pointers.
    // I think I can take the where from tik, and split on row size?
    uint32_t r = where/mask.cols;
    uint32_t c = where%mask.cols;
    if((r<0 || r>mask.rows)||(c<0 || c>mask.cols)){
        fprintf(stderr,"Attempted invalid lookup at (%d,%d)\n",r,c);
    }
    double centergain = gainherenow(mask.at<uchar>(r, c),center);
#ifdef CHATTY
    //if(where == 90000)
    printf("Center Gain is %lf, interval is %lf\n", centergain, len);
#endif
    return centergain * len;
}

//Read a grayscale PGM Image as the mask
int readMask(char * maskfile)
{
    printf("Reading mask from %s\n",maskfile);
    mask = imread(maskfile , IMREAD_GRAYSCALE );
    if ( !mask.data )
    {
        printf("No image data in mask\n");
        return -1;
    }
    return 0;
}

//A helper to print out all the currently loaded gain functions in
    the same format they are accepted
void dumpGainFns()
{
    printf("Read functions:\n");
    for(int i=0;i<256;i++)
    {
        if(fnc[i] != 0)

```

```

    {
        printf("M%d{" ,i);
        for(int j=0;j<fnc[i];j++)
        {
            printf("[%lf,%lf]",fns[i][j].time , fns[i][j].gain);
            if(j==fnc[i]-1){printf("}\n");}
            else { printf(","); }
        }
    }
}

int readGainFns(char * gainFnFile)
{
    printf("Reading gain functions from %s\n",gainFnFile);
    FILE *ffp;
    ffp = fopen(gainFnFile, "r");
    if(ffp == NULL)
    {
        fprintf(stderr,"Could Not Open Gain Function File %s",
            gainFnFile);
        exit(1);
    }

    //Read a set of exposure functions
    char line [MAXLINE];
    char *tok;
    char *tup;
    int maskval;

    double gn;
    double tn;

    while(fgets(line, sizeof line , ffp) != NULL) //Strip Lines
    {
        tok = strtok(line, "{"); // Split header from list
        if(tok != NULL){
            //if(tok[0] != 'M'){continue;} // Skip lines not shaped like
            //functions.
            sscanf(tok,"M%d",&maskval);
            if( maskval >= 0 && maskval < 256){ //Check if it's a valid
            //mask value
                //printf("Found function for Mask Value %d", maskval);
                if(fnc[maskval]!=0){
                    fprintf(stderr,"Warning: Mask value %d multiply defined\n",
                        maskval);
                }
                int pt = 0;
                tok = strtok(NULL, "{"); //Get the list
                tup = strtok(tok, ","); //Split Tuples
                while(tup != NULL){
                    sscanf(tup,"[%lf:%lf]",&tn, &gn);
                    fns[maskval][pt].time = tn;
                    fns[maskval][pt].gain = gn;
                }
            }
        }
    }
}

```

```

        pt++;
        if(pt > MAXPTS) {
            fprintf(stderr, "Too many points defined for mask value
                %d, max of %d\n", maskval, MAXPTS);
            return (-1);
        }
        tup = strtok(NULL, ",");
    }
    fnc[maskval]=pt; //Store the number of points for this
        value
    }
    else{//Maskval out of range
        fprintf(stderr, "Mask value %d out of range (only 0-255
            supported)\n", maskval);
        return (-1);
    }
}
}
printf("Read mask of size %d x %d\n", mask.cols, mask.rows);
return 0;
}

//Returns the time (in ns) of the NEXT control point specified in
    the input for the current mask
// To use in partitioning
// Special case 0 to mean "no relevant time partition?" for times
    after the last control point?
double nextControlTime(uint32_t where, double now){
    int after = -1;

    //Coordinate fix
    uint32_t r = where/mask.cols;
    uint32_t c = where%mask.cols;
    if((r<0 || r>mask.rows)||(c<0 || c>mask.cols)){
        fprintf(stderr, "Attempted invalid lookup at (%d,%d)\n", r, c);
    }
    int maskval = mask.at<uchar>(r, c);

    if(fnc[maskval] == 0){
        fprintf(stderr, "No function defined for value %d\n", maskval);
        return 0;
    }

    //now before first control point
    if(now < fns[maskval][0].time){
        return fns[maskval][0].time;
    }
    //now after last control point
    if(now > fns[maskval][fnc[maskval]-1].time)
    {
        return numeric_limits<double>::infinity(); //We read off the end
            of the control interval
    }
    // Have to search

```

```

int i = 0;
while((after == -1) && (i < fnc[maskval]-1))
{
    if(fns[maskval][i].time < now && fns[maskval][i+1].time >= now){
        //Find closest point after
        return fns[maskval][i+1].time;
    }
    i++;
}
//fprintf(stderr, "Exited nextControlTime for function %d time %ld
with no time found!\n", maskval, now );
return 0;
}

/*Locate the control point _before_ the first non-zero gain in the
function spec*/
// One before because interpolation includes the prior point
double FirstLive()
{
    double first = numeric_limits<double>::infinity();
    for(int i=0;i<256;i++)
    {
        if(fnc[i] != 0)
        {
            for(int j=0;j<fnc[i];j++)
            {
                //The next point has non-zero gain and
                // the current point has an earlier time than previously
                seen
                // Update the earliest
                if((fns[i][j+1].gain != 0) && (fns[i][j].time<first))
                {
                    first = fns[i][j].time;
                }
            }
        }
    }
}
#if CHATTY
    printf("First_live_control_time_is_%lf\n",first);
#endif
return first;
}

/*Locate the control point after the last non-zero gain in the
function spec*/
// One past because interpolation includes the next point
double LastLive()
{
    double last = 0;
    for(int i=0;i<256;i++)
    {
        if(fnc[i] != 0)
        {

```



```

xinu(unsigned int x)
{
    unsigned int y;

    *(((char *) &y) + 0) = *(((char *) &x) + 3);
    *(((char *) &y) + 1) = *(((char *) &x) + 2);
    *(((char *) &y) + 2) = *(((char *) &x) + 1);
    *(((char *) &y) + 3) = *(((char *) &x) + 0);
    return(y);
}

static void
TIKrenderWriteFile(register int r)
{
    char outfile[4*1024];
    char *s;

    sprintf(outfile, e_outfile, r);
    INFO("writing \"%s\" as frame %d (%1.3fs @ %1.3fs) from \"%s\" with quality %1.3f\n",
        outfile,
        r,
        (STOP-START) / 1000000000.0,
        START / 1000000000.0,
        infile,
        QUAL);

    if ((s = tdc12jpeg(outfile, IMAGE)) != 0) {
        ERROR(ERROR_WRITE,
            "%s %s\n",
            outfile,
            s);
    }

    MORE = 0;
    free(IMAGE);
    IMAGE = ((double *) 0);
}

void
badformat()
{
    ERROR(ERROR_FORMAT, "bad format in TIK_RGB_file\n");
}

void
TIKrenderSimul(void)
{
    //printf("Beginning TIKrenderSimul\n");
    register uint8 *p;
    register int r;

    double fnfirstlive=FirstLive();
    double fnlastlive =LastLive();

```

```

printf("Control_Function_live_range_from[%lf,%lf]",fnfirstlive ,
      fnlastlive);
printf(" expose-b%lf-t%lf\n",fnfirstlive/1e9,(fnlastlive-
      fnfirstlive)/1e9);

/* Anything requested? */
if (rendersp < 1) {
    ERROR(ERROR_EXPOSE,
          "no exposures requested\n");
}

/* Open the input file */
if (dottik) {
    if (0 > (PNMfd = open(infile, O_RDONLY))) {
        ERROR(ERROR_OPEN,
              "could not open TIK file %s\n",
              infile);
    }
} else {
    start_opencv(infile);
}

/* Initialize wave stuff */
memcpy(&wavework, &waveref, sizeof(waveref));
if (waveref.x > 0) {
    /* Non-zero X means this is next frame */
    wavework.b += waveref.f;
}
wavep = &wavework;

/* Check we have an image */
if (p = PNMreader()) {
    double gamma[256];
    register double invgamma;
    register uint32 xy;
    register uint32 xyc;
    register double *from;
    register uint8 *ref;
    register double wf;
    register double wt;
    register double now;
    register uint32 where;
    register int i, off, n, r;

    memcpy(&waveref, &wavework, sizeof(waveref));
    xy = wavex * wavey;
    xyc = xy * ((wavetype == wavePNM) ? 3 : wavec);
    from = ((double *) calloc(xy, sizeof(double)));

    /* Mark all frames as no pixels rendered */
    FOR_RENDER MORE = xy;

    ref = p; /* Set initial TDCI values */

```

```

wf = ((wavetype == wavePNM) ? (1000000000.0 / 24) : wavef);
wt = (((wavet < 1) || (wavet > wavef)) ? wavef : wavet);
now = (waveb / 1000000000.0) + wf;
n = 0;

/* Create gamma mapping info */
if (e_gamma == 0) {
    e_gamma = ((waveg == 0) ? 1.0 : (waveg / 1000000.0));
}
for (i=0; i<256; ++i) {
    gamma[i] = ((e_gamma == 1) ?
        ((double) i) :
        pow(((double) i), e_gamma));
}
invgamma = 1.0 / e_gamma;

/* Stuff specific to different formats */
switch (wavetype) {
case waveRGB:

    /* Should be 0 separator; skip over it */
    if (PNMnextc()) badformat();
    PNMnextc();

    /* Process TDCI until a little past stop...
       past stop because we need frame after so we can
       interpolate the slope in the gap between samples
       Initialize where to inc past end of first frame
    */
    where = xy - 1;
    while (!PNMtimedout) {
        register uint32 shift = 0;
        register int c;
        uint8 v[3 + 1]; /* +1 to allow PNMnextbn hack below */
        register int natstart = n;
        register int left = 0;

        /* Skip to next changed pixel */
        ++where;
        do {
            /* 7 bits of skip at a time, low first */
            where += (((c = PNMc) & 0x7f) << shift);
            shift += 7;
            while (where >= xy) {
                /* In another frame... */
                where -= xy;
                now += wf;
                ++n;
                INFO("Frame %d: %1.3fs\n",
                    n,
                    (now / 1000000000.0));
            }
        } while (PNMnextc());
        if (PNMtimedout) badformat();
    }
}

```

```

    } while (c & 0x80);

    /* Where are we? */
    off = where * wavec;

    /* Get value of this sample */
#ifdef NOTNOW
    for (i=0; i<wavec; ++i) {
        v[i] = PNMc;
        PNMnextc();
        if (PNMtimedout) badformat();
    }
#else
    v[0] = PNMc;
    PNMnextbn(&(v[1]), wavec);
    if (PNMtimedout) badformat();
    PNMc = v[wavec];
#endif

    /* Add contribution from previous sample to sum */
    if (now > minstart) {

        FOR_RENDER {
            if ((MORE > 0) && (now > START)) {
                double f = from[where];
                double g = now - (wf - wt); /* start of gap between
                    samples */
                double fstart = ((START > f) ? START : f);
                double fstop = ((g > STOP) ? STOP : g);
                double gstart = ((START > g) ? START : g);
                double gstop = ((now > STOP) ? STOP : now);
                uint32 off = where * wavec;
                //PSE Look up the next control point in the
                    integration function for this location to segment
                    on
                double nextcontrolpoint = nextControlTime(where, (
                    unsigned long) now);
                // STILL NEED TO SEGMENT... but maybe need to rejigger
                    time input

                /* Newly rendering this frame? */
                if (IMAGE == ((double *) 0)) {
                    if (!(IMAGE = ((double *) calloc(rendersp, xyc *
                        sizeof(double)))) {
                        ERROR(ERROR_EXPOSE,
                            "cannot allocate memory for TIK virtual
                                exposure");
                    }
                    //printf("Starting frame in WaveRGB\n");
                }

                // gonna have to rethink START and STOP in terms of
                    functions I think
            }
        }
    }

```

```

/* Add portion of previous sample */
if (fstart < fstop) {
    double sfstop = fstop; //Assume it's the end for now
    double sfstart = fstart; //Assume it's the beginning
        for now
    double nexttcp=nextControlTime(where, sfstart);
    //Split on control points
    while(nexttcp< fstop){
    if(where == WATCHSPOT){
    printf("Cracking leading sample into [%lf,%lf] on
        control point %lf\n",sfstart,sfstop,nexttcp);
    }
        //
        sfstop = nexttcp;
        double w = sfstop - fstart;
        double weight = weightherebetween(where, sfstart,
            sfstop);
        if(where == WATCHSPOT){
            printf("Including leading sample from [%lf,%lf],
                weight %lf\n",sfstart,sfstop,weight);
        }
        for (i=0; i<wavec; ++i) SUM(off+i) += (gamma[ref[
            off+i]] * weight);
        /* Add-in fraction from real data frames */
        QUAL += (1.0 + (n - natstart)) * (w / (now - f));
        //Advance the interval
        sfstart=sfstop+1;
        nexttcp=nextControlTime(where, sfstart);
    }
    // Do the remainder after the last control point
    double w = fstop - sfstart;
    double weight = weightherebetween(where, sfstart,
        fstop);

    if(where == WATCHSPOT){
    printf("Including end of leading sample interval
        from [%lf,%lf], weight %lf\n", sfstart,fstop,
        weight);
    }
        for (i=0; i<wavec; ++i) SUM(off+i) += (gamma[ref[
            off+i]] * weight);
        /* Add-in fraction from real data frames */
        QUAL += (1.0 + (n - natstart)) * (w / (now - f));
    }/* End Previous Sample Portion*/
    //printf("Finished Previous Sample\n");

    /* Add portion of gap as a slope */
    /* This code is only called if the input shutter angle
        is expressly specified*/
    if (gstart < gstop) {
        double wstart = (gstart - g) / (now - g); //(start-
            beginning of gap)/(now-beginning of gap)
        double wstop = (gstop - g) / (now - g);
        double wgap = gstop - gstart;

```

```

double nexttcp=nextControlTime(where, gstart);
double sgstart = gstart;
double sgstop = gstop;
//Need to chop the gap not the end model
// double sstart = wstart;
// double sstop = wstop;
double swgap = gstop - gstart;

double weight;

if(where == WATCHSPOT){printf("Handling gap from [%f, %f]\n", gstart, gstop);}
while(nexttcp < gstop)//Input function changes during gap
{
    //Cut a partition
    if(where == WATCHSPOT){printf("Split gap on %f\n", nexttcp);}
    sgstop=nexttcp;

    weight = weightherebetween(where, sgstart, sgstop);
    ;
    if(where == WATCHSPOT){printf("Processed gap from [%f, %f] with weight %f\n", sgstart, sgstop, weight);}
    for (i=0; i<wavec; ++i) {
        /* Compute gap end values, then average * wgap to get area */
        double vstart = (ref[off+i] * (1.0 - wstart)) + (gamma[v[i]] * wstart);
        double vstop = (ref[off+i] * (1.0 - wstop)) + (gamma[v[i]] * wstop);
        SUM(off+i) += (weight * ((vstart + vstop) / 2.0));
    }
    /* Add-in gap fraction as if it is from one frame */
    QUAL += (wgap / (now - f));
    sgstart=sgstop+1;
    nexttcp=nextControlTime(where, sgstart);
}
//Otherwise just do the remainder in one shot
weight = weightherebetween(where, sgstart, sgstop);
if(where == WATCHSPOT){printf("Processed trailing gap from [%f, %f] with weight %f\n", sgstart, sgstop, weight);}
for (i=0; i<wavec; ++i) {
    /* Compute gap end values, then average * wgap to get area */
    double vstart = (ref[off+i] * (1.0 - wstart)) + (gamma[v[i]] * wstart);
    double vstop = (ref[off+i] * (1.0 - wstop)) + (gamma[v[i]] * wstop);
}

```

```

        SUM(off+i) += (weight * ((vstart + vstop) / 2.0));
    }
    /* Add-in gap fraction as if it is from one frame */
    QUAL += (wgap / (now - f));
}/* End Gap Portion */

/* Update more from a trailing sample*/
//This part is spatially traveling in the inner for
loop by pos not where!
if ( now > STOP+wf) {
    /* Add-in data for other pixels */
    int pos;
    int off = 0;
    for (pos=0; pos<xy; ++pos) {
        double f = from[pos];
        //Segment!
        double sf = ((f < START) ? START : f); //The most
            recent time to update here
        double sstop = STOP;
        double nextcp=nextControlTime(pos, sf);

        while(nextcp < STOP){
            if(pos == WATCHSPOT){
                printf("Cracking_trailing_sample_interval_[%lf,%
                    lf]_on_control_point_%lf_at_position_%d\n",sf
                        ,sstop,nextcp,pos);
            }
            sstop = nextcp;
            register double w = sstop - sf;
            double weight = weightherebetween(pos, sf, sstop
                );
            if(pos == WATCHSPOT){//307190
                printf("Processing_trailing_sample_interval_
                    from_[%lf,%lf],_weight_%lf\n",sf,sstop,
                        weight);
            }
            //TIK handled an edge case by detecting
            negatives.
            if (w < 0) //This MUST squash if the interval is
                negative!
            {
                w = 0;
                weight = 0;
                if(pos == WATCHSPOT){
                    printf("Squashed_negative_interval_segment\n")
                        ;
                }
            }
            off=pos*wavec;
            for (i=0; i<wavec; ++i) {
                SUM(off) = (SUM(off) + (gamma[ref[off]] *
                    weight)) * DIVBY;
                if (e_gamma != 1) {
                    SUM(off) = pow(SUM(off), invgamma);
                }
            }
        }
    }
}

```

```

    }
    ++off; //PSE: This is NOW just color channel
    ++QUAL;
}
sf=sstop+1;
nexttcp=nextControlTime(pos, sf);
sstop=((nexttcp<STOP)?nexttcp:STOP);
if(pos == WATCHSPOT){
printf("Next trailing interval [%lf,%lf], next
control point %lf\n",sf,sstop,nexttcp);
}
}
//Do the remainder after the last control point (
sf to sstop)
double w = STOP - (sf);
off=0; // CAN NOT reset off here
double weight = weightherebetween(pos, sf, sstop
);
if(pos == WATCHSPOT){
printf("Processing trailing remainder from [%lf
,%lf], weight %lf\n",sf,sstop,weight);

//printf("pos out of range, found %d, max is %d\
n",pos,xy-1);
}
//off = 0; //reset off? No change.
//TIK handled an edge case by detecting
negatives.
if (w < 0) //This MUST squash if the interval is
negative!
{
w = 0;
weight = 0;
if(pos == WATCHSPOT){
printf("Squashed negative interval segment\n")
;
}
}
off=pos*wavec; //Reset the offset based on pos
for (i=0; i<wavec; ++i) {
//Segfaulting here before 20240703 - offset
was being advanced as a side-effect of the
outer loop, causing illegal references
SUM(off) = (SUM(off) + (gamma[ref[off]] *
weight)) * DIVBY;
if (e_gamma != 1) {
SUM(off) = pow(SUM(off), invgamma);
}
}
++off; //PSE: This is NOW just color channel
++QUAL;
}

} //ends pos
/* Correct exposure quality */

```

```

        QUAL /= xy;
        /* Done with this virtual exposure; write the file
        */
        TIKrenderWriteFile(r);
    }/*End Trailing Sample Portion*/
}

/* Still any images left incomplete? */
left += (MORE > 0);
}

/* Check to see if any frames not yet rendered */
if (left < 1) goto noneleft;
}

/* Record this sample */
from[where] = now;
for (i=0; i<wavec; ++i) ref[off+i] = v[i];
}

/* Update image with last samples...
which we'll assume persist until stop,
because we can't know otherwise ;-)
Also divide by time to get average values.
*/
FOR_RENDER
if (MORE > 0) {
    char outfile[4*1024];
    char *s;

    off = 0;
    for (where=0; where<xy; ++where) {
        register double f = from[where];
        register double w = STOP - ((f < START) ? START : f);

        if (w < 0) w = 0;
        for (i=0; i<wavec; ++i) {
            SUM(off) = (SUM(off) + (gamma[ref[off]] * w)) * DIVBY;
            if (e_gamma != 1) {
                SUM(off) = pow(SUM(off), invgamma);
            }
            ++off;

            /* Add-in fraction from real data */
            ++QUAL;
        }
    }
}

/* Correct exposure quality */
QUAL /= xy;

/* Done with this virtual exposure; write the file */
TIKrenderWriteFile(r);
}

```

```

break;

case waveUYVYYYold:
    /* Should be a P5 header next...
       we know how to read that!
    */
    for (where=0; where<xyc; where+=6) {
        ref[where] += 128;
        ref[where+2] += 128;
    }
    p = P5reader();
    while (p) {
        register double f = now - wf;
        register double g = now - (wf - wt); /* start of gap between
            samples */
        register int left = 0;

        FOR_RENDER {
            if ((MORE > 0) && (now > START)) {
                register double fstart = ((START > f) ? START : f);
                register double fstop = ((g > STOP) ? STOP : g);
                register double gstart = ((START > g) ? START : g);
                register double gstop = ((now > STOP) ? STOP : now);
                register double wstart = (gstart - g) / (now - g);
                register double wstop = (gstop - g) / (now - g);
                register double wgap = gstop - gstart;

                /* Newly rendering this frame? */
                if (IMAGE == ((double *) 0)) {
                    if (!(IMAGE = ((double *) calloc(rendersp, xyc *
                        sizeof(double)))))) {
                        ERROR(ERROR_EXPOSE,
                            "cannot allocate memory for UYVYYY virtual
                            exposure");
                    }
                }
            }

            /* Update quality */
            ++QUAL;

            for (where=0; where<xyc; where+=6) {
                p[where] += 128;
                p[where+2] += 128;
            }
            for (where=0; where<xyc; ++where) {
                /* Add contribution from previous sample to sum */
                if (now > START) {
                    /* Add portion of previous sample */
                    if (fstart < fstop) {
                        register double w = fstop - fstart;
                        SUM(where) += (gamma[ref[where]] * w);
                    }

                    /* Add portion of gap as a slope */

```

```

        if (gstart < gstop) {
            /* Compute gap end values, then average * wgap to
               get area */
            register double vstart = (ref[where] * (1.0 -
                wstart)) + (gamma[p[where]] * wstart);
            register double vstop = (ref[where] * (1.0 - wstop
                )) + (gamma[p[where]] * wstop);
            SUM(where) += (wgap * ((vstart + vstop) / 2.0));
        }
    }

    /* Update more and write file */
    if (now >= STOP) {
        /* Done with this virtual exposure; write the file */
        TIKrenderWriteFile(r);
    }
}

/* Still any images left incomplete? */
left += (MORE > 0);
}

/* Check to see if any frames not yet rendered */
if (left < 1) goto noneleft;

/* Next image */
now += wf;
free(ref);
ref = p;
p = P5reader();
}

/* Did we get another? If so, discard it. */
if (p) free(p);

/* Update image with last samples...
   which we'll assume persist until stop,
   because we can't know otherwise ;- )
   Also divide by time to get average values.
*/
FOR_RENDER
if (MORE > 0) {
    /* Newly rendering this frame? */
    if (IMAGE == ((double *) 0)) {
        if (!(IMAGE = ((double *) calloc(rendersp, xyc * sizeof(
            double)))) {
            ERROR(ERROR_EXPOSE,
                "cannot allocate memory for UYVYYY virtual
                exposure");
        }
    }
}
}

/* Update quality */

```

```

++QUAL;

for (where=0; where<xyc; ++where) {
    register double f = now - wf;
    register double w = STOP - ((f < START) ? START : f);

    if (w < 0) w = 0;
    SUM(where) = (SUM(where) + (gamma[ref[where]] * w)) *
        DIVBY;
    if (e_gamma != 1) {
        SUM(where) = pow(SUM(where), invgamma);
    }
}

/* Done with this virtual exposure; write the file */
TIKrenderWriteFile(r);
}
break;

case waveUYVYYY:
    /* Make all values signed */
    for (where=0; where<xyc; where+=6) {
        ref[where] += 128;
        ref[where+2] += 128;
    }

    /* Resize from[] */
    free(from);
    from = ((double *) calloc(xyc, sizeof(double)));

    /* Process TDCI until a little past stop...
       past stop because we need frame after so we can
       interpolate the slope in the gap between samples
       Initialize where to inc past end of first frame
    */
    PNMnextc();
    where = 0;
    while ((!PNMtimedout) && (PNMnextw() != 1)) {
        register uint32 change = PNMw;
        register int left = 0;

        if (change & 1) {
            /* This is a span record */
            int skip = 0;
            where += ((change + change) & ~3);

            /* Skip complete frames */
            while (where >= xyc) {
                now += wf;
                ++skip;
                where -= xyc;
            }

            if (skip > 0) printf("now_=_%gs\n", now/1000000000.0);

```

```

} else {
    /* Correct sample signedness */
    for (i=0; i<4; ++i) {
        switch ((where+i) % 6) {
            case 0:
            case 2:
                *(((uint8 *) &PNMw) + i) ^= 128;
        }
    }

    /* Add contribution from previous sample to sum */
    if (now > minstart) {
        double refd[4], newd[4];

        /* Map the old and new values */
        for (i=0; i<4; ++i) {
            refd[i] = ref[where+i];
            newd[i] = *(((uint8 *) &PNMw) + i);
        }

        FOR_RENDER {
            if ((MORE > 0) && (now > START)) {
                register double f = from[where];
                register double g = now - (wf - wt); /* start of gap
                    between samples */
                register double fstart = ((START > f) ? START : f);
                register double fstop = ((g > STOP) ? STOP : g);
                register double gstart = ((START > g) ? START : g);
                register double gstop = ((now > STOP) ? STOP : now);

                /* Newly rendering this frame? */
                if (IMAGE == ((double *) 0)) {
                    if (!(IMAGE = ((double *) calloc(rendersp, xyc *
                        sizeof(double)))))) {
                        ERROR(ERROR_EXPOSE,
                            "cannot allocate memory for TIK virtual
                            exposure");
                    }
                }

                /* Add portion of previous sample */
                if (fstart < fstop) {
                    register double w = fstop - fstart;

                    for (i=0; i<4; ++i) {
                        SUM(where+i) += refd[i] * w;
                    }

                    /* Add-in fraction from real data frames */
                    QUAL += (w / (now - f));
                }

                /* Add portion of gap as a slope */
                if (gstart < gstop) {

```

```

register double wstart = (gstart - g) / (now - g);
register double wstop = (gstop - g) / (now - g);
register double wgap = gstop - gstart;

for (i=0; i<4; ++i) {
    /* Compute gap end values, then average * wgap
       to get area */
    register double vstart = (refd[i] * (1.0 -
        wstart)) + (newd[i] * wstart);
    register double vstop = (refd[i] * (1.0 - wstop)
        ) + (newd[i] * wstop);
    SUM(off+i) += (wgap * ((vstart + vstop) / 2.0));
}

/* Add-in gap fraction as if it is from one frame
   */
QUAL += (wgap / (now - f));
}

/* Update more */
if (now > STOP+wf) {
    /* Add-in data for other pixels */
    register int pos;

    for (pos=0; pos<xyc; ++pos) {
        register double f = from[pos];
        register double w = STOP - ((f < START) ? START
            : f);
        if (w < 0) w = 0;
        SUM(pos) = (SUM(pos) + (ref[pos] * w)) * DIVBY;
        ++QUAL;
    }

    /* Correct exposure quality */
    QUAL /= (xyc / 4);

    /* Done with this virtual exposure; write the file
       */
    TIKrenderWriteFile(r);
}
}

/* Still any images left incomplete? */
left += (MORE > 0);
}

/* Check to see if any frames not yet rendered */
if (left < 1) goto noneleft;
}

/* Update from pixel data */
for (i=0; i<4; ++i) {
    ref[where+i] = *(((uint8 *) &PNMw) + i);
    from[where+i] = now;
}

```

```

    }
    where += 4;
    while (where >= xyc) {
        now += wf;
        where -= xyc;
    }
}
}

/* Update image with last samples...
   which we'll assume persist until stop,
   because we can't know otherwise ;- )
   Also divide by time to get average values.
*/
FOR_RENDER
if (MORE > 0) {
    /* Newly rendering this frame? */
    if (IMAGE == ((double *) 0)) {
        if (!(IMAGE = ((double *) calloc(rendersp, xyc * sizeof(
            double)))) {
            ERROR(ERROR_EXPOSE,
                "cannot allocate memory for UYVYYY virtual
                exposure");
        }
    }
}

/* Update quality */
++QUAL;

for (where=0; where<xyc; ++where) {
    register double f = now - wf;
    register double w = STOP - ((f < START) ? START : f);

    if (w < 0) w = 0;
    SUM(where) = (SUM(where) + (ref[where] * w)) * DIVBY;
}

/* Done with this virtual exposure; write the file */
TIKrenderWriteFile(r);
}
break;

case wavePNM:
    /* Should be a P6 header next...
       we know how to read that!
    */
    p = P6reader();
    while (p) {
        register double f = now - wf;
        register double g = now - (wf - wt); /* start of gap between
            samples */
        register int left = 0;

        FOR_RENDER { //For every output frame

```

```

if ((MORE > 0) && (now > START)) { //that still needs work
    register double fstart = ((START > f) ? START : f); //
        Start as far into the current sample this output
        frame starts at
    register double fstop = ((g > STOP) ? STOP : g); // If
        the end of this input frame is after the end of the
        output frame, stop short
    register double gstart = ((START > g) ? START : g); //
        This is the beginning of the part interpolated from
        the gap between samples
    register double gstop = ((now > STOP) ? STOP : now); //
        End of the part of the output interval in the gap
    register double wstart = (gstart - g) / (now - g); //
        This is the next gap interval, that gets constrained
        by the vstart/vstop values on the fly below?
    register double wstop = (gstop - g) / (now - g);
    register double wgap = gstop - gstart;

    /* Newly rendering this frame? */
    if (IMAGE == ((double *) 0)) {
        if (!(IMAGE = ((double *) calloc(rendersp, xyc *
            sizeof(double)))) {
            ERROR(ERROR_EXPOSE,
                "cannot allocate memory for PNM virtual
                exposure");
        }
    }
}

/* Update quality by denoting another sample has been
    included*/
++QUAL;

for (where=0; where<xyc; ++where) {
    /* Add portion of previous sample */
    if (fstart < fstop) {
        register double w = fstop - fstart; //How long is
            this input sample contributing to the output
            frame
        SUM(where) += (gamma[ref[where]] * w); //gamma for
            correction, w is weighting by the amount of time
            it is contributing
        printf("PSE: Contribution Added in WavePNM\n");
    }
}

/* Add portion of gap as a slope */
//Wstart wstop are the weighting for the gap length
if (gstart < gstop) {
    /* Compute gap end values, then average * wgap to
        get area */
    register double vstart = (ref[where] * (1.0 - wstart
        )) + (gamma[p[where]] * wstart);
    register double vstop = (ref[where] * (1.0 - wstop))
        + (gamma[p[where]] * wstop);
    SUM(where) += (wgap * ((vstart + vstop) / 2.0));
}

```

```

    }
}

/* Update more and write file */
if (now > STOP+wf) {
    for (where=0; where<xyc; ++where) {
        SUM(where) = (SUM(where) * DIVBY);
        if (e_gamma != 1) {
            SUM(where) = pow(SUM(where), invgamma);
        }
    }

    /* Done with this virtual exposure; write the file */
    TIKrenderWriteFile(r);
}

/* Still any images left incomplete? */
left += (MORE > 0);
}

/* Check to see if any frames not yet rendered */
if (left < 1) goto noneleft;

/* Next image */
now += wf;
free(ref);
ref = p;
p = P6reader();
}

/* Did we get another? If so, discard it. */
if (p) free(p);

/* Update image with last samples...
   which we'll assume persist until stop,
   because we can't know otherwise ;-)
   Also divide by time to get average values.
*/
FOR_RENDER
if (MORE > 0) {
    /* Newly rendering this frame? */
    if (IMAGE == ((double *) 0)) {
        if (!(IMAGE = ((double *) calloc(rendersp, xyc * sizeof(
            double)))) {
            ERROR(ERROR_EXPOSE,
                "cannot allocate memory for PNM virtual exposure")
                ;
        }
    }
}

/* Update quality */
++QUAL;

```

```

    for (where=0; where<xyc; ++where) {
        register double f = now - wf;
        register double w = STOP - ((f < START) ? START : f);

        if (w < 0) w = 0;
        SUM(where) = (SUM(where) + (gamma[ref[where]] * w)) *
            DIVBY; // Add in some guesses for data after the last
                sample
        if (e_gamma != 1) {
            SUM(where) = pow(SUM(where), invgamma);
        }
    }

    /* Done with this virtual exposure; write the file */
    TIKrenderWriteFile(r);
}

break;

default:
    badformat();
}

/* Clean-up */
noneleft:
    free(ref);
    free(from);

    /* Close the input file */
    if (dottik) {
        close(PNMfd);
    }
}

void
TIKrenderFile(int d, char *filename)
{
    dottik = d;
    infile = filename;
    rendersp = 0;
}

void
TIKrender(double start, double stop)
{
    /* Normalize start, stop and convert to nanoseconds */
    start *= 1000000000.0;
    stop *= 1000000000.0;
    if (stop < start) { double t = start; start = stop; stop = t; }

    /* When does the first frame start? */
    if ((rendersp == 0) || (start < minstart)) minstart = start;
}

```

```

    /* Queue it up */
    render[rendersp].start = start;
    render[rendersp].stop = stop;
    render[rendersp].qual = 0;
    render[rendersp].divby = 1.0 / (stop - start);
    render[rendersp].image = ((double *) 0);
    ++rendersp;
}

```

Listing B.4: MaskGain.h

```

/* tik.cpp

    Temporal Image Kentucky/Kontainer

    Original by Henry Dietz, June 2016

    See tik.h for notices.
*/

#include "tik.h"

char *myname; /* For error messages, name of this program */

FILE *TDCIfile = 0;

double e_begin = 0;
char *e_noisefile = 0;
double e_fps = 0; /* Frames Per Second */
double e_gamma = 0; /* Encoding gamma (0 means not set) */
int e_n = 0;
char *e_outfile = 0;
char *e_outtik = ((char *) "pnm.tik");
char *e_outimage = ((char *) "tik%05d.jpg");
double e_percent = 4.55;
double e_quality = 75;
double e_t = 0; /* Shutter time, Tv in seconds */
int e_what = WHAT_UNSPEC;
int e_interactive = 0; /* Interactive mode? */
time_t e_update;
int e_maketype = MAKE_UNSPEC;

//PSE: Probably need to made a default mode that always returns 1?
char *e_maskfile = 0;
char *e_finfile = 0;

double
atofrac(char *s)
{
    /* Atof, but allowing fractions with 1/ */
    if ((s[0] == '1') && (s[1] == '/')) {
        return(1.0 / atof(&(s[2])));
    }
}

```

```

    }
    return(atoi(s));
}

int
main(register int argc,
register char **argv)
{
    register char *s;
    register int i, n;
    register char *fname = 0;
    register double now;
    time_t real_time = (e_update = time(0));

    /* Set interactive mode based on stderr */
    e_interactive = isatty(2);

    /* Process command line... */
    myname = argv[0];
    if (argc < 2) {
usage:
        fprintf(stderr,
            "Usage: %s {exposure_settings}\n"
            "-a#Set Tv by shutter angle; Tv=(angle/360)/FPS\n"
            "-b#Begin exposure time in seconds (default 0); needs .tik input\n"
            "-eNAME Error model is NAME; blank creates from video of a constant scene\n"
            "-f#Frames per second, FPS (default 24)\n"
            "-g#Gamma of encoded data (1.0 linear default; 2.2 typical JPEG)\n"
            "-i#Interactive progress update seconds -1 (default %d, 0 means never, -i toggles)\n"
            "-kFNFILE Specify a function spec file for exposure functions\n"
            "-mMASKFILE Specify a (PGM) mask file to define areas for exposure\n"
            "-n#Number of frames to encode/decode (default 1 output, all input)\n"
            "-oNAME Output filename is NAME (default %s)\n"
            "-p#Minimum % probability same to factor (default %0.2f; std. dev. are 32, 5, 0.3)\n"
            "-q#Quality % (default %0.0f; for JPEG output or TIK encoding)\n"
            "-t#Shutter speed in seconds, Tv (default to 1/FPS or 1/60s)\n"
            "-v Input is a video to be converted to .tik TDCI output\n"
            "FILENAME Process file as specified by earlier options, .tik assumed to be TDCI\n",
            myname,
            e_interactive,
            e_outtik,
            e_percent,

```

```

    e_quality);
    exit(ERROR_USAGE);
}

for (i=1; i<argc; ++i) {
    if (*argv[i] == '-') {
        switch (*(argv[i]+1)) {
            case 'a':
                e_t = atofrac(argv[i]+2);
                if (e_fps == 0) {
                    ERROR(ERROR_ARG,
                        "cannot set shutter angle before -f to set FPS\n");
                }
                if (e_t <= 0) {
                    ERROR(ERROR_ARG,
                        "shutter angle must be greater than 0, not %s\n",
                        (argv[i]+2));
                }
                e_t = (e_t / (e_fps * 360.0));
                break;
            case 'b':
                e_begin = atofrac(argv[i]+2);
                e_what |= WHAT_TIK;
                break;
            case 'e':
                e_noisefile = (argv[i]+2);
                if (*e_noisefile) {
                    /* Read error model file */
                    uint8 *p;

                    if ((0 > (PNMfd = open(e_noisefile, O_RDONLY))) ||
                        (0 == (p = PNMreader()))) ||
                        (PNMx != 256) ||
                        (PNMy != 256) ||
                        (PNMmaxval > 255)) {
                        ERROR(ERROR_READ,
                            "could not read error model file %s\n",
                            e_noisefile);
                    }
                    if (wavetype != waveNOISE) {
                        WARN("file %s used, but not marked as TIK NOISE\n",
                            e_noisefile);
                    }
                }

                memcpy(&(PNMerr[0][0][0]), p, (256*256*3));
                close(PNMfd);
                free(p);

                /* Only makes sense for encoding */
                e_what |= WHAT_VIDEO;
            } else {
                /* Force create error model file */
                e_what = WHAT_ERRMOD;
            }
        }
    }
}

```

```

    break;
case 'f':
    e_fps = atofrac(argv[i]+2);
    break;
case 'g':
    e_gamma = atofrac(argv[i]+2);
    break;
case 'i':
    if (*(argv[i]+2) == 0) {
        e_interactive = !e_interactive;
    } else {
        e_interactive = atoi(argv[i]+2);
        if (e_interactive < 1) e_interactive = 1;
    }
    break;

//PSE20240626: Add k and m cases for NU
case 'k':
    e_fnfile = argv[i]+2;
    readGainFns(e_fnfile);
    dumpGainFns();
    break;
case 'm':
    e_maskfile = argv[i]+2;
    readMask(e_maskfile);
    break;

case 'n':
    if (*(argv[i]+2) == 0) {
        e_n = 0;
    } else {
        e_n = atoi(argv[i]+2);
        if (e_n < 1) e_n = 1;
    }
    break;
case 'o':
    e_outfile = (argv[i]+2);

/* Guess type based on end of filename... */
if (e_maketype == MAKE_UNSPEC) {
    register char *p = argv[i] + 2;
    register int len = strlen(p);

    switch (len) {
    case 1:
        if (*p != '-') break;
        /* Fall through... */
    case 0:
        /* PPM stream to stdout for "-o-" or "-o" */
        e_outfile = ((char *) "-");
        e_maketype = MAKE_PPM;
        if (e_what != WHAT_ERRMOD) e_what |= WHAT_TIK;
        break;
    case 2:

```

```

case 3:
    /* Too short to say... */
    break;
default:
    /* Does it end in something we know? */
    p += (len - 4);
    if (p[0] == '.') {
        if (((p[1] == 'J') || (p[1] == 'j')) &&
            ((p[2] == 'P') || (p[2] == 'p')) &&
            ((p[3] == 'G') || (p[3] == 'g'))) {
            e_maketype = MAKE_JPEG;
            e_what |= WHAT_TIK;
        }
        if (((p[1] == 'P') || (p[1] == 'p')) &&
            ((p[2] == 'P') || (p[2] == 'p') || (p[2] == 'N')
             || (p[2] == 'n')) &&
            ((p[3] == 'M') || (p[3] == 'm'))) {
            e_maketype = MAKE_PPM;
            if (e_what != WHAT_ERRMOD) e_what |= WHAT_TIK;
        }
    }
}
break;
case 'p':
    e_percent = atofrac(argv[i]+2);
    if ((e_percent < 0) || (e_percent > 100)) {
        ERROR(ERROR_ARG,
              "%s is not valid; must be between -p0 and -p100\n",
              argv[i]);
    }
    e_what |= WHAT_VIDEO;
    break;
case 'q':
    e_quality = atofrac(argv[i]+2);
    if ((e_quality < 0) || (e_quality > 100)) {
        ERROR(ERROR_ARG,
              "%s is not valid; must be between -q0 and -q100\n",
              argv[i]);
    }
    break;
case 't':
    e_t = atofrac(argv[i]+2);
    break;
case 'v':
    e_what |= WHAT_VIDEO;
    break;
default:
    goto usage;
}
} else {
    /* What are we supposed to do with this file?
       Can't be nothing or more than one thing.
    */

```

```

register char *p = argv[i];
register int dottik = 0;

/* Guess based on end of filename... */
while (*p) ++p;
p -= 4;
if ((p[0] == '.') &&
    ((p[1] == 'T') || (p[1] == 't')) &&
    ((p[2] == 'I') || (p[2] == 'i')) &&
    ((p[3] == 'K') || (p[3] == 'k'))) {
    /* Force encoding exposures */
    e_what = WHAT_TIK;
    dottik = 1;
} else {
    if (e_what == WHAT_UNSPEC) e_what = WHAT_VIDEO;
}

//      if (e_t && (e_fps == 0)) e_fps = 1.0 / e_t;
//      if (e_fps && (e_t == 0)) e_t = 1.0 / e_fps;
switch (e_what) {
case WHAT_ERRMOD:
    if (e_n == 0) e_n = E_N_MAX;
    if (e_outfile == 0) e_outfile = e_outtik;
    INFO("creating_error_model_\ "%s\" from_\ "%s\""\n",
        e_outfile,
        argv[i]);
    start_opencv(argv[i]);
    PNMnoise(e_outfile);
    break;
case WHAT_VIDEO:
    if (e_n == 0) e_n = E_N_MAX;
    if (e_outfile == 0) e_outfile = e_outtik;
    if (e_noisefile == 0) {
        /* No error model specified; make one */
        register int x, y;
        for (y=0; y<256; ++y) {
            for (x=0; x<256; ++x) {
                int z = 255 - ((x > y) ? (x-y) : (y-x));
                if (z < 0) z = 0;
                z -= ((255 - z) * (255 - z));
                if (z < 0) z = 0;
                PNMerr[x][y][0] = z;
                PNMerr[x][y][1] = z;
                PNMerr[x][y][2] = z;
            }
        }
    }
    start_opencv(argv[i]);
    PNMtdci(e_outfile);
    break;
case WHAT_TIK:
    if (e_outfile == 0) e_outfile = e_outimage;
    now = ((e_begin < 0) ? 0 : e_begin);
    if (e_n <= 1) {

```

```

    /* One frame only */
    e_n = 1;
    if (e_t == 0) e_t = ((e_fps > 0) ? (1.0/e_fps) : (1.0/60))
        ;
    if (e_fps == 0) e_fps = e_t;
} else {
    /* Video sequence */
    if (e_fps == 0) e_fps = 24;
    if (e_t == 0) e_t = 1.0 / e_fps;
}

/* Create exposures */
/*PSE: Hack this to default to the functions in -k if
supplied
if a spec file is loaded,
FirstLive() and LastLive() can replace now and now+e_t
... But don't do it until any problems and edge cases are
worked out
*/
//if(e_fnfile){TIKrender(FirstLive(), LastLive());}

TIKrenderFile(dottik, argv[i]);
for (n=0; n<e_n; ++n) {
    TIKrender(now, now+e_t);
    now += (1.0 / e_fps);
}

/* Simultaneously render all frames */
TIKrenderSimul();

/* Done with this file */
break;
default:
    ERROR(ERROR_ARG,
        "what to do with %s? %s %s\n",
        argv[i],
        ((e_what & WHAT_ERRMOD) ? "Make error model" : ""),
        ((e_what & WHAT_VIDEO) ? "Encode as TIK" : ""),
        ((e_what & WHAT_TIK) ? "Make exposures" : ""));
}
}
}

INFO("completed in %d seconds\n", ((int)(time(0) - real_time)));
return(0);
}

```

Listing B.5: MaskGain.h

```

#!/usr/bin/python3
# Plots a gain function file for human viewing
import sys
import matplotlib.pyplot as plt
import parse as ps

```

```

if len(sys.argv) != 2:
    print ("Usage: _FnPlotter_FnFile.fn")

fns=[];

# Line format is M$n{$t0:$g0},...,$tm:$gm}}
with open(sys.argv[1],"r") as ffile:
    for line in ffile:
        # Echo it back at each step for testing
        #print(line.strip())
        ef={}
        if line.startswith('M'):
            tokens=line.split("{")
            #print(tokens)
            fnum=int(tokens[0][1:])
            #print("fnum=" + str(fnum) + "\n")
            ef["maskval"]=fnum
            #Do in' a little parsing to strip the trailing curly and
            newline
            tuples = tokens[1][:-2].split(",")
            times=[]
            gains=[]
            for pts in tuples:
                #print(pts)
                vals=ps.parse("[{}:{}] ",pts)
                #print("Time: " + vals[0] + " Gain: " + vals[1])
                times.append(float(vals[0]))
                gains.append(float(vals[1]))
            ef["times"]=times
            ef["gains"]=gains
            fns.append(ef)

#Print the data structure serialization if it looks like the sketchy
    parser is broken
#print(fns)

# Special case the single function in a file case because matplotlib
    is a little dumb
if len(fns) == 1:
    fig, ax = plt.subplots()
    fig.suptitle(sys.argv[1])
    ax.plot(ef["times"],ef["gains"])
    ax.set(title=ef["maskval"])
    #ax[i].set(xlabel='time (ns)', ylabel='gain',title=ef["maskval"])
    ax.grid()

else:
    fig, ax = plt.subplots(len(fns),sharex=True,sharey=True,
        gridspec_kw={'hspace': 0.505})
    fig.suptitle(sys.argv[1])
    i=0
    for ef in fns:

```

```
ax[i].plot(ef["times"],ef["gains"])
ax[i].set(title=ef["maskval"])
#ax[i].set(xlabel='time (ns)', ylabel='gain',title=ef["maskval
    ")
ax[i].grid()
i=i+1

# fig.savefig("fn.png")
plt.show()
```

Bibliography

- [1] J. R. Janesick, “Scientific charge-coupled devices,” in Bellingham: SPIE, 2001, ch. 1:History, Operation, Performance, Design, Fabrication and Theory, ISBN: 9780819480392. DOI: 10.1117/3.374903. [Online]. Available: <https://www.spiedigitallibrary.org/ebooks/PM/Scientific-Charge-Coupled-Devices/>.
- [2] H. G. Dietz, “Frameless, time domain continuous image capture,” in *Electronic Imaging 2014*, vol. 9022, 2014, pp. 7–12. DOI: 10.1117/12.2040016. [Online]. Available: <http://dx.doi.org/10.1117/12.2040016>.
- [3] H. Dietz, P. Eberhart, J. Fike, K. Long, C. Demaree, and J. Wu, “Tik: A time domain continuous imaging testbed using conventional still images and video,” *Electronic Imaging*, vol. 2017, no. 15, pp. 58–65, 2017, ISSN: 2470-1173. DOI: doi:10.2352/ISSN.2470-1173.2017.15.DPMI-081. [Online]. Available: <http://www.ingentaconnect.com/content/ist/ei/2017/00002017/00000015/art00010>.
- [4] J. Poskanzer, B. Henderson, and C. netpbm, *Netpbm*, Jan. 2014. [Online]. Available: <http://netpbm.sourceforge.net/doc/>.
- [5] K. Long, H. Dietz, and C. Demaree, “A canon hack development kit implementation of time domain continuous imaging,” *Electronic Imaging*, vol. 2017, no. 15, pp. 66–72, 2017, ISSN: 2470-1173. DOI: doi:10.2352/ISSN.2470-1173.2017.15.DPMI-075. [Online]. Available: <http://www.ingentaconnect.com/content/ist/ei/2017/00002017/00000015/art00011>.
- [6] ISO, *INTERNATIONAL STANDARD ISO12232-2006 - Photography - Digital still cameras - Determination of exposure index, ISO speed ratings, standard output sensitivity, and recommended exposure index*, 2006.
- [7] D. Kerr, “Apex - the additive system of photographic exposure,” Tech. Rep., 2007. [Online]. Available: <http://dougkerr.net/Pumpkin/articles/APEX.pdf>.
- [8] C. S. Committee, *Cipa dc-008-2016: Exchangeable image file format for digital still cameras: Exif version 2.31*, Jul. 2016. [Online]. Available: <http://www.cipa.jp/std/documents/e/DC-008-Translation-2016-E.pdf>.
- [9] H. G. Dietz, “Fujifilm x10 white orbs and deorbit,” *SPIE Conference Proceedings*, vol. 8660, pp. 8660–8675, 2013. DOI: 10.1117/12.2004411. [Online]. Available: <https://doi.org/10.1117/12.2004411>.
- [10] M. F. Tompsett, G. F. Amelio, and G. E. Smith, “Charge coupled 8-bit shift register,” *Applied Physics Letters*, vol. 17, no. 3, pp. 111–115, 1970. DOI: 10.1063/1.1653327. [Online]. Available: <https://doi.org/10.1063/1.1653327>.
- [11] N. Tompsett Michael Francis (Summit, *Charge transfer imaging devices*, Apr. 1978. [Online]. Available: <http://www.freepatentsonline.com/4085456.html>.

- [12] R. Cicala, *Sensor stack thickness: When does it matter?* L. R. Blog, Ed., Jun. 2014. [Online]. Available: <https://www.lensrentals.com/blog/2014/06/sensor-stack-thickness-when-does-it-matter/>.
- [13] A. Darmont, “Spectral response of silicon image sensors,” Aphesa, Tech. Rep., Apr. 2009. [Online]. Available: <http://www.aphesa.com/downloads/download2.php?id=1>.
- [14] J. Nakamura, *Image Sensors and Signal Processing for Digital Still Cameras*. Boca Raton, FL, USA: CRC Press, Inc., 2005, ISBN: 0849335450.
- [15] “Trichromatic colour reproduction and the additive principle,” in *The Reproduction of Colour*. Wiley-Blackwell, 2005, ch. 2, pp. 9–17, ISBN: 9780470024270. DOI: 10.1002/0470024275.ch2. eprint: <https://onlinelibrary.wiley.com/doi/pdf/10.1002/0470024275.ch2>. [Online]. Available: <https://onlinelibrary.wiley.com/doi/abs/10.1002/0470024275.ch2>.
- [16] Eric R. Jeschke, *Converting color images to b&w*, I’m sure there’s a more academic source for the 30/59/11 RGB ratio, but this is what I know it from, 2002. [Online]. Available: <https://www.gimp.org/tutorials/Color2BW/>.
- [17] S. Farsiu, M. Elad, and P. Milanfar, “Multiframe demosaicing and super-resolution of color images,” *IEEE Transactions on Image Processing*, vol. 15, no. 1, pp. 141–159, Jan. 2006, ISSN: 1057-7149. DOI: doi:10.1109.
- [18] H. Dietz, P. Eberhart, J. Fike, K. Long, and C. Demaree, “Temporal super-resolution for time domain continuous imaging,” *Electronic Imaging*, vol. 2017, no. 15, 2017.
- [19] A. Davies and P. Fennessy, *Digital Imaging for Photographers with CD (Audio)*, 4th. Newton, MA, USA: Butterworth-Heinemann, 2001, Accessed via Google Books, ISBN: 0240515900. [Online]. Available: <https://books.google.com/books?vid=ISBN0240515900>.
- [20] H. Dietz and P. Eberhart, “Shuttering methods and the artifacts they produce,” *Electronic Imaging*, vol. 2019, no. 4, pp. 590-1-590–7, 2019, ISSN: 2470-1173. [Online]. Available: <https://www.ingentaconnect.com/content/ist/ei/2019/00002019/00000004/art00010>.
- [21] H. G. Dietz, “Credible repair of sony main-sensor pdaf striping artifacts,” *Electronic Imaging*, vol. 2019, no. 4, pp. 585-1-585–7, 2019, ISSN: 2470-1173. [Online]. Available: <https://www.ingentaconnect.com/content/ist/ei/2019/00002019/00000004/art00006>.
- [22] Á. R.-V. Juan A. Leñero-Bardallo Jorge Fernández-berni, “Review of adcs for imaging,” vol. 9022, 2014, pp. 9022 - 9022 –6. DOI: 10.1117/12.2041682. [Online]. Available: <https://doi.org/10.1117/12.2041682>.
- [23] E. R. Fossum, J. Ma, S. Masoodian, L. Anzagira, and R. Zizza, “The Quanta Image Sensor: Every Photon Counts,” *Sensors (Basel)*, vol. 16, no. 8, Aug. 2016.

- [24] H. G. Dietz, “Programmable nanocontrollers for nanodevices,” University of Kentucky, Tech. Rep., 2003. [Online]. Available: <http://aggregate.org/KYARCH/cases2003.pdf>.
- [25] G. Gallego, T. Delbrück, G. Orchard, *et al.*, “Event-based vision: A survey,” *CoRR*, vol. abs/1904.08405, 2019. arXiv: 1904.08405. [Online]. Available: <http://arxiv.org/abs/1904.08405>.
- [26] C. Posch, D. Matolin, and R. Wohlgenannt, “A qvga 143 db dynamic range frame-free pwm image sensor with lossless pixel-level video compression and time-domain cds,” *IEEE Journal of Solid-State Circuits*, vol. 46, no. 1, pp. 259–275, Jan. 2011. DOI: 10.1109/JSSC.2010.2085952.
- [27] C. Hahne. “The standard plenoptic camera.” (), [Online]. Available: <http://www.plenoptic.info/index.html> (visited on 06/07/2024).
- [28] E. Adelson and J. Wang, “Single lens stereo with a plenoptic camera,” *IEEE Transactions on Pattern Analysis and Machine Intelligence*, vol. 14, no. 2, pp. 99–106, 1992. DOI: 10.1109/34.121783.
- [29] R. Ng, “Digital light field photography,” Ph.D. dissertation, Stanford University, 2006.
- [30] M. Kosoff, “Lytro, a ‘magic’ camera startup that raised \$140 million, announces layoffs and pivots to virtual reality,” *Business Insider*, Feb. 26, 2015. [Online]. Available: <https://www.businessinsider.in/lytro-a-magic-camera-startup-that-raised-140-million-announces-layoffs-and-pivots-to-virtual-reality/articleshow/46387133.cms>.
- [31] M. Zhang, “The first plenoptic camera on the market,” *petapixel*, Sep. 23, 2010. [Online]. Available: <https://petapixel.com/2010/09/23/the-first-plenoptic-camera-on-the-market/>.
- [32] *Canon hack development kit*. [Online]. Available: <http://chdk.wikia.com/wiki/CHDK>.
- [33] S. G. Corporation. “Sony global - source code distribution service.” (), [Online]. Available: <https://oss.sony.net/Products/Linux/common/search.html> (visited on 03/14/2024).
- [34] D. Coffin, *Decoding raw digital photos in linux*. [Online]. Available: <https://www.cybercom.net/~dcoffin/dcraw/>.
- [35] S. W. Hasinoff, “Photon , poisson noise (preprint),” in *Computer Vision; A Reference Guide*, K. Ikeuchi, Ed., Oxford: Springer US, 2014, pp. 608–610. [Online]. Available: <https://people.csail.mit.edu/hasinoff/pubs/hasinoff-photon-2012-preprint.pdf>.
- [36] J. L. Barron, D. J. Fleet, and S. S. Beauchemin, “Performance of optical flow techniques,” *International Journal of Computer Vision*, vol. 12, no. 1, pp. 43–77, Feb. 1994, ISSN: 0920-5691. DOI: 10.1007/BF01420984. [Online]. Available: <http://dx.doi.org/10.1007/BF01420984>.

- [37] J. J. Gibson, *The perception of the visual world / James J. Gibson*, English. Houghton Mifflin Boston, 1950, xii, 235 p. :
- [38] P. Pérez, M. Gangnet, and A. Blake, “Poisson image editing,” *ACM Transactions on Graphics*, vol. 22, no. 3, pp. 313–318, Jul. 2003, ISSN: 0730-0301. DOI: 10.1145/882262.882269. [Online]. Available: <http://doi.acm.org/10.1145/882262.882269>.
- [39] E. H. Land and J. J. McCann, “Lightness and retinex theory,” *Journal of the Optical Society of America*, vol. 61, no. 1, pp. 1–11, Jan. 1971. DOI: 10.1364/JOSA.61.000001. [Online]. Available: <http://www.osapublishing.org/abstract.cfm?URI=josa-61-1-1>.
- [40] alex. “Dynamic range improvement for some canon dslrs by alternating iso during sensor readout.” (), [Online]. Available: http://phd-sid.ethz.ch/debian/magiclantern/dual_iso.pdf (visited on 07/14/2014).
- [41] B. K. Karch and R. C. Hardie, “Robust super-resolution by fusion of interpolated frames for color and grayscale images,” *Frontiers in Physics*, vol. 3, 2015, ISSN: 2296-424X. DOI: 10.3389/fphy.2015.00028. [Online]. Available: <https://www.frontiersin.org/articles/10.3389/fphy.2015.00028>.
- [42] H. Dietz, C. Demaree, P. Eberhart, C. Kuball, and J. Y. Wu, “Lessons from design, construction, and use of various multicameras,” *Electronic Imaging*, vol. 30, no. 5, pp. 182-1–182-1, 2018. DOI: 10.2352/ISSN.2470-1173.2018.05.PMII-182. [Online]. Available: <https://library.imaging.org/ei/articles/30/5/art00004>.
- [43] T. Williams, C. Kelley, and many others, *Gnuplot 4.6: An interactive plotting program*, <http://gnuplot.sourceforge.net/>, Apr. 2013.
- [44] H. Dietz, W. Davis, and P. Eberhart, “Characterization of camera shake,” *Electronic Imaging*, vol. 32, no. 7, pp. 228-1–228-1, 2020. DOI: 10.2352/ISSN.2470-1173.2020.7.ISS-228. [Online]. Available: <https://library.imaging.org/ei/articles/32/7/art00011>.
- [45] H. G. Dietz and P. S. Eberhart, “Iso-less?” In *Electronic Imaging 2014*, vol. 9404, 2015, pp. 94040L-94040L–14. DOI: 10.1117/12.2080168. [Online]. Available: <http://dx.doi.org/10.1117/12.2080168>.
- [46] H. Dietz, P. Eberhart, and C. Demaree, “Multispectral, high dynamic range, time domain continuous imaging,” *Electronic Imaging*, vol. 2018, no. 5, pp. 409-1-409–9, Jan. 28, 2018, ISSN: 2470-1173. DOI: doi:10.2352/ISSN.2470-1173.2018.05.PMII-409. [Online]. Available: <https://www.ingentaconnect.com/content/ist/ei/2018/00002018/00000005/art00012>.
- [47] A. A. with Robert Baker, “The print,” in 3. 1271 Avenue of the Americas, New York, NY 10020: Little, Brown and Company, 1995, vol. Ansel Adams Photography, ch. The Fine Print: Control of Values, pp. 89–127, ISBN: 0-8212-2187-6.

- [48] P. Baumgarten, “Focus stacking & bracketing with om-d,” OM Digital Solutions Corporation, Tech. Rep., 2016. [Online]. Available: <https://learnandsupport.getolympus.com/learn-center/photography-tips/macro/focus-stacking-bracketing-with-om-d>.
- [49] E. E. Catmull and R. Rom, “A class of local interpolating splines,” *Computer Aided Geometric Design*, pp. 317–326, 1974. [Online]. Available: <https://api.semanticscholar.org/CorpusID:118383557>.
- [50] R. Burden and J. Faires, “Numerical analysis,” in Cengage Learning, 2010, ch. 3, pp. 144–153, ISBN: 9780538733519. [Online]. Available: <https://books.google.com/books?id=zXnSxY9G2JgC>.
- [51] P. Eberhart and H. G. Dietz, “Non-uniform integration of tdc captures,” *Electronic Imaging*, vol. 32, no. 7, pp. 330-1–330-1, 2020. DOI: 10.2352/ISSN.2470-1173.2020.7.ISS-330. [Online]. Available: <https://library.imaging.org/ei/articles/32/7/art00017>.
- [52] G. Bradski, “The OpenCV Library,” *Dr. Dobb’s Journal of Software Tools*, 2000.
- [53] *Sony playmemories camera apps, a camera application download service*. [Online]. Available: <https://www.playmemoriescameraapps.com>.
- [54] S. G. Corporation. “Playmemories camera apps ending.” (), [Online]. Available: <https://www.sony.com/electronics/support/articles/00289030> (visited on 03/14/2024).
- [55] k. oz_paulb kenan, *Fwtool*, 2012. [Online]. Available: <http://www.personal-view.com/faqs/sony-hack/fwtool>.
- [56] malco, *Fwtool.py*, 2018. [Online]. Available: <http://www.personal-view.com/faqs/sony-hack/fwtool>.
- [57] malco, *Sony-pmca-re*, 2018. [Online]. Available: <https://github.com/malco/Sony-PMCA-RE>.
- [58] malco, *Openmemories:tweak*, 2018. [Online]. Available: <https://github.com/malco/OpenMemories-Tweak>.
- [59] K. Shirriff. “Understanding sony ir remote codes, lirc files, and the arduino library.” (Mar. 21, 2010), [Online]. Available: <https://www.righto.com/2010/03/understanding-sony-ir-remote-codes-lirc.html> (visited on 03/21/2024).
- [60] C. Inc. “Canon technology — dryos (archived).” (), [Online]. Available: https://web.archive.org/web/20080116050120/http://www.canon.com/technology/canon_tech/explanation/dryos.html (visited on 11/20/2008).
- [61] H. Dietz, C. Parrish, and K. D. Donohue, “Self-contained, passive, non-contact, photoplethysmography: Real-time extraction of heart rates from live view within a canon powershot,” *Electronic Imaging*, vol. 31, no. 13, pp. 146-1–146-1, 2019. DOI: 10.2352/ISSN.2470-1173.2019.13.COIMG-146. [Online]. Available: <https://library.imaging.org/ei/articles/31/13/art00012>.

- [62] *The magic lantern project*. [Online]. Available: <https://www.magiclantern.fm/>.
- [63] alex et.al. “Magic lantern forum: Topic: Edmac internals.” (), [Online]. Available: <https://www.magiclantern.fm/forum/index.php?topic=18315.msg245609> (visited on 12/20/2023).
- [64] K. Ushida, Y. Naoi, Y. Katahira, and K. Morishita, “Image processing apparatus and image processing method,” US7817297B2, Dec. 2010. [Online]. Available: <https://patents.google.com/patent/US7817297>.
- [65] The Magic Lantern Community. “Register magic lantern firmware wiki: Register map.” (), [Online]. Available: https://magiclantern.fandom.com/wiki/Register_Map (visited on 12/20/2023).
- [66] David Milligan, et.al. “Magic lantern forum: Topic: Mlv lite.” (), [Online]. Available: <https://www.magiclantern.fm/forum/index.php?topic=16650.0> (visited on 12/20/2023).
- [67] I. Sibiryakov. “Mlv-app: All in one mlv processing app.” (), [Online]. Available: <https://github.com/ilia3101/MLV-App> (visited on 12/20/2023).
- [68] CarVac. “Librtprocess: A project to make rawtherapee’s processing algorithms more readily available.” (), [Online]. Available: <https://github.com/CarVac/librtprocess> (visited on 12/20/2023).
- [69] D. Milligan. “Mlvfs: Mlv (magic lantern raw video format) ”converter” that uses fuse to allow ”mounting” of mlv files as filesystems.” (), [Online]. Available: <https://bitbucket.org/dmilligan/mlvfs/src/master/> (visited on 12/20/2023).
- [70] P. S. Eberhart and H. Dietz, “Magic lantern as a platform for digital photography research,” *Electronic Imaging*, 2024.
- [71] A.-T. Technology. “Esp32-cam camera development board.” (), [Online]. Available: <https://docs.ai-thinker.com/en/esp32-cam> (visited on 05/06/2024).
- [72] H. Dietz and P. Eberhart, “An ultra-low-cost large-format wireless iot camera,” *Electronic Imaging*, vol. 33, no. 7, pp. 70-1–70-1, 2021. DOI: 10.2352/ISSN.2470-1173.2021.7.ISS-070. [Online]. Available: <https://library.imaging.org/ei/articles/33/7/art00005>.
- [73] H. Dietz, D. Abney, P. Eberhart, *et al.*, “Esp32-cam as a programmable camera research platform,” *Electronic Imaging*, vol. 34, no. 7, pp. 232-1–232-1, 2022. DOI: 10.2352/EI.2022.34.7.ISS-232. [Online]. Available: <https://library.imaging.org/ei/articles/34/7/ISS-232>.
- [74] J. D. Hunter, “Matplotlib: A 2d graphics environment,” *Computing in Science & Engineering*, vol. 9, no. 3, pp. 90–95, 2007. DOI: 10.1109/MCSE.2007.55.
- [75] C. Odenbach. “The canon ae-1: A new kind of slr.” (2016), [Online]. Available: <https://www.678vintagecameras.ca/blog/the-canon-ae-1-a-new-kind-of-slr> (visited on 06/09/2024).

- [76] M. Johnston. “A (very) brief and somewhat lighthearted history of modes.” (2014), [Online]. Available: https://theonlinephotographer.typepad.com/the_online_photographer/2014/04/a-very-brief-history-of-modes.html (visited on 06/09/2024).
- [77] THE INTERNATIONAL TELEGRAPH AND TELEPHONE CONSULTATIVE COMMITTEE, “CODEC FOR AUDIOVISUAL SERVICES AT $n \times 384$ kbit/s,” INTERNATIONAL TELECOMMUNICATION UNION, Standard, 1988.
- [78] ISO/IEC JTC 1/SC 29, “Iso/iec 1172: Coding of moving pictures and associated audio for digital storage media at up to about 1.5 mbit/s,” International Organization for Standardization, Geneva, CH, Standard, 1993.
- [79] J. Ma, D. Zhang, D. Robledo, L. Anzagira, and S. Masoodian, “Ultra-high-resolution quanta image sensor with reliable photon-number-resolving and high dynamic range capabilities,” *en, Sci. Rep.*, vol. 12, no. 1, p. 13 869, Aug. 2022.
- [80] J. Fisher, “Hands on: Sony’s speedy a9 iii has a global shutter, 120fps burst rate,” *PCMag*, Nov. 9, 2023. [Online]. Available: <https://www.pcmag.com/news/hands-on-sonys-speedy-a9-iii-has-a-global-shutter-120fps-burst-rate>.
- [81] R. Butler, “Sony a9 iii: Global shutter comes with an image quality cost,” *dpreview*, Jan. 4, 2024. [Online]. Available: <https://www.dpreview.com/articles/6717086661/sony-a9-iii-image-quality-dynamic-range-analysis>.
- [82] A. Lee, “Review: The light 116 is brilliant and braindead,” *petapixel*, Dec. 8, 2017. [Online]. Available: <https://petapixel.com/2017/12/08/review-light-116-brilliant-braindead/>.
- [83] J. Schneider, “Samsung argues that there is no such thing as a real picture,” *petapixel*, Feb. 5, 2024. [Online]. Available: <https://petapixel.com/2024/02/05/samsung-argues-that-there-is-no-such-thing-as-a-real-picture/>.
- [84] R. Amadeo, “Moon-gate: Samsung fans are mad about ai-processed photos of the moon,” *Ars Technica*, Mar. 16, 2023. [Online]. Available: <https://arstechnica.com/gadgets/2023/03/samsung-says-it-adds-fake-detail-to-moon-photos-via-reference-photos/>.

Vita

Paul Selegue Eberhart of Lexington, KY has collected Bachelors of Science in Electrical Engineering, Computer Engineering, and Computer Science, and a Masters of Science in Electrical Engineering at the University of Kentucky.